Pliocene-Quaternary volcanic rocks of NW Armenia: magmatism and lithospheric dynamics within an active orogenic plateau

I. Neill[1*], Kh. Meliksetian[2], M.B. Allen[1], G. Navarsardyan[2], S. Karapetyan[2]

[1]Department of Earth Sciences, Durham University, Science Site, DH1 3LE, Durham, UK

[2]Institute of Geological Sciences, National Academy of Sciences of Armenia, Marshal Baghramian Avenue, Yerevan 0019, Armenia

*Corresponding author. E-mail: iain.neill@durham.ac.uk. Phone: +44 1913 342356.

Abstract

The Pliocene-Quaternary volcanic rocks of Armenia are a key component of the Arabia-Eurasia collision, representing intense magmatism within the Turkish-Iranian plateau, tens of millions of years after the onset of continental collision. Here we present whole rock elemental and Nd-Sr isotope data from mafic, intermediate, and felsic lava flows and cinder cones in Shirak and Lori provinces, NW Armenia. Magmatism appears to be controlled locally by extension related to major strike-slip faults within the plateau. Major and trace element results show that the three series – valley-filling medium-K alkali basalt flows, ridge-forming andesite to rhyolite flows, and andesitic cinder cones – form a compositional continuum linked by a crystallisation sequence dominated by two pyroxenes, plagioclase and amphibole. There is petrographic and major and trace element evidence for magma mixing

processes and potentially crustal contamination by Mesozoic-early Cenozoic arc-related rocks, which has not significantly affected the isotopic signature. Modelling of the basaltic rocks indicates that they formed by moderate degrees of partial melting (~3-4 %) of an incompatible element enriched, subduction-modified, lithospheric mantle source. Samples have a distinctive high Zr/Hf ratio and high Zr concentrations, which are an intrinsic part of the source or the melting process, and are much more commonly found in ocean island basalts. Regional models for magmatism often argue for whole-scale delamination of the mantle lithosphere beneath Eastern Anatolia and the Lesser Caucasus, but this scenario is hard to reconcile with limited crustal signatures and the apparent lack of asthenospheric components within many studied centres.

Highlights

- Whole-rock study of Pliocene-Quaternary lavas from the Armenian Highlands
- Compositional range controlled by fractional crystallisation, magma mixing and possible crustal contamination
- Low-degree melting of a shallow metasomatised lithospheric mantle source
- Exploring triggers for <10 Myr increase in magmatic activity in the Arabia-Eurasia collision zone

Keywords

Armenia; geochemistry; petrogenesis; orogenic plateau

1. Introduction

Orogenic plateaux such as the modern Turkish-Iranian, Bolivian Altiplano-Puna and Tibetan plateaus form in response to plate convergence and collision, and represent a primary topographic feature of the continents. In spite of their thickened crust, plateaus are also sites of intense, ultimately mantle-derived magmatism (e.g. Williams et al., 2004; Mo et al., 2007). Such magmatism is often attributed to asthenospheric upwelling following the break-off of the subducted oceanic slab (e.g. Keskin, 2003), or the delamination of the lithosphere inboard of the plate suture (e.g. Kay and Kay, 1993).

The Turkish-Iranian plateau (Fig. 1) is a product of the Cenozoic Arabia-Eurasia collision, and magmatism post-dating initial collision is particularly voluminous from the Late Miocene until the present day, in numerous locations across eastern Turkey, Armenia, and much of Iran (Fig. 1). Erupted products range from mafic to felsic, and sodic to ultrapotassic (Pearce et al., 1990; Karapetian et al., 2001; Davidson et al., 2004; Azizi and Moinevaziri, 2009; Saadat et al., 2011; Saadat and Stern, 2012; Allen et al., 2013). In nearby Georgia and the Greater Caucasus, the most recent magmatism appears to have started slightly earlier, in the Middle Miocene, and continued with some gaps in the record until recent times (Lebedev et al., 2006a,b; 2007; 2008a,b; Adamia et al., 2011).

This plateau-wide ‘recent’ magmatism may be only partly explained by partial melting of asthenospheric or mantle lithosphere sources due to break-off of the southern Neo-Tethys slab (e.g. Keskin, 2003; 2007; Şengör et al., 2008; Dilek et al., 2010; van Hunen and Allen, 2011). Miocene to recent magmatism extends to at least 500 km from the Bitlis-Zagros suture zone, a spatial scale akin to the Cenozoic ‘ignimbrite flare-up’ of the western United States (Johnson, 1991). The wide extent of Miocene-Quaternary magmatism hundreds of

kilometres from the suture zone indicates that whole-scale lithospheric delamination (Pearce et al., 1990), or other unrecognised processes may be collectively responsible for magmatism in this region.

To further consider the origin of such magmatism, this paper focuses on Armenia (Fig. 1), where recent volcanism has been under-represented in the international literature. We present whole rock elemental and Nd-Sr isotope data from three series of mafic to felsic Pliocene-Quaternary volcanic rocks in the north of Shirak and west of Lori administrative provinces in the northwest of the country (herein referred to as 'Shirak') (Fig. 2). The local tectonic setting and relationship to magmatism is highlighted, alongside discussion on magmatic evolution, mantle sources and partial melting. We finish by assessing how the results fit with regional geodynamic models.

2. Geological setting, structure, and petrography

2.1. The Turkish-Iranian plateau

The Turkish-Iranian orogenic plateau (Fig. 1) developed following the closure of the Neo-Tethys Ocean (Şengör and Kidd, 1979). The basement of the plateau consists of Mesozoic to Early Cenozoic accretionary belts and arc rocks and also older, Gondwanaland-related micro-continental fragments that all accreted to the southern margin of Eurasia. It is widely assumed that the Neo-Tethys oceanic crust was divided into a northern and a southern segment; the former closed either during the Late Cretaceous (Lordkinpanidze, 1980; Keskin, 2008) or the Paleocene-Early Eocene (Sosson et al., 2010). The two segments of Neo-Tethys were separated by micro-continental fragments such as the South Armenian Block and Tauride-

100 Anatolide terranes (Sosson et al., 2010). Destruction of the southern segment of Neo-Tethys
101 brought Arabia and Eurasia together along the Bitlis-Zagros suture zone (Fig. 1).
102
103 The timing of initial collision between Arabia and Eurasia is debated, although most
104 estimates range between 35 and 20 Ma (Agard et al., 2005; Allen and Armstrong, 2008;
105 Morley et al., 2009; Okay et al., 2010; Ballato et al., 2011; McQuarrie and van Hinsbergen,
106 2013). Marine carbonates deposited across much of central Iran and eastern Turkey in the
107 Early Miocene indicate that growth of the orogenic plateau is a later phenomenon (Bottrill et
108 al., 2012). Deformation is presently focussed on the plateau margins, from the Greater
109 Caucasus and Alborz in the north to the Zagros in the south, with no active crustal thickening
110 or thinning occurring between (Jackson et al., 1995; Allen et al., 2011). Lithospheric
111 thickness is highly variable, from >200 km in Iran near the Zagros suture, to only 60 km or
112 less in eastern Anatolia (Priestley and McKenzie, 2006; Angus et al., 2006). The current
113 height of the plateau, ~1750 m above sea level, has been attributed to a combination of Late
114 Cenozoic crustal shortening, and also to the detachment of mantle lithosphere and/or
115 subducted Tethyan slabs beneath the plateau, allowing the upwelling of hot, buoyant
116 asthenosphere beneath the region (Keskin, 2003).
117
118 The Cenozoic magmatic record of the plateau is divided into several stages (see Dilek
119 et al., 2010; Chiu et al., 2013 for reviews). First is an Eocene 'flare-up' of arc magmatism
120 immediately prior to the onset of continental collision, focussed predominantly on the
121 Urumieh-Dokhtar arc in southwest Iran, the Lut Block, Kopeh Dag and Alborz regions of
122 eastern and northern Iran (Verdel et al., 2011), and also in Armenia (Lordkinpanidze et al.,
123 1988). The flare-up has been attributed to back-arc extension (Vincent et al., 2005), an
124 episode of flat subduction (Berberian and Berberian, 1981), perhaps coupled with enhanced

slab roll-back (Verdel et al., 2011), or break-off of the northern Neo-Tethyan slab in Armenia and North-Central Turkey (Keskin et al., 2008; Sosson et al., 2010). The second stage is a magmatic 'gap' which comprised some 20-30 Myr of limited magmatic activity between the Eocene and the Late Miocene as continental collision proceeded (Verdel et al., 2011; Richards et al., 2011). The third and final stage is the aforementioned upsurge of mantle-derived volcanism from the Middle to Late Miocene until the present day (Chiu et al., 2013), which forms the basis of this study.

2.2. Basement and structure in Armenia

Armenia, including the Lesser Caucasus mountain range, lies at the northern side of the plateau (Figs. 1, 2). Southern Armenia is underlain by the aforementioned South Armenian Block (SAB), a micro-continental fragment rifted during the early Mesozoic, separating the northern and southern branches of the Neo-Tethyan seaway (Stampfli, 2000). The SAB consists of Proterozoic gneisses, mica schists and amphibolites partially overlain by Devonian to Jurassic sediments, Jurassic and younger ophiolitic material, and Paleocene to Early Oligocene volcanic rocks related to subduction of the southern branch of Neo-Tethys (Rolland et al., 2009). In the north of Armenia, the Armenian Highlands represent the former active continental margin of Eurasia and contain arc and discontinuous ophiolite sequences formed during the closure of the northern branch of the Neo-Tethyan seaway (Adamia et al., 1981; 2011). The largest tract of ophiolitic material in Armenia forms the Sevan-Akera suture zone, a 400 km-long boundary between the SAB and the Mesozoic arc of the Lesser Caucasus to the north. Immediately south of our field area, between Amasia and Stepanavan, is a belt of blueschist-facies mélange (part of the Sevan-Akera ophiolite suite), tectonically

149 overlain by Jurassic to Cretaceous mafic rocks, and two sequences of Cretaceous to Early
150 Oligocene subduction-related volcano-sedimentary rocks (Rolland et al., 2009).
151
152 Following the Eocene amalgamation of the Armenian crustal blocks (Rolland et al.,
153 2009), north-directed subduction of the southern Neo-Tethys terminated along the Bitlis-
154 Zagros suture, some 300 km south of Armenia. After the last subduction-related magmatism,
155 the magmatic 'gap' in Armenia extended until the Late Miocene (~10 Ma), based on
156 groundmass and mineral K-Ar ages from the oldest volcanic rocks of the Gegham Highlands
157 (Arutyunyan et al., 2007). The most voluminous volcanism is of Pliocene-Quaternary age,
158 covering much of Aragatsotn, Shirak, Kotayk, Gegharkunik, and Syunik provinces, an area
159 >10,000 km^2 (Mitchell and Westaway, 1999; Karapetian et al., 2001; Lebedev et al., 2011)
160 (Fig. 2).
161
162 2.3. Pliocene - Quaternary magma series
163
164 The geology of NW Armenia was first studied in detail during Soviet times (Kharazyan,
165 1983). The oldest Pliocene – Quaternary volcanism is represented by poorly-exposed
166 rhyolites and obsidians at Aghvorik (Fig. 2), covered by dolerites which drape much of the
167 lowest topography in Shirak, often part-filling river valleys for tens of kilometers.
168 Relationships with sedimentary deposits dated using mammalian fossils lead authors to
169 conclude that these mafic lavas were of Late Pliocene age (Kharazyan, 1983 and references
170 therein). A K-Ar age determination from dolerite from the Akhurian river basin within our
171 study area gave a result of 2.5 ± 0.2 Ma (Chernyshev et al., 2002). Groundmass K-Ar results
172 from numerous mafic to felsic volcanic rocks across the Javakheti Highlands in southern
173 Georgia gave ages of 4.6 ± 0.2 to 1.54 ± 0.10 Ma (Late Pliocene to Quaternary) (Lebedev et

al., 2008a,b). The mafic rocks in Armenia and southern Georgia may have resulted from fissure eruptions (Jrbashyan et al., 1996), but the actual source of these lavas has never been found, and may be buried by younger flows.

On top of the plateau-like topography formed by the mafic flows in Shirak, are hills of intermediate-felsic composition of up to 600 m prominence, including the north-south trending Javakheti, or Kechut, ridge (Fig. 2). Kharazyan (1983) distinguished two units within the Armenian part of the Javakheti ridge. The first unit (Lower Kechut Suite) is said to contain two-pyroxene basaltic andesites, andesites and hornblende andesites which cover the valley series and are thus assumed to be of Early Pleistocene age (Kharazyan, 2005). SHRIMP U-Pb zircon dating of andesitic vent-proximal ash and breccia layers deposited on the eastern flank of the Javakheti ridge in Lori province at the Karakhach archaeological site (Fig. 2) gives maximum eruption ages of 1.94 ± 0.05 to 1.80 ± 0.03 Ma (Presnyakov et al., 2012). This study also noted two Eocene zircons (40-50 Ma) consistent with Eocene arc rocks found to the east of the study area, plus five Proterozoic grains, consistent with an origin in the underthrust SAB. It is uncertain whether or not these old grains were from xenoliths ripped up during explosive volcanism or zircons assimilated during magma ascent. The Javakheti Ridge extends into southern Georgia, where it is higher and has a sharp little denuded topographic profile compared to further south. Groundmass K-Ar dating revealed younger ages of <1 Ma for the Samsari volcanic centre to the north of the Javakheti Ridge (Chernyshev et al., 2006). Kharazyan (1983) also defined an Upper Kechut Suite supposedly containing lavas erupted from cinder cones on the western part of the ridge, and considered to be of Middle Pleistocene age (Kharazyan, 2005). We did not find clear evidence of this unit during our studies. The only other Pliocene-Quaternary volcanic products in this part of Shirak are cinder cones to the west of the Javakheti Ridge around Lake Arpi (Fig. 2), which

199 are estimated to be of Early-Middle Pleistocene age, based on relationships with the mafic
200 rocks and some river terraces (Kharazyan, 1983).
201
202 Overall there have been no comprehensive geochronological studies carried out in
203 Shirak using a single reliable technique, unlike those for similar sequences in Georgia
204 (Lebedev et al., 2008a,b). A lack of continuous exposure hampers judgement of the relative
205 age of the different lavas. We have decided to sub-divide the entire Pliocene-Quaternary suite
206 close to the Javakheti Ridge into three components: mafic flows (the dolerites) largely
207 covering the topography developed on the basement (herein termed the *Valley Series*); more
208 evolved flows built up into hills above the mafic flows (*Ridge Series*); and scattered cinder
209 cones (*Cone Series*) (Fig. 2).
210
211 *2.3.1. Valley Series*
212
213 The Valley Series consists of mafic flows with a maximum cumulative thickness of 200 m in
214 eastern Lori province (Fig. 2). In the study area, the exposed sequence comprises at most four
215 or five stacked flows up to 40 m thick in total, and directly overlies the Sevan-Akera suture
216 and ophiolite sequence in the Dzoraged gorge and near Amasia (Fig. 2). We have collected
217 samples from these locations, as well as from Lake Arpi and near Tashir in western Lori
218 Province (Fig. 2). Valley Series samples collected from near Lake Arpi, Amasia, and Tashir
219 (Fig. 2), consist of vesicular sub-ophitic dolerites with rare clinopyroxene or optically zoned
220 plagioclase phenocrysts, set in a groundmass of 1-2 mm grain size consisting of
221 clinopyroxene, plagioclase and oxides (see Supplementary Item 1). Clinopyroxene is
222 commonly rimmed or almost totally replaced by red-brown amphibole, and there is
223 occasional interstitial quartz and rare rounded quartz blebs. Some samples contain very rare

224 iddingsite crystals, and the few olivines found in thin section are rounded and <0.5 mm in
225 diameter.
226
227 *2.3.2. Ridge Series*
228
229 Magmatism in this series is restricted to intermediate to felsic lavas built up into prominent
230 topographic features. The highest of these is the north to south-trending Javakheti Ridge (Fig.
231 2), consisting of rounded and glacially eroded peaks reaching ~3100 m above sea level,
232 following a clear north-south trend running north into Georgia (Fig. 2). A second series of
233 hills lie north of the Akhuryan River parallel to the Georgian border, but these are more
234 topographically muted, reaching a maximum elevation of ~2400 m. Rock types from both
235 ridges are almost exclusively andesitic to dacitic flows, with rare black dacites and rhyolitic
236 obsidians (Karapetian et al., 2001). Analysed flows range from basaltic trachyandesites to
237 dacites, and there is much compositional and textural variation. Some of the least evolved
238 samples (<60 wt.% SiO_2) contain 1-3 mm phenocrysts and glomerocrysts of clinopyroxene
239 (rarely orthopyroxene) and plagioclase, set in a flow-banded groundmass of plagioclase,
240 clinopyroxene and Fe-Ti oxides, with accessory apatite and zircon. More evolved samples
241 tend to contain significantly more plagioclase phenocrysts, and several have abundant 1-3
242 mm euhedral green-brown pleochroic amphiboles, but the presence of amphibole is not
243 ubiquitous even in samples of similar SiO_2 and MgO concentrations. Many plagioclase
244 crystals are sieve-textured and some have corroded margins, usually taken to imply the
245 occurrence of magma mixing processes (Tsuchiyama, 1985; Tepley et al., 1999), and many
246 crystals are also optically zoned. Other evidence for magma mixing is the common
247 occurrence of rounded quartz blebs with dark reaction coronas, and ubiquitous opaque rims
248 on primary hornblende crystals (Tepley et al., 1999; Supplementary Item 1). A black dacite

contains a few clinopyroxene glomerocrysts, but mostly consists of a fine-grained groundmass dominated by prismatic to acicular feldspars. The Ridge Series includes the only crustal xenoliths noted from our sampling, at a single site near Darik, north of Lake Arpi (Fig. 2). The xenoliths consist of a coarse-grained groundmass of plagioclase, clinopyroxene, oxide, and rare iddingsite after olivine; and 2-3 mm phenocrysts of clinopyroxene and plagioclase, most consistent with inclusion of material from the Valley Series. A slight chilled margin is observed within the host.

2.3.3. Cone Series

Scattered cinder cones are present in the Akhuryan valley near Lake Arpi (Fig. 2), often tens of metres high and several hundred metres across. We have collected samples from Sepasar, Eznasar, and Kaputkogh cones (Fig. 2). Most are composed of poorly welded unsorted glass or scoria fragments, and more coherent scoria bombs reaching a few tens of centimetres in diameter. The Cone Series compositions mirror the least evolved of the ridge series, the majority of samples containing differing proportions of plagioclase and clinopyroxene as phenocrysts and groundmass (Supplementary Item 1). Bombs from Kaputkogh and Eznasar contain ubiquitous mm-scale rounded quartz xenocrysts, whereas those at Sepasar appear more mafic, and devoid of foreign material.

3. Analytical methods

Samples were powdered in an agate ball mill at Durham University. Major element analysis was conducted on fused glass beads using a PANalytical Axios Advanced X-Ray Fluorescence (XRF) spectrometer at the University of Leicester. Leftover fractions of the

274 powder from XRF analysis were digested using a standard HF and HNO_3 technique prior to
275 trace element analysis. Solutions were run on a Thermo X2 inductively-coupled plasma mass
276 spectrometer (ICP-MS) at the Northern Centre for Isotopic and Elemental Tracing (NCIET)
277 at Durham University. Accuracy, precision, and reproducibility were monitored using blanks,
278 multi-run and within-run duplicates, Re-Rh spike solutions, and five international reference
279 standards. Standard W2 (n = 15) gave first relative standard deviations of 5% or better for
280 most transition metals (excepting 10% for Sc, 12% for Cr, 6% for Ni), the large ion lithophile
281 elements (LILE) and the rare earth elements (REE) (7% for La, 6% for Ce). Elemental results
282 are recorded in Table 1 and Supplementary Item 2, the latter also containing standard results.
283
284 Radiogenic Nd and Sr isotope analysis was conducted at NCIET, with column
285 chemistry for elemental pre-concentration based on the method of Dowall et al. (2007).
286 Powders were digested in HF and HNO_3, and solutions run through 1 ml pipettes containing
287 several drops of dilute Sr-spec resin to collect the Sr-bearing fraction. The high field strength
288 element (HFSE)- and rare earth element (REE)-bearing fraction from these columns was run
289 through 10 ml Bio-Rad polypropylene columns containing 1 ml of Bio-Rad AG1-X8 200-400
290 mesh anion-exchange resin. Neodymium was collected as part of a general rare earth element
291 fraction. Analysis was conducted on a Thermo Neptune Mass Collector ICP-MS. Strontium
292 was run in a single batch during which time blanks averaged 88 pg Sr (n = 6). International
293 reference standard NBS987 gave a mean of $^{87}Sr/^{86}Sr = 0.710263 \pm 0.000012$ (2σ, n = 12),
294 comparable to a preferred value of 0.710240, and providing a minimum uncertainty of
295 16 ppm (2σ). No correction was applied to the final results. Neodymium was run in two
296 separate batches, with blanks averaging 10 pg Nd (n = 6). During the first run, a combination
297 of the J&M standard and a Sm-doped version gave a mean $^{143}Nd/^{144}Nd = 0.511098 \pm$
298 0.000007 (2σ, n = 13), and a minimum uncertainty of 13 ppm (2σ). During the second run,

299 $^{143}Nd/^{144}Nd = 0.511100 \pm 0.000007$ (2σ, n = 13), giving an uncertainty of 14 ppm (2σ). For
300 consistency between the runs, all results were normalised to a preferred value of 0.511110.
301 Results are presented in Table 2.
302
303 **4. Geochemistry**
304
305 4.1. Sample freshness
306
307 We collected the freshest available samples at each locality, and this is reflected in loss-on-
308 ignition (LOI) values typically <1 wt.%, mostly un-weathered feldspars and mafic minerals,
309 and an overall lack of sericite and chlorite in thin section. Major and trace element data,
310 particularly element vs. SiO_2 plots (see Section 4.2), have trends consistent with magmatic
311 processes, particularly for CaO, MgO, K_2O, and Na_2O, as opposed to the widespread scatter
312 expected during sub-solidus alteration which easily mobilises these elements (e.g. Cann,
313 1970; Pearce, 1996). $^{87}Sr/^{86}Sr$ isotope results are commonly affected by hydrothermal
314 alteration, but here are depleted with no sign of a trend towards high $^{87}Sr/^{86}Sr$ at constant
315 $^{144}Nd/^{143}Nd$ (Table 2); nor is there a correlation between LOI and isotopic ratios.
316 Furthermore, the samples were erupted in an intra-continental high plateau so have not
317 interacted with high $^{87}Sr/^{86}Sr$ seawater or been exposed to tropical weathering.
318
319 4.2. Major and trace element characteristics
320
321 *4.2.1. Valley Series*
322

323 The Valley Series lavas (~49-55 wt.% SiO_2) are mostly mildly alkaline trachybasalts based
324 on the total alkali-silica classification (Le Bas et al., 1986; Fig. 3a), and belong to the
325 medium-K series of Peccerillo and Taylor (1976; Fig. 3b). They are evolved, with 4-7 wt.%
326 MgO and low molar Mg# from 46 to 58. Overall the samples have low TiO_2, moderate-high
327 Al_2O_3, and a sodic character (Na_2O/K_2O = 2.7-4.1) (Fig. 4). Trace element abundances and
328 trends can be seen on Figure 5. Also, the lavas have low Sc (<25 ppm), moderate Cr, Ni, and
329 large ion lithophile element (LILE) abundances (e.g. Ba = 280-450 ppm and Sr = 540-720
330 ppm). Chondrite-normalised (CN) REE abundances are light REE (LREE) enriched
331 (La/Yb_{CN} = 5-9; calc-alkaline), with flat heavy REE (HREE) patterns around 15-20 times
332 chondritic abundances (Fig. 6a). The patterns are split into two groups, one with lower LREE
333 and higher HREE concentrations and vice versa, the patterns crossing over at around Pr-Nd.
334 There are some very slight negative Eu anomalies relative to the MREE. The extended
335 Primitive Mantle-normalised (PMN) plot (Fig. 6b) shows that the samples have spiky LILE
336 patterns (modest positive Ba, Rb, Th, Sr anomalies), prominent negative K, Nb-Ta, and Ti
337 anomalies and positive Zr-Hf anomalies relative to the REE, with super-chondritic Zr/Hf
338 ratios of 47-55.
339
340 *4.2.2. Ridge Series*
341
342 The more evolved Ridge Series (~57-68 wt.% SiO_2, 2-5 wt.% MgO, Mg# = 41-55) has a
343 wide range of sub-alkaline compositions from basaltic trachy-andesite through to dacite (Fig.
344 3a). Samples largely belong to the medium-K series, although two plot in the high-K field
345 (Fig. 3b). They have noticeably lower TiO_2, $Fe_2O_{3(t)}$ and P_2O_5 concentrations compared to the
346 valley series, and are slightly less sodic (Na_2O/K_2O = 1.4-2.5) (Fig. 4). Transition metal
347 abundances are lower than the Valley Series, but the Ridge Series has higher Ba and Zr and

lower Sr and Nb concentrations compared to the mafic lavas (Fig. 5). Chondrite-normalised LREE patterns (Fig. 6c) are similar to the Valley Series, again splitting into two groups with higher or lower LREE concentrations. Ridge samples have La/Yb_{CN} from 8 to 18, with a highly fractionated M-HREE distribution such that some samples have a U-shaped pattern. There are small negative Eu anomalies. Primitive Mantle-normalised patterns (Fig. 6d) differ slightly from the Valley Series in having positive Rb spikes, and more pronounced negative Nb-Ta, P and Ti anomalies.

4.2.3. Cone Series

The Cone Series splits into three groups, the most mafic being the two cones at Sepasar (58 wt.% SiO_2, but low Mg# = 43), and the most felsic at Eznasar (62 wt.% SiO_2, Mg# = 52). The large cone at Kaputkogh has intermediate silica content relative to the other cones, although it has the highest Mg# of 54. The cones have higher Nb and Zr concentrations relative to the other series (Fig. 5); REE patterns for the Cone Series are clearly bimodal (Fig. 6e), whilst the Primitive Mantle-normalised plots look similar to the Valley Series (Fig. 6f).

4.3. Radiogenic isotope geochemistry

Most samples span a narrow range from $^{87}Sr/^{86}Sr$ = 0.70416 to 0.70446 and $^{143}Nd/^{144}Nd$ = 0.51280 to 0.51287, giving a range of values in epsilon notation from εNd = +3.1 to +4.6. No age corrections were applied owing to the young age of the rocks. On Figure 7a, there is overlap between samples from the Valley, Ridge, and Cone series, and the samples display only a little isotopic enrichment with major element evolution (Fig. 7b). Overall, the samples lie on the mantle array between bulk silicate earth and depleted MORB mantle, and there is

no clear evidence of any trends which might be related to mixing of different mantle end members (e.g. EMI or EMII) or old, isotopically enriched crustal contaminants. The Cone and Ridge Series samples containing quartz xenocrysts are not isotopically different from the other samples.

Regionally, the samples are significantly more depleted than most Pliocene-Quaternary centres in north-west Iran and Mount Damavand (Alborz), and Tendürek volcano in Eastern Anatolia (Fig. 7a). The Iranian volcanic rocks were erupted through thicker lithosphere than beneath Armenia (e.g. Liotard et al., 2008; Kheirkhah et al., 2009; Mirnejad et al., 2010; Davidson et al., unpublished data; Allen et al., 2013). Samples are also more depleted than asthenospheric melts from eastern Iran which have trends towards the EM-II mantle end member (Saadat et al., 2011; Saadat and Stern, 2012). Instead, results are closest to the few analyses conducted on the large stratovolcano, Mount Ararat, close to the Armenian border (Pearce et al., 1990; Kheirkhah et al., 2009), and nearly identical in terms of $^{143}Nd/^{144}Nd$ to six analyses of the ~3.25-2.05 Ma valley series lavas from southern Georgia, and from eight Late Miocene sub-alkaline basalts in central Georgia (Lebedev et al., 2006; 2007). Radiogenic isotope results are not yet widely published from other Armenian Pliocene-Quaternary centres, but Savov et al. (2007) and Lin et al. (2011) reported values from $^{87}Sr/^{86}Sr$ = 0.7041 to 0.7051 and $^{143}Nd/^{144}Nd$ = 0.5128 to 0.5129 from various locations.

5. Discussion

5.1. Volcano-tectonic interaction

Before considering the petrogenesis of the magma series, we first address the location of volcanic activity with respect to major crustal structures. The internal part of the orogenic plateau is not undergoing contractile deformation (Jackson et al., 1995; Vernant et al., 2004), but internal reorganisation of the plateau during the on-going convergence between Arabia and Eurasia means that Eastern Anatolia, the Lesser Caucasus, and northwest Iran are criss-crossed by numerous active strike-slip fault systems (Rebaï et al., 1993; Koçyiğit et al., 2001). These systems, which often tally with pre-existing crustal discontinuities, have been widely implicated in providing a locus for Quaternary magmatic activity through the production of highly localised pull-apart zones (Dewey et al., 1986; Karakhanian et al., 1997, 2002; Avagyan et al., 2010; Shabanian et al., 2012).

In Armenia, the active Pambak-Sevan-Syunik right-lateral strike-slip fault system is one such structure exploiting the existing discontinuity of the Sevan-Akera suture zone (Fig. 2). All of the magmatism described in this study originated just to the north of the fault zone, and so we propose that this location sat over a region of localised upper crustal extension at the time of magmatism. No active extension is recorded from the Shirak region from earthquake focal mechanisms or geomorphic features. Blanket coverage of most pre-existing fault structures by the Valley Series, and the absence of linear arrays of cinder cones (e.g. Dewey et al., 1986), may have helped obscure this association between faulting and magmatism. The south-eastern termination of the Pambak-Sevan-Syunik fault in the Syunik region is characterised by widespread volcanism in the area south of the fault, with little volcanism to the north (Kharakhanian et al., 2004). The Syunik centres therefore appear to have developed along the complementary trailing imbricate fan (Woodcock and Fischer, 1986) to the Shirak volcanic rocks. The north-south trending volcanism along the Javakheti Ridge is consistent with this idea.

Not all young Armenian centres fit a simple fault-control hypothesis: Aragats volcano, the largest centre in the country, is situated in a region apparently not crossed by presently-active faults (Kharakhanian et al., 2004). It is possible that older faults may be obscured by lava flows, or that some other control on the location of Aragats may apply, such as a local thin-spot in the lithosphere which focussed melting beneath the plateau.

5.2. Fractionation and contamination processes

5.2.1. Fractional crystallisation – minerals involved

No sample from the mafic Valley Series lavas is close to a primary melt (MgO is typically < 7 wt.%), so it is assumed that they have already evolved at depth involving a typical fractionation assemblage of olivine and spinel. In the major element data, clear falling trends for the Valley Series against typical indices of fractionation, such as SiO_2, TiO_2, MgO, and CaO (Fig. 4), corroborate with the observed mineral assemblages in confirming that clino- and orthopyroxene and Fe-Ti oxides were important in Valley Series evolution. Al_2O_3 concentrations cover a narrow range with no trends, indicating that feldspar fractionation was not an important feature of the Valley Series; likewise with P_2O_5 concentrations and apatite. Trace element abundances, such as Ba, Th, and La, display rising trends against SiO_2 in the Valley Series, which confirms their incompatible behaviour (Fig. 5). In the more evolved Ridge and Cone Series, clear falling trends emerge against SiO_2 for Al_2O_3, P_2O_5, Sr, Nb, Zr and La, pointing to addition of plagioclase, along with small proportions of zircon and apatite, to the fractionating assemblage.

The overall pattern of Shirak magmatism can be compared with Eastern Anatolia. Volcanic centres that display either high- or low-Y trends relative to Rb, are associated with fractionation of anhydrous (plagioclase, olivine, pyroxenes, and magnetite), or hydrous assemblages (including amphibole, which is compatible with Y) respectively (Pearce et al., 1990) (Fig. 8). The mafic Valley Series rocks in Shirak follow the same moderate to low-Y trend as the Kars plateau/Mt. Ararat systems, which may indicate amphibole fractionation has taken place at depth, given that amphibole is not seen in any of the Valley Series thin sections. Another indication of amphibole fractionation is the compatible middle to heavy REE (Sm-Lu) showing falling trends as the three series evolve (Fig. 6). The ridge series lavas have a steeply falling trend for Y against Rb, which may reflect increased partition coefficients for both clinopyroxene and amphibole for Y as these minerals fractionate from more evolved rocks (Pearce et al., 1990).

5.2.2. Magma mixing

The petrographic evidence for magma mixing (zoned plagioclases, sieve textures, reaction rims and quartz blebs) also needs to be reconciled with geochemical data. Major element plots, especially TiO_2, CaO and MgO vs. SiO_2 (Fig. 4) have straight line trends which are widely associated with mixing of two compositionally distinct magmas (Langmuir et al., 1978), rather than the curved trends associated with fractional crystallisation. In the field, the key observation is that the most evolved rocks found in the area, the obsidians at Agvorik, underlie the mafic Valley Series, so felsic magmas had already been erupted by the time of mafic magma injection.

5.2.3. Crustal contamination

Many models (e.g. Keskin et al., 1998) consider assimilation-fractional crystallisation (AFC) processes to be important in magma genesis in the plateau. Keskin et al. (1998) argue that recent mafic to felsic samples from Eastern Anatolia have undergone significant amounts of AFC coinciding with enriched $^{87}Sr/^{86}Sr$ ratios up to 0.7065 (Pearce et al., 1990). In Shirak, samples have only a slight variation in isotope ratios relative to SiO_2 (Fig. 7b), and samples containing quartz xenocrysts do not have different isotopic ratios to the other lavas - a feature that should strongly support the hypothesis that fractionation and magma mixing were the dominant processes. Also, preliminary results from elsewhere in Armenia, including the Aragats volcanic system, show little clear isotopic evidence for contamination (Savov et al., 2007; Lin et al., 2011) in spite of Aragats erupting through the SAB basement which has enriched $^{87}Sr/^{86}Sr$ ratios of up to 0.7303 - any contamination should be easily indentified (Bagdasaryan and Gukasyan, 1985). However, along-strike from Shirak at Artvin in eastern Turkey, Eocene rocks have measured $^{143}Nd/^{144}Nd$ of 0.512663 - 0.512854 and $^{87}Sr/^{86}Sr$ of 0.705148 - 0.704233 (Aydinçakir and Şen, in press). These values are very similar to the Shirak lavas (Fig. 7), so partial melting or assimilation of similar Eocene crust may be very difficult to decipher geochemically.

On a Th/Yb vs. Ta/Yb plot (Pearce, 1983) (Fig. 9), the three series form a consistent linear trend sub-parallel to the mantle array, with the felsic rocks having compositions more enriched than those of typical continental crust (Rudnick and Gao, 2003). On this diagram, the fractional crystallisation trend for a typical amphibole-bearing assemblage is shown. The samples plot to the left of the fractionation trend which suggests that AFC processes may be operating - although choice of mineral assemblages and partition coefficients can easily affect the FC trend. AFC modelling (Powell, 1984) using the average composition of the Artvin

497 rocks (Aydinçakir and Şen, in press) quite reasonably reproduces the trend of the Shirak
498 lavas, but the ratio of assimilation to fractionation is high at 0.8. Modelling thus shows that
499 large volumes of isotopically similar material can be incorporated into the Shirak lavas
500 without a significant effect on trace element evolution. Studies of disequilibrium textures and
501 mineral chemistry might better elucidate the processes involved in magma evolution.
502
503 5.3. Mantle source and partial melting
504
505 *5.3.1. Mantle source of the Valley Series*
506
507 The presence of LILE and HFSE anomalies on normalised plots of mafic rocks (Fig. 6b) are
508 normally taken to indicate a subduction-modified mantle source owing to the retention of
509 HFSE in the slab, and the comparative mobility of the LILE/REE during slab heating and
510 dewatering into the overlying mantle wedge (e.g. Pearce and Peate, 1995). We have already
511 introduced the Th/Yb vs. Ta/Yb diagram (Fig. 9). The alkali basalts from Shirak plot above
512 the mantle array which is commonly taken to indicate the presence of a subduction-modified
513 source. However, they also have very much higher Ta/Yb ratios than many subduction-
514 related rocks. The Shirak lavas are therefore derived from an incompatible element-enriched
515 mantle source, or are derived from a limited degree of melt extraction. As these lavas erupted
516 >20 Myr after the end of Neo-Tethyan subduction, and there is no evidence for a slab at
517 shallow depths beneath Eastern Anatolia and Armenia at the present day (Zor et al., 2008), it
518 is improbable that a normal supra-subduction zone hydrated asthenospheric mantle wedge
519 was involved in the origin of the Shirak lavas. Therefore, the subduction-like characteristics
520 are likely to be derived from a fertile source within the mantle that had been inherited its
521 slab-related geochemical component from earlier Neo-Tethyan subduction. Crustal

522 contamination is unlikely be responsible for the subduction-like characteristics of the Shirak
523 lavas, as LILE and HFSE anomalies are significant in even the most mafic samples.
524
525 Some of the trace element characteristics of the valley series may help constrain the
526 mineralogy of the mantle source. Overall, the flat normalised HREE patterns (Fig. 6a)
527 indicate a spinel-facies mantle source at <70 km, unless the degree of partial melting was
528 very high (>25%) in order to completely consume any garnet present at depths of >70 km.
529 This is unlikely given the overall LREE-enriched and Nb-Ta/HREE-enriched trace element
530 patterns (Fig. 6b) which point towards modest degrees of partial melting of an enriched
531 source. Low Sc concentrations (<25 ppm) in all Valley Series samples may indicate residual
532 clinopyroxene, another indicator of a low degree of partial melting, but it is also possible that
533 extensive pyroxene fractionation prior to eruption has resulted in these low values. Intra-
534 LILE variations, including low Ba/Rb (<25) and Rb/Sr ratios (<0.05), do not point towards
535 amphiboles or phlogopite playing an important role during melting (e.g. Furman and Graham,
536 1999). Melting therefore took place beneath the Armenian crust at depths of ~45-70 km.
537
538 One unusual feature of the Shirak lavas is high ocean island basalt (OIB)-like Zr
539 concentrations (~200 ppm) and Zr/Hf ratios (41-52) relative to MOR and arc basalts, the
540 latter having chondritic Zr/Hf ratios of 35-39 (Weaver et al., 1987; David et al., 2000;
541 Pfänder et al., 2007). Nb/Ta ratios range from 16-22 relative to the chondritic ratio of 19.9
542 (Pfänder et al., 2007). Mafic samples from other nearby centres in the plateau, including
543 Tendürek and Ararat, show similar features (Fig. 10). Lower ratios in the Ridge Series
544 compared to the Valley Series might be explained by contamination with crustal material
545 such as the Eocene basement (Fig. 10). However, the high Zr/Hf ratios of 47-52 in the less
546 evolved Valley Series are a primary feature of the magmas.

There is little correlation between Zr and Zr/Hf ratios (not shown), indicating that zircon accumulation cannot be directly responsible for the high Zr-Zr/Hf character of the Shirak lavas. HFSE fractionation in OIBs may be due to: (1) residual or fractionating clinopyroxene (David et al., 2000); (2) fractionation of Ti-bearing phases such as rutile, ilmenite, and amphibole (Foley et al., 2000; Tiepolo et al., 2001); (3) melting of recycled eclogite or garnet pyroxenite (Pfänder et al., 2007); or (4) the occurrence of carbonate metasomatism (Dupuy et al., 1992). For option (1), fractionation of clinopyroxene only has a modest effect upon Zr/Hf ratios (Pfänder et al., 2000). Our modelling of pure clinopyroxene fractional crystallisation from a starting composition with Zr/Hf and Nb/Ta of primitive mantle shows that unrealistic amounts of fractionation are required to generate the Shirak samples (Fig. 10). In option (2), fractionation of titanate phases such as rutile and ilmenite can generate very high Zr/Hf and Nb/Ta ratios, with $D_{Zr/Hf}$ and $D_{Nb/Ta}$ both <1 (Pfänder et al., 2000); however, titanate fractionation would also strongly reduce overall Nb concentrations, a feature not seen in the Valley Series. Partial melting of garnet-bearing lithologies (option 3) is invoked in many OIB examples (see Pfänder et al., 2007) but can be ruled out here on the basis of flat normalised HREE patterns in the Shirak lavas – these are not OIB-like magmas (Fig. 6b). Where carbonates are invoked in the mantle source (e.g. Dupuy et al., 1992; Hoernle et al., 2002) (option 4), resultant alkaline melts or mantle xenoliths have very high Sr and Ba of >>1000 ppm, and in spite of high Zr/Hf ratios many carbonatites have very low concentrations of these elements (Ionov et al., 1993). This is not the signature of the Shirak samples hence carbonate metasomatism is unlikely in this case. Several studies have shown that amphibole and phlogopite fractionate the HFSE (Moine et al., 2001; Tiepolo et al., 2001; Chakhmouradian, 2006), with Chakhmouradian (2006) demonstrating that low-Ti amphiboles have high Zr/Hf ratios of ~60-200. Hence these minerals can impart high Zr/Hf on a melt; but

572 it is still unclear what the high overall Zr concentrations in the Shirak lavas are caused by -
573 this feature is normally attributed to ancient recycled oceanic crust in OIBs (Weaver, 1991).
574
575 *5.3.2. Modelling of partial melting*
576
577 Any model of partial melting conditions for Shirak has to be based on the HREE and HFSE,
578 making the assumption that neither set of elements were transported into the lithospheric
579 mantle source in a slab-derived fluid (Pearce and Peate, 1995). Therefore, we have
580 constructed non-modal batch melting curves using Dy, Yb and Nb (ignoring Zr owing to its
581 anomalous behaviour), in order to constrain the degree of partial melting needed to form the
582 Valley Series. We have taken the approach of Pearce et al. (1990) in assuming that hydrous
583 phases such as amphibole and phlogopite (if present) are completely consumed during
584 melting and do not contribute to the melt model. Given the high Ta/Yb ratios of even the least
585 evolved Valley Series samples (Fig. 9), it is reasonable to compare the melting of depleted
586 MORB mantle (DMM) (Workman and Hart, 2005) with a more incompatible-element
587 enriched source, in this case primitive mantle with 1% bulk continental crust extracted, as
588 used by Fitton and Godard (2004) for the Ontong Java oceanic plateau.
589
590 Although we can easily model HREE and HFSE ratios (see below), fractional
591 crystallisation of olivine, spinel, plagioclase and pyroxene versus fractionation of amphibole
592 from primary magma have competing effects on absolute REE and HFSE concentrations.
593 Often, elemental values for basalts in modelling are back-calculated to 9 wt.% MgO to negate
594 the effects of plagioclase and pyroxene crystallisation (Pearce & Parkinson, 1993). However,
595 valley series Dy and Yb concentrations are near-constant in spite of varying MgO and SiO_2
596 (Fig. 6a), probably due to the competing effects of amphibole and clinopyroxene

fractionation, so no realistic back-calculation can be applied. Therefore, we simply attempt to model the elemental ratios of the last-evolved Valley Series lava (7 wt.% MgO) and assume that this best reflects the conditions of partial melting.

Modelling results (Fig. 11) indicate that melting of a garnet peridotite cannot reproduce the compositions of the Valley Series lavas, a finding consistent with the flat normalised HREE patterns (Fig. 6a). Spinel peridotite partial melting curves do intersect the valley series at low degrees of melting, with the DMM melting curve on Figure 11 giving 0.1-0.5% melting. In contrast the more fertile source gives 2-5% melting, which is perhaps more realistic than the tiny proportion of melting required from a DMM source and the difficulties of extracting such a small volume of melt (e.g. Hirth and Kohlstedt, 1995). This spinel peridotite melting outcome is also consistent with geophysical surveys indicating a seismically slow mantle at depths of ~50 km beneath Armenia (e.g. Koulakov et al., 2012).

5.4. Reconciliation with geophysical and geodynamic models

5.4.1. Extent of lithospheric delamination

Debate exists over the extent of lithospheric delamination beneath Eastern Anatolia following the cessation of subduction beneath the Bitlis-Zagros suture (e.g. Keskin, 2003). Seismic surveys indicate a crustal thickness of ~40-45 km, but with significant negative P- and S-wave seismic velocity anomalies beneath, extending from ~50 to ~250 km depth, between eastern Turkey, Armenia, the Black Sea and northwest Iran, concurrent with many Pliocene-Quaternary volcanic centres (e.g. Piromallo and Morelli, 2003; Maggi & Priestley, 2005; Zor et al., 2008; Koulakov et al., 2012). The anomaly has been used by these authors to argue for

622 the presence of hot, perhaps partially molten, asthenosphere, but several authors extend these
623 conclusions to the possibility that there is also no mantle lithosphere 'lid' beneath the
624 Anatolian crust (e.g. Keskin, 2003; Zor et al., 2008) and the Caucasus (Koulakov et al.,
625 2012). In this case, mafic magmatism in Shirak would have to have an asthenospheric source.
626
627 There are significant implications for magmatism in this scenario. The impact of hot
628 upwelling asthenosphere on the thickened Lesser Caucasus arc crust should result in
629 extensive lower crustal melting, as observed in the Puna Plateau of the Andes, and the Great
630 Basin Altiplano in the western U.S. (Allmendinger et al., 1997; Babeyko et al., 2002; Best et
631 al., 2009). Going back to our geochemical results, this model of whole-scale lithospheric
632 delamination proposed for the Puna Plateau is incompatible with the observed silica-
633 undersaturated magmatism in Shirak, which bears little evidence for large-scale crustal
634 interaction. We conclude that there is sufficient lithospheric mantle beneath the Armenian
635 crust to act as a thermal barrier between the asthenosphere and crust (Fig. 12), protecting the
636 crust from melting and infiltration by hot asthenospheric melts in the manner described by
637 Babeyko et al. (2002). An asthenospheric source for the Shirak magmas cannot have been
638 influenced by a subducting slab, because subduction processes ended prior to the Miocene.
639 Hence the Shirak magmas would not have subduction-like trace element characteristics, and
640 instead should closely resemble OIB. There are asthenosphere-derived OIB-like lavas
641 without subduction-related geochemical signatures in Eastern Iran (Saadat et al., 2010;
642 Saadat and Stern, 2012) and in the Arabian foreland (Lustrino et al., 2010). The Iranian alkali
643 olivine basalts show trends towards an EMII-like isotope signature (particularly with respect
644 to Pb isotope ratios) (Zindler and Hart, 1986). They also and contain pyroxenite xenoliths
645 from the lithospheric mantle, plagioclase megacrysts of uncertain origin, and some lower
646 crustal gabbroic xenoliths (Saadat and Stern, 2012). These lavas are distinct in terms of

xenolith content, trace element signatures and isotope geochemistry from those erupted in Shirak.

5.4.2. Geodynamic model

Our geodynamic model is presented schematically in Figure 12. We propose that, upon the termination of Neo-Tethyan subduction along the Bitlis-Zagros suture during the Oligocene, Armenia lay in a continental back-arc position relative to the former subducting slab and mantle wedge. Modelling studies have suggested that an old slab may be able to persist or 'stall' in the upper mantle without breaking off for up to 20 Myr after terminal collision (van Hunen and Allen, 2011). Delayed break-off of the Neo-Tethyan slab from Arabia beneath Eurasia may thus be responsible for the upsurge in magmatism since 10 Ma, and particularly in the Pliocene-Quaternary, across the orogenic plateau (e.g. Keskin, 2003), concurrent with the influx of hot asthenosphere into the region the slab once occupied. In Eastern Anatolia, the region immediately above the detached slab might lack mantle lithosphere, and asthenospheric and crustal melting would combine to produce arc-like magmas (Fig. 12) (Keskin, 2003). However, as we have already discussed, it is improbable that whole-scale lithospheric mantle delamination occurred beneath Armenia because we do not see attendant whole-scale lower crustal melting. The former asthenospheric mantle wedge of the Neo-Tethyan arc system would be refrigerated by the presence of a stalled slab, and rapidly converted into lithospheric mantle over the 15-25 Myr following terminal collision (c.f. Holt et al., 2010). This depleted lithospheric mantle could be stable and buoyant enough to be at least partially preserved following the eventual detachment of the underlying oceanic slab, whilst the aforementioned influx of convecting asthenosphere would trigger partial melting in

671 the overlying lithospheric mantle, as well as providing a thermal support for the orogenic
672 plateau (Fig. 12).
673
674 Another potentially important consideration is that, although much of the LILE and
675 LREE budget of the southern Neo-Tethyan slab may have been delivered to the lithosphere
676 before continental collision, a stalled slab and associated sediments would continue
677 dewatering before break-off. This would contribute to the subduction-like signature on the
678 mantle frozen-in beneath Armenia. Other Pliocene-Quaternary centres in the collision zone,
679 such as the foreland volcanic system at Karacadağ, may result from asthenospheric melting
680 beneath thin spots in the lithosphere (Lustrino et al., 2010; Ekici et al., 2012). Mantle-derived
681 volcanism is also apparent even in the 50+ km thick crust of the Elbrus region of the Greater
682 Caucasus (Lebedev et al., 2006b; Koulakov et al., 2012), and it is here that magmatism may
683 be related to melting during collisional thickening of lithospheric mantle and the breakdown
684 of hydrous mineral phases such as micas and amphiboles (e.g. Pearce et al., 1990; Allen et
685 al., 2013) or to asthenospheric upwelling during lithospheric dripping (see Sosson et al.,
686 2010) (Fig. 12).
687
688 **6. Conclusions**
689
690 • Mafic and more evolved Pliocene-Quaternary lavas in Shirak, NW Armenia, were
691 emplaced through a former continental margin arc sequence as a result of localised
692 extensional tectonics within the present-day Arabia-Eurasia collision zone.
693 • Magmas evolved from mafic through to dacitic compositions by fractional
694 crystallisation dominated by pyroxene, amphibole and plagioclase; and although
695 evolved samples contain quartz xenocrysts, none preserves clear isotopic evidence for

large-scale crustal assimilation - magma mixing appears to be the dominant petrogenetic process. We conclude that if assimilation did occur, it was of local arc-related crust of a similar isotopic composition to the Shirak melts.

- The least-evolved magmas preserve trace element evidence for derivation by moderate degrees of melting (~3-4%) from a shallow, spinel-facies lithospheric mantle source with an inherited subduction component probably related to earlier Tethyan subduction processes. They contain high Zr concentrations and high Zr/Hf ratios which are an intrinsic feature of the source or partial melting process.
- The presence of lithospheric mantle beneath Armenia is a requirement for geodynamic models of the region in order to prevent the occurrence of whole-scale lower crustal melting.

Acknowledgements

This work is funded by the Natural Environment Research Council project, 'Orogenic Plateau Magmatism' [NE/H021620/1]. Nick Marsh conducted the XRF analyses; Geoff Nowell and Chris Ottley assisted with, and partly conducted, radiogenic isotope and trace element analyses, respectively. We are grateful to *Lithos* guest editor Ioan Seghedi, along with Evgenii Sharkov and an anonymous reviewer for their constructive comments. Ivan Savov and Douwe van Hinsbergen are thanked for discussion on some of the ideas presented within.

References

719 Adamia, S.A., Chkhotua, T., Kekelia, M., Lordkipanidze, M., Shavishvili, I., 1981. Tectonics
720 of the Caucasus and adjoining regions: implications for the evolution of the Tethys ocean.
721 Journal of Structural Geology 3, 437-447.
722
723 Adamia, S.A., Zakariadze, G., Chkhotua, T., Sadradze, N., Tsereteli, N., Chabukiani, A.,
724 Gventsadze, S., 2011. Geology of the Caucasus: A Review. Turkish Journal of Earth Sciences
725 20, 489-544.
726
727 Agard, P., Omrani, J., Jolivet, L., Mouthereau, F., 2005. Convergence history across Zagros
728 (Iran): constraints from collisional and earlier deformation. International Journal of Earth
729 Sciences 94, 401-419.
730
731 Allen, M.B., Armstrong, H.A., 2008. Arabia-Eurasia collision and the forcing of mid
732 Cenozoic global cooling. Palaeontology Palaeoclimatology Palaeoecology 265, 52-58.
733
734 Allen, M.B., Kheirkhah, M., Emami, M.H., Jones, S.J., 2011. Right-lateral shear across Iran
735 and kinematic change in the Arabia-Eurasia collision zone. Geophysical Journal International
736 184, 555-574.
737
738 Allen, M.B., Kheirkhah, M., Neill, I., Emami, M.H., McLeod, C.L., 2013. Generation of arc
739 and within-plate chemical signatures in collision zone magmatism: Quaternary lavas from
740 Kurdistan Province, Iran. Journal of Petrology 54, 887-911.
741
742 Allmendinger, R.W., Isacks, B.L., Jordan, T.E., Kay, S.M., 1997. The evolution of the
743 Altiplano-Puna plateau of the Central Andes. Annual Reviews of Earth Science 25, 139-174.

744

745 Angus, D.A., Wilson, D.C., Sandvol, E., Ni, J.F., 2006. Lithospheric structure of the Arabian
746 and Eurasian collison zone in eastern Turkey from S-wave receiver functions. Geophysical
747 Journal International 166, 1335-1346.

748

749 Avagyan, A., Sosson, M., Karakhanian, A., Philip, H., Rebai, S., Rolland, Y., Melkonyan, R.,
750 Davtyan, V., 2010. Recent tectonic stress evolution in the Lesser Caucasus and adjacent
751 regions. In: Sosson, M., Kaymakci, N., Stephenson, R.A., Bergerat, F., Starostenko, V.
752 (Eds.). Sedimentary Basin Tectonics from the Black Sea and Caucasus to the Arabian
753 Platform. Geological Society of London Special Publications, v. 340, p.p. 393-408.

754

755 Aydinçakir, E., Şen, C, in press. Petrogenesis of the post-collisional volcanic rocks from the
756 Borçka (Artvin) area: Implications for the evolution of the Eocene magmatism in the Eastern
757 Pontides (NE Turkey). Lithos, doi:10.1016/j.lithos.2013.04.007.

758

759 Azizi, H., Moinevaziri, H., 2009. Review of the tectonic setting of Cretaceous to Quaternary
760 volcanism in northwestern Iran. Journal of Geodynamics 47, 167-179.

761

762 Babeyko, A.Yu., Sobolev, S.V., Trumbull, R.B., Oncken, O., Lavier, L.L., 2002. Numerical
763 models of crustal-scale convection and partial melting beneath the Altiplano-Puna plateau.
764 Earth and Planetary Science Letters 199, 373-388.

765

766 Baghdasaryan, G.P., Ghukasyan, R.Kh., 1985. Geochronology of magmatic, metamorphic
767 and ore formations of Armenian SSR. Publication of the Academy of Sciences of Armenian
768 Soviet Socialist Republic (in Russian).

Ballatto, P., Uba, C.E., Landgraf, A., Strecker, M.R., Sudo, M., Stockli, D.F., Friedrich, A., Tabatabaei, S.H., 2011. Arabia-Eurasia continental collision: Insights from late Tertiary foreland-basin evolution in the Alborz Mountains, northern Iran. Geological Society of America Bulletin 123, 106-131.

Berberian, F., Berberian M., 1981. Tectono-plutonic episodes in Iran. In: Gupta, H.K., Delany, F.M. (Eds.). Zagros, Hindu Kush, Himalaya Geodynamic Evolution. American Geophysical Union Geodynamic Series v. 3, p.p. 5-32.

Best, M.G., Barr, D.L., Christiansen, E.H., Gromme, S., Deino, A.L., Tingey, D.G., 2009. The Great Basin Altiplano during the middle Cenozoic ignimbrite flareup: insights from volcanic rocks. International Geology Review 51, 589-633.

Bottrill, A.D., van Hunen, J., Allen, M.B., 2012. Insight into collision zone dynamics from topography: numerical modelling results and observations. Solid Earth 3, 387-399.

Cann, J.R., 1970. Rb, Sr, Zr and Nb in some ocean floor basaltic rocks. Earth and Planetary Science Letters 10, 7-11.

Chakhmouradian, A., 2006. High-field-strength elements in carbonatitic rocks: Geochemistry, crystal chemistry and significance for constraining the source of carbonatites. Chemical Geology 235, 138-160.

793 Chernyshev, I.V., Lebedev, V.A., Arakelyants, M.M., Jrbashyan, R.T., Ghukasyan, Y.G.,
794 2002. Geochronology of the Aragats volcanic centre, Armenia: Evidence from K-Ar dating.
795 Doklady Earth Sciences 384, 393-398 (in Russian).
796
797 Chernyshev, I.V., Lebedev, V.A., Arakelyants, M.M., 2006. K-Ar dating of Quaternary
798 volcanics: Methodology and interpretation of results. Petrologiya (Petrology) 14, 69-89.
799
800 Chiu, H.-Y., Chung, S.-L., Zarrinkoub, M.H., Mohammadi, S.S., Khatib, M.M., Iizuka, Y.,
801 2013. Zircon U-Pb constraints from Iran on the magmatic evolution related to Neotethyan
802 subduction and Zagros orogeny. Lithos 162, 70-87.
803
804 David, K., Schiano, P., Allégre, C.J., 2000. Assessment of the Zr/Hf fractionation in oceanic
805 basalts and continental materials during petrogenetic processes. Earth and Planetary Science
806 Letters 178, 285-301.
807
808 Davidson, J.P., Hassanzadeh, J., Berzins, R., Stockli, D.F., Bashukooh, B., Turrin, B.,
809 Pandamouz, A., 2004. The geology of Damavand volcano, Alborz Mountains, northern Iran.
810 Geological Society of America Bulletin 116, 16-29.
811
812 Dewey, J.F., Hempton, M.R., Kidd, W.S.F., Saroglu, F., Şengör, A.M.C., 1986. Shortening
813 of continental lithosphere: the neotectonics of Eastern Anatolia – a young collision zone. In:
814 Coward, M.P., Ries, A.C. (Eds.). Collision Tectonics. Geological Society of London Special
815 Publication, v. 19, p.p. 3-36.
816

817 Dilek, Y., Imamverdiyev, N., Altunkaynak, Ş., 2010. Geochemistry and tectonics of
818 Cenozoic volcanism in the Lesser Caucasus (Azerbaijan) and the peri-Arabian region:
819 collision-induced mantle dynamics and its magmatic signature. International Geology Review
820 52, 536-578.
821
822 Dowall, D.P., Nowell, G.M., Pearson, D.G., 2007. Chemical pre-concentration procedures for
823 high-precision analysis of Hf-Nd-Sr isotopes in geological materials by plasma ionisation
824 multi-collector mass spectrometry (PIMMS) techniques. In: Holland, J.G., Tanner, S.D.
825 (Eds.) Plasma Source Mass Spectrometry: Applications and Emerging Technologies.
826 Cambridge: The Royal Society of Chemistry, p.p. 321-337.
827
828 Drew, S.T., Ducea, M.N., Schoenbohm, L.M., 2009. Mafic volcanism on the Puna Plateau,
829 NW Argentina: Implications for lithospheric composition and evolution with an emphasis on
830 lithospheric foundering. Lithosphere 1, 305-318.
831
832 Dupuy, C., Liotard, J.M., Dostal, J., 1992. Zr/Hf fractionation in intraplate basaltic rocks:
833 Carbonate metasomatism in the mantle source. Geochimica et Cosmochimica Acta 56, 2417-
834 2423.
835
836 Ekici, T, Macpherson, C.G., Otlu, N, 2012. Polybaric melting of a single mantle source
837 during the Neogene Siverek phase of the Karacadağ Volcanic Complex, SE Turkey. Lithos
838 146, 152-163.
839
840 Fitton, J.G., Godard, M., 2004. Origin and evolution of magmas on the Ontong Java Plateau.
841 In: Fitton, J.G., Mahoney, J.J., Wallace, P.J., Saunders, A.D. (Eds.). Origin and Evolution of

842 the Ontong Java Plateau. Geological Society of London Special Publication, v. 229, p.p. 151-
843 178.
844
845 Foley, S.F., Barth, M.G., Jenner, G.A., 2000. Rutile/melt partition coefficients for trace
846 elements and an assessment of the influence of rutile on the trace element characteristics of
847 subduction zone magmas. Geochimica et Cosmochimica Acta 64, 933-939.
848
849 Furman, T., Graham, D., 1999. Erosion of lithospheric mantle beneath the East African Rift
850 System: geochemical evidence from the Kivu volcanic province. Lithos 48, 237-262.
851
852 Jackson, J., Haines, J., Holt, W., 1995. The accommodation of Arabia-Euasia Plate
853 convergence in Iran. Journal of Geophysical Research 100, B8, P15205.
854
855 Johnson, C.M., 1991. Large-scale crust formation and lithosphere modification beneath
856 middle to late Cenozoic calderas and volcanic fields, western North America. Journal of
857 Geophysical Research 96, 13485-13507.
858
859 Jrbashian, R.T., Kazarian, G.A., Karapetian, S.G., Meliksetian, Kh.B., Mnatsakanian, A.,
860 Shirinian, K.G., 1996. Meso-Cenozoic basaltic volcanism in the northeastern part of
861 Armenian Highland. Letters of the Armenian Academy of Sciences, Earth Sciences 49, 19-32
862 (in Russian).
863
864 Hirth, G., Kohlstedt, D.L., 1995. Experimental constraints on the dynamics of the partially
865 molten upper mantle: deformation in diffusion creep regime. Journal of Geophysical
866 Research 100, 1981-2001.

Hoernle, K., Tilton, G., Le Bas, M.J., Duggan, S., Garbe-Schönberg, D., 2002. Geochemistry of oceanic carbonatites compared with continental carbonatites: mantle recycling of oceanic crustal carbonate. Contributions to Mineralogy and Petrology 142, 520-542.

Holt, P.J., Allen, M.B., van Hunen, J., Bjørnseth, H.M., 2010. Lithospheric cooling and thickening as a basin forming mechanism. Tectonophysics 495, 184-194.

Ionov, D.A., Dupuy, C., O'Reilly, S.Y., Kopylova, M.G., Genshaft, Y.S., 1993. Carbonated peridotite xenoliths from Spitsbergen: implications for trace element signature of mantle carbonate metasomatism. Earth and Planetary Science Letters 119, 283-297.

Karapetian, S.G., Jrbashian, R.T., Mnatsakanian, A.Kh., 2001. Late collision rhyolitic volcanism in the north-eastern part of the Armenian Highland. Journal of Volcanology and Geothermal Research 112, 189-220.

Kharazyan, E.Kh., 1983. Geology of recent volcanism of north-west part of Armenian SSR (basins of rivers Dzoraget and Akhuryan). PhD thesis, unpublished, ArmGeologia, Yerevan, 55 pp.

Kharazyan, E.Kh., 2005. Geological Map of Armenia. Ministry of Nature Protection of Republic of Armenia.

890 Keskin, M., Pearce, J.A., Mitchell, J.G., 1998. Volcano-stratigraphy and geochemistry of
891 collision-related volcanism on the Erzurum-Kars Plateau, northeastern Turkey. Journal of
892 Volcanology and Geothermal Research 85, 355-405.
893
894 Keskin, M., 2003. Magma generation by slab steepening and breakoff beneath and
895 subduction-accretion complex: An alternative model for collision-related volcanism in
896 Eastern Anatolia, Turkey. Geophysical Research Letters 30, 1-4.
897
898 Keskin, M., 2007. Eastern Anatolia: a hot spot in a collision zone without a mantle plume. In:
899 Foulger, G.R., Jurdy, D.M. (Eds.) Plates, Plumes, and Planetary Processes. Geological
900 Society of America Special Paper, vol. 409, p.p. 1-25.
901
902 Keskin, M., Can Genç, Ş, Tüysüz, O., 2008. Petrology and geochemistry of post-collisional
903 Middle Eocene volcanic units in North-Central Turkey: Evidence for magma generation by
904 slab breakoff following the closure of the Northern Neotethys Ocean. Lithos 104, 267-305.
905
906 Karakhanian, A.S., Trifonov, V.G., Azizbekian, O.G., Hondkarian, D.G., 1997. Relationship
907 of late Quaternary tectonics and volcanism in the Khanarassar active fault zone, the
908 Armenian Upland. Terra Nova 9, 131-134.
909
910 Karakhanian, A., Djrbashian, R., Trifonov, V., Philip, H., Arakelian, S., Avagian, A., 2002.
911 Holocene-historical volcanism and active faults as natural risk factors for Armenia and
912 adjacent countries. Journal of Volcanology and Geothermal Research 113, 319-344.
913

914 Karakhanian, A., Abgaryan, Y., 2004. Evidence of historical seismicity and volcanism in the
915 Armenian Highland (from Armenian and other sources). Annals of Geophysics 47, 793-810.
916
917 Kay, R.W., Kay, S.M., 1993. Delamination and delamination magmatism. Tectonophysics
918 219, 177-189.
919
920 Kheirkhah, M., Allen, M.B., Emami, M.H., 2009. Quaternary syn-collision magmatism from
921 the Iran/Turkey borderlands. Journal of Volcanology and Geothermal Research 182, 1-12.
922
923 Koçyiğit, A., Yilmaz, A., Adamia, S., Kuloshvili, S., 2001. Neotectonics of East Anatolian
924 Plateau (Turkey) and Lesser Caucasus: implications for transition from thrusting to strike-slip
925 faulting. Geodinamica Acta 14, 177-195.
926
927 Langmuir, C.H., Vocke, R.D., Hanson, G.N., Hart, S.R., 1978. A general mixing equation
928 with applications to Icelandic basalts. Earth and Planetary Science Letters 37, 380-392.
929
930 Koulakov, I., Zabelina, I., Amanatashvili, I., Meskhia, V., 2012. Nature of orogenesis and
931 volcanism in the Caucasus region based on results of regional tomography. Solid Earth 3,
932 327-337.
933
934 Lebedev, V.A., Chernyshev, I.V., Chugaev, A.V., Dudauri, O.Z., Vashakidze, G.T., 2006a.
935 K-Ar age and Sr-Nd characteristics of subalkali basalts in the Central Georgian neovolcanic
936 region. Doklady Earth Sciences 408, 657-661.
937

938 Lebedev, V.A., Bubnov, S.N., Chernyshev, I.V., Gol'tsman, Y.V., 2006b. Basic magmatism
939 in the geological history of the Elbrus neovolcanic area, Greater Caucasus: Evidence from K-
940 Ar and Sr-Nd isotope data. Doklady Earth Sciences 406, 37-44.
941
942 Lebedev, V.A., Bubnov, S.N., Chernyshev, I.V., Chugaev, A.V., Dudauri, O.Z., Vashakidze,
943 G.T., 2007. Geochronology and genesis of subalkaline basaltic lava rivers at the Dzhavakheti
944 Highland, Lesser Caucasus: K-Ar and Sr-Nd isotopic data. Geochemistry International 45,
945 211-225.
946
947 Lebedev, V.A., Bubnov, S.N., Dudauri, O.Z., Vashakidze, G.T., 2008a. Geochronology of
948 Pliocene volcanism in the Dzhavakheti Highland (the Lesser Caucasus). Part 1: Western part
949 of the Dzhavakheti Highland. Stratigraphy and Geological Correlation 16, 204-224.
950
951 Lebedev, V.A., Bubnov, S.N., Dudauri, O.Z., Vashakidze, G.T., 2008b. Geochronology of
952 Pliocene volcanism in the Dzhavakheti Highland (the Lesser Caucasus). Part 2: Eastern part
953 of the Dzhavakheti Highland. Regional geological correlation. Stratigraphy and Geological
954 Correlation 16, 553-574.
955
956 Lebedev, V.A., Chernyshev, I.V., Chugaev, A.V., Gol'tsman, Y.V., Bairova, E.D., 2010.
957 Geochronology of eruptions and parental magma sources of Elbrus volcano, the Greater
958 Caucasus: K-Ar and Sr-Nd-Pb isotope data. Geochemistry International 48, 41-67.
959
960 Lebedev, V.A., Chernyshev, I.V., Yakushev, A.I., 2011. Initial time and duration of
961 Quaternary magmatism in the Aragats neovolcanic area (Lesser Caucasus, Armenia).
962 Doklady Earth Sciences 437, 532-536.

963

964 Le Bas, M.J., Le Maitre, R.W., Streckeisen, A., Zanettin, B., 1986. A chemical classification
965 of volcanic rocks based on the total alkali-silica diagram. Journal of Petrology 27, 745-750.

966

967 Lin, Y.C., Chung, S.L., Karakhanian, A., Jrbashyan, R., Navasardyan, G., Galoyan, G., Chiu,
968 H.Y., Lin, I.J., Chu, C.H., Lee, H.Y., 2011. Geochemical and Sr-Nd isotopic constraints on
969 the petrogenesis of pre- to post-collisional volcanic rocks in Armenia. Geophysical Research
970 Abstracts 13, EU2011-5422.

971

972 Liotard, J.M., Dautria, J.M., Bosch, D., Condomines, M., Mehdizadeh, H., Ritz, J.F., 2008.
973 Origin of the absarokite-banakite association of the Damavand volcano (Iran): trace elements
974 and Sr, Nd, Pb isotope constraints. International Journal of Earth Sciences 97, 89-102.

975

976 Lordkipanidze, M., 1980. Alpine volcanism and geodynamics of the central segment of the
977 Mediterranean belt. Metsniereba, Tiblisi (in Russian).

978

979 Lordkipanidze, M., Meliksetian, B., Jrbashian, R., 1988. Mesozoic-Cenozoic magmatic
980 evolution of the Pontian-Crimean-Caucasian region. Mémoire de la Société Géologique de
981 France 154, 103-124.

982

983 Lustrino, M., Keskin, M., Mattioli, M., Lebedev, V.A., Chugaev, A., Sharkov, E., Kavak, O.,
984 2010. Early activity of the largest Cenozoic shield volcano in the circum-Mediterranean area:
985 Mt. Karacadağ, SE Turkey. European Journal of Mineralogy 22, 343-362.

986

Maggi, A., Priestley, K., 2005. Surface waveform tomography of the Turkish-Iranian plateau. Geophysical Journal International 160, 1068-1080.

McDonough, W.F., Sun, S.-S., 1995. The composition of the Earth. Chemical Geology 120, 223-253.

McQuarrie, N., van Hinsbergen, D.J.J., 2013. Retrodeforming the Arabia-Eurasia collision zone: Age of collision versus magnitude of continental subduction. Geology 41, 315-318.

Mirnejad, H., Hassanzadeh, J., Cousens, B.J., Taylor, B.E., 2010. Geochemical evidence for deep mantle melting and lithospheric delamination as the origin of the inland Damavand volcanic rocks of northern Iran. Journal of Volcanology and Geothermal Research 198, 288-296.

Mitchell, J., Westaway, R., 1999. Chronology of Neogene and Quaternary uplift and magmatism in the Caucsus: constraints from K-Ar dating of volcanism in Armenia. Tectonophysics 304, 157-186.

Mo, X., Hou, Z., Niu, Y., Dong, G., Qu, X., Zhao, Z., Yang, Z., 2007. Mantle contributions to crustal thickening during continental collision: Evidence from Cenozoic igneous rocks in southern Tibet. Lithos 96, 225-242.

Moine, B.N., Grégoire, M., O'Reilly, S.Y., Sheppard, S.M.F., Cottin, J.Y., 2001. High field strength element fractionation in the upper mantle: evidence from amphibole-rich composite

mantle xenoliths from the Kerguelen Islands (Indian Ocean). Journal of Petrology 42, 2145-2167.

Morley, C.K., Kongwung, B., Julapour, A.A., Abdolghafourian, M., Hajian, M., Waples, D., Warren, J., Otterdoom, H., Srisuriyon, K., Kazemi, H., 2009. Structural development of a major late Cenozoic basin and transpressional belt in central Iran: The Central Basin in the Qom-Saveh area. Geosphere 5, 325-362.

Okay, A.I., Zattin, M., Cavazza, W., 2010. Apatite fission-track data for the Miocene Arabia-Eurasia collision. Geology 38, 35-38.

Pagé, P., Bédard, J.H., Tremblay, A., 2009. Geochemical variations in a depleted fore-arc mantle: The Ordovician Thetford Mines Ophiolite. Lithos 113, 21-47.

Pearce, J.A., 1983. Role of the sub-continental lithosphere in magma genesis at active continental margins. In: Hawkesworth, C.J., Norry, M.J. (Eds.). Continental Basalts and Mantle Xenoliths. Shiva, Natwich, p.p. 230-249.

Pearce, J.A., Bender, J.F., Delong, S.E., Kidd, W.S.F., Low, P.J., Guner, Y., Sargolu, F., Yilmaz, Y., Moorbath, S., Mitchell, J.G., 1990. Genesis of collision volcanism in eastern Anatolia, Turkey. Journal of Volanology and Geothermal Research 44, 189-229.

Pearce, J.A., Parkinson, I.J., 1993. Trace element models for mantle melting: application to volcanic arc petrogenesis. In: Prichard, H.M., Alabaster, T., Harris, N.B.W., Neary, C.R. (Eds.). Geological Society Special Publication 76, 373-403.

Pearce, J.A., Peate, D.W., 1995. Tectonic implications of the composition of volcanic arc magmas. Annual Review of Earth and Planetary Sciences 23, 251-285.

Pearce, J.A., 1996. A users guide to basalt discrimination diagrams. In: Wyman, D.A. (Ed.). Trace Element Geochemistry of Volcanic Rocks: Applications for Massive Sulphide Exploration. Geological Association of Canada Short Course Notes 12, 79-113.

Peccerillo, R., Taylor, S.R., 1976. Geochemistry of Eocene calc-alkaline volcanic rocks from the Kastamonu area, northern Turkey. Contributions to Mineralogy and Petrology 58, 63-81.

Pfänder, J.A., Münker, C., Stracke, A., Mezger, K., 2007. Na/Ta and Zr/Hf in ocean island basalts – Implications for crust-mantle differentiation and the fate of Niobium. Earth and Planetary Science Letters 254, 158-172.

Piromallo, C., Morelli, A., 2003. P-wave tomography of the mantle under the Alpine-Mediterranean area. Journal of Geophysical Research 108, B2, doi:10.1029/2002JB001757.

Powell, R., 1984. Inversion of the assimilation and fractional crystallisation (AFC) equations; characterisation of contaminants from isotope and trace element relationships in volcanic suites. Journal of the Geological Society of London 141, 447-452.

Presnyakov, S.L., Belyaeva, E.V., Lyubin, V.P., Rodionov, N.V., Antonov, A.V., Saltykova, A.K., Berezhnaya, N.G., Sergeev, S.A., 2012. Age of the earliest Paleolithic sites in the

northern part of the Armenian Highland by SHRIMP-II U-Pb geochronology of zircons from volcanic ashes. Gondwana Research 21, 929-938.

Priestley, K.F., McKenzie, D.P., 2006. The thermal structure of the literature from shear wave velocities. Earth and Planetary Science Letters 244, 285-301.

Rebaï, S., Philip, H., Dorbath, L., Borissoff, B., Haessler, H., Cisternas, A., 1993. Active tectonics in the Lesser Caucasus: coexistence of compressive and extensional structures. Tectonics 12, 1089-1114.

Richards, J.P., Spell, T., Rameh, E., Razique, A., Fletcher, T., 2012. High Sr/Y magmas reflect arc maturity, high magmatic water content, and porphyry Cu ± Mo ± Au potential: examples from the Tethyan arcs of central and eastern Iran and western Pakistan. Economic Geology 107, 295-332.

Rolland, Y., Billo, S., Corsini, M., Sosson, M., Galoyan, G., 2009. Blueschists of the Amassia-Stepanavan suture zone (Armenia): linking Tethys subduction history from E-Turkey to W-Iran. International Journal of Earth Sciences 98, 533-550.

Saadat, S., Karimpour, M.H., Stern, C., 2010. Petrochemical characteristics of Neogene and Quaternary alkali olivine basalts from the western margin of the Lut Block, eastern Iran. Iranian Journal of Earth Sciences 2, 87-106.

Saadat, S., Stern, C.R., 2012. Petrochemistry of a xenolith-bearing Neogene alkali olivine basalt from northeastern Iran. Journal of Volcanology and Geothermal Research 225, 13-29.

Savov, I.P., Luhr, J., D'Antonio, M., Connor, C., Karakhanian, A., Ghukasyan, Y., Djrbashian, R., 2007. Variable slab and subarc mantle signatures within dying arc setting – clues from the volcanology and geochemistry of Quaternary volcanic rocks from Armenia. American Geophysical Union Spring Meeting Abstracts, V53A-02.

Sen, P.A., Temel, A., Gourgaud, A., 2004. Petrogenetic modelling of Quaternary post-collisional volcanism: a case study of central and eastern Anatolia. Geological Magazine 141, 81-98.

Şengör, A.M.C., Kidd, W.S.F., 1979. Post-collisional tectonics of the Turkish-Iranian plateau and a comparison with Tibet. Tectonophysics 55, 361-376.

Şengör, A.M.C., Özeren, M.S., Keskin, M., Sakinç, M., Özbakir, A.D., Kayan, I., 2008. Eastern Turkish high plateau as a small Turkic-type orogen: Implications for post-collisional crust-forming processes in Turkic-type orogens. Earth Science Reviews 90, 1-48.

Shabanian, E., Acocella, V., Gioncada, A., Ghasemi, H., Bellier, O., 2012. Structural control on volcanism in intraplate post collisional settings: Late Cenozoic to Quaternary examples of Iran and Eastern Turkey. Tectonics 31, TC3013, doi:10.1029/2011TC003042.

Skhirtladse, N.N., 1958. Post-Paleogene Volcanism in Georgia (Postpaleogenovyi effuzivnyi vulkanizm Gruzii). Report of the Georgian Soviet Socialist Republic Academy of Sciences, Tblisi, 368 pp (in Russian).

1110 Sosson, M., Rolland, Y., Müller, C., Danelian, T., Melkonyan, R., Kekelia, S., Adamia, A.,
1111 Babazadeh, V., Kangarli, T., Avagyan, A., Galoyan, G., Mosar, J., 2010. Subudctions,
1112 obduction and collision in the Lesser Caucasus (Armenia, Azerbaijan, Georgia), new insights.
1113 In: Sosson, M., Kaymakci, N., Stephenson, R.A., Bergerat, F., Starostenko, V. (Eds.).
1114 Sedimentary Basin Tectonics from the Black Sea and Caucasus to the Arabian Platform.
1115 Geological Society of London Special Publications 340, 329-352.
1116
1117 Stampfli, G.M., 2000. Tethyan oceans. In: Bozkurt, E., Winchester, J.A., Piper, J.D.A. (Eds.).
1118 Tectonics and Magmatism in Turkey and the Surrounding Area. Geological Society of
1119 London Special Publications 173, 1-23.
1120
1121 Sun, S.-S., McDonough, W.F., 1989. Chemical and isotopic systematics of oceanic basalts:
1122 implications for mantle composition and processes. In: Saunders, A.D., Norry, M.J. (Eds.)
1123 Magmatism in the Ocean Basins. Geological Society of London Special Publication, vol.42,
1124 p.p. 313-345.
1125
1126 Tepley, F.J., Davidson, J.P., Clynne, M.A., 1999. Magmatic interactions as recorded in
1127 plagioclase phenocrysts of Chaos Crags, Lassen Volcanic Centre, California. Journal of
1128 Petrology 40, 787-806.
1129
1130 Tiepolo, M., Bottazzi, P., Foley, S.F., Oberti, R., Vannucci, R., Zanetti, A., 2001.
1131 Fractionation of Nb and Ta from Zr and Hf at mantle depths: the role of Titanian pargasite
1132 and kaersutite. Journal of Petrology 42, 221-232.
1133

1134 Tsachiyama, A., 1985. Dissolution kinetics of plagioclase in the melt system diopsite-albite-
1135 anorthite, and origin of dusty plagioclase in andesites. Contributions to Mineralogy and
1136 Petrology 89, 1-16.
1137
1138 van Hunen, J., Allen, M.B., 2011. Continental collision and slab break-off: A comparison of
1139 3-D numerical models with observations. Earth and Planetary Science Letters 302, 27-37.
1140
1141 Verdel, C., Wernicke, B.P., Hassanzadeh, J., Guest, B., 2011. A Paleogene extensional arc
1142 flare-up in Iran. Tectonics 30, TC3008, doi:10.1029/2010TC002809.
1143
1144 Vernant, P., Nilforoushan, F., Hatzfeld, D., Abbassi, M., Vigny, C., Masson, F., Nankali, H.,
1145 Martinod, J., Ashtiani, A., Bayer, R., Tavakoli, F., Chery, J., 2004. Contemporary crustal
1146 deformation and plate kinematics in Middle East constraints by GPS measurements in Iran
1147 and northern Iran. Geophysical Journal International 157, 381-398.
1148
1149 Vincent, S.B., Allen, M.B., Ismail-Zadeh, A.D., Flecker, R., Foland, K.A., Simmons, M.B.,
1150 2005. Insights from the Talysh of Azerbaijan into the Paleogene evolution of the South
1151 Caspian region. Geological Society of America Bulletin 117, 1513-1533.
1152
1153 Weaver, B.L., Wood, D.A., Tarney, J., Joron, J.L., 1987. Geochemistry of ocean island
1154 basalts from the South Atlantic: Ascension, St. Helena, Gough and Tristan da Cunha. In:
1155 Fitton, J.G., Upton, B.G.J. (Eds.). Alkaline Igneous Rocks. Geological Society of London
1156 Special Publications 30, 253-267.
1157

1158 Weaver, B.L., 1991. The origin of ocean island basalt end-member compositions: trace
1159 element and isotope constraints. Earth and Planetary Science Letters 104, 381-397.
1160
1161 Williams, H.M., Turner, S.P., Pearce, J.A., Kelley, S.P., Harris, N.B.W., 2004. Nature of the
1162 source regions for post-collisional, potassic magmatism in southern and northern Tibet from
1163 geochemical variations and inverse trace element modelling. Journal of Petrology 45, 555-
1164 607.
1165
1166 Woodcock, N.H., Fischer, M., 1986. Strike-slip duplexes. Journal of Structural Geology 8,
1167 725-735.
1168
1169 Workman, R.K., Hart, S.R., 2005. Major and trace element composition of the depleted
1170 MORB mantle (DMM). Earth and Planetary Science Letters 231, 53-72.
1171
1172 Zindler, A., Hart, S., 1986. Chemical Geodynamics. Annual Reviews in Earth and Planetary
1173 Sciences 14, 493-571.
1174
1175 Zor, E., 2008. Tomographic evidence of slab detachment beneath eastern Turkey and the
1176 Caucasus. Geophysical Journal International 175, 1273-1282.
1177
1178

Table captions

Table 1. Major and trace element data for selected samples from the valley, ridge, and cone series, Shirak. LOI = loss-on-ignition.

Table 2. Measured Nd and Sr isotope compositions of the valley, ridge, and cone series, Shirak.

Supplementary Items

Item 1. Selected photomicrographs of samples from the valley, ridge, and cone series, Shirak.

Item 2. Complete whole rock major and trace element data for the Shirak lavas, including trace element standards.

Figures

Figure 1. Map of the Turkish- Iranian plateau with shaded digital topography, showing locations of Pliocene-Quaternary volcanic centres (cones) and the study area (rectangle).

Figure 2. Digital topography map of the study region with geological features simplified from work by Khachatur Meliksetian, Gevorg Navasardyan and Sergey Karapetyan of the Institute of Geology of the National Academy of Sciences of Armenia, plus outline map of Armenia showing administrative boundaries and regional coverage of Late Miocene-Quaternary magmatic products.

Figure 3. (a) Total alkali-silica classification (Le Bas et al., 1986) and (b) K_2O vs. SiO_2 classification (Peccerillo and Taylor, 1976).

Figure 4. Major element variation diagrams for the Shirak lavas.

Figure 5. Minor and trace element variation in the Shirak lavas.

Figure 6. Rare earth element and extended trace element normalised plots. Chondrite normalisation values from McDonough and Sun (1995) and Primitive Mantle and OIB values from Sun and McDonough (1989).

Figure 7. (a) Nd-Sr isotope plot for Shirak lavas, compared to mafic centres within the collision zone. Pliocene-Pleistocene valley series in southern Georgia and Late Miocene mafic lavas from the Elbrus region of Southern Russia - Lebedev et al. (2007; 2010); NW

Iran minor centres, Tendurek, Ararat, Kurkistan - Kheirkhah et al. (2009), Allen et al. (2013); Damavand - Davidson et al. (unpublished data), Mirnejad et al. (2010); Artvin, Eastern Turkey - Aydiçakir and Şen, in press). Mantle end members and array - Zindler & Hart (1986). (b) Variation of Nd and Sr isotopes as a function of magmatic evolution.

Figure 8. Fractional crystallisation (FC) trends within the Shirak lavas (symbols as per previous diagrams). Data and FC vectors for basic to acidic rocks for Eastern Anatolia are from Pearce et al. (1990). pl = plagioclase; o = olivine; opx = orthopyroxene; cpx = clinopyroxene; hb = hornblende; gnt = garnet.

Figure 9. Th/Yb vs. Ta/Yb diagram (Pearce, 1983) for the Shirak lavas, showing an FC vector for a hydrous assemblage, taking into account increasing partition coefficients during magmatic evolution (after Keskin et al., 1998), and an AFC vector as described on the figure. Eocene rocks from Eastern Turkey, likely to be similar to those directly underlying the Shirak lava series, are plotted (Aydinçakir and Şen, in press). Crust (UCC: upper continental crust; MCC: middle crust; LCC: lower crust; BCC: bulk continental crust, all from Rudnick and Gao, 2003). Active margins - Pearce (1983). See text for discussion.

Figure 10. Zr/Hf vs. Nb/Ta plot for Shirak lavas and selected mafic Pliocene-Quaternary lavas from the Arabia-Eurasia collision. Ararat and Tendürek are from lithospheric mantle sources, Karacadağ in southern Turkey has an OIB source. Sources: Tendürek, Ararat – Kheirkhah et al. (2009); Karacadağ - Sen et al. (2004), Lustrino et al. (2010); clinopyroxene fractionation based on partition coefficients of Pagé et al. (2009); other references as per Figure 9.

1245 Figure 11. Non-modal batch partial melting models for the valley series lavas using depleted
1246 MORB mantle (Workman and Hart, 2005) and incompatible element enriched oceanic
1247 plateau (Fitton and Godard, 2004) sources. Source modes: spinel lherzolite - ol = 0.578, opx
1248 = 0.27, cpx = 0.119, sp = 0.033; garnet lherzolite - 0.598, 0.211, 0.076, gnt = 0.115. Melt
1249 modes: spinel lherzolite - 0.1, 0.27, 0.5, sp = 0.13; garnet lherzolite - 0.05, 0.2, 0.3, gnt =
1250 0.45. Partition coefficients are from the GERM Partition Coefficient Database
1251 (http://earthref.org/KDD).
1252
1253 Figure 12. A schematic cross-section through the present-day Arabia-Eurasia collision zone
1254 highlighting potential processes involved in Pliocene-Quaternary magmatism. Hatchings
1255 represent regions of partial melting. Crustal thicknesses estimated from Zor et al. (2008).

Pliocene-Quaternary volcanic rocks of NW Armenia: magmatism and lithospheric dynamics within an active orogenic plateau

I. Neill[1*], Kh. Meliksetian[2], M.B. Allen[1], G. Navarsardyan[2], S. Karapetyan[2]

[1]Department of Earth Sciences, Durham University, Science Site, DH1 3LE, Durham, UK

[2]Institute of Geological Sciences, National Academy of Sciences of Armenia, Marshal Baghramian Avenue, Yerevan 0019, Armenia

*Corresponding author. E-mail: iain.neill@durham.ac.uk. Phone: +44 1913 342356.

Abstract

The Pliocene-Quaternary volcanic rocks of Armenia are a key component of the Arabia-Eurasia collision, representing intense magmatism within the Turkish-Iranian plateau, tens of millions of years after the onset of continental collision. Here we present whole rock elemental and Nd-Sr isotope data from mafic, intermediate, and felsic lava flows and cinder cones in Shirak and Lori Provinces, NW Armenia. Magmatism appears to be controlled locally by extension related to major strike-slip faults within the plateau. Major and trace element results show that the three series – valley-filling medium-K alkali basalt flows, ridge-forming andesite to rhyolite flows, and andesitic cinder cones – form a compositional continuum linked by a crystallisation sequence dominated by two pyroxenes, plagioclase and amphibole. There is ~~some~~ petrographic and major and trace element evidence for magma

mixing processes and potentially crustal contamination by Mesozoic-early Cenozoic arc-related rocks, which has not significantly affected the isotopic signature. Modelling of the basaltic rocks indicates that they formed by moderate degrees of partial melting (~3-4 %) of an incompatible element enriched, subduction-modified, lithospheric mantle source. Samples have a distinctive high Zr/Hf ratio and high Zr concentrations, which are an intrinsic part of the source or the melting process, and are much more commonly found in ocean island basalts. Regional models for magmatism commonly often argue for whole-scale delamination of the mantle lithosphere beneath Eastern Anatolia and the Lesser Caucasus, but this scenario is hard to reconcile with limited crustal signatures and the apparent lack of asthenospheric components within many studied centres.

Highlights

- Whole-rock study of Pliocene-Quaternary lavas from the Armenian Highlands
- Range of alkali basalts through to rhyolitesCompositional range controlled by fractional crystallisation, magma mixing and possible limited crustal contamination
- Low-degree melting of a shallow metasomatised lithospheric mantle source
- Exploring triggers for <10 Myr increase in magmatic activity in Armenia and elsewhere in the Arabia-Eurasia collision zone

Keywords

Armenia; geochemistry; petrogenesis; orogenic plateau

1. Introduction

Orogenic plateaus such as the modern Turkish-Iranian, Bolivian Altiplano-Puna and Tibetan plateaus form in response to plate convergence and collision, and represent a primary topographic feature of the continents. In spite of their thickened crust and compression tectonics, plateaus are also sites of intense, ultimately mantle-derived magmatism (e.g. Williams et al., 2004; Mo et al., 2007). Such magmatism is often attributed to asthenospheric upwelling following the break-off of the subducting oceanic slab (e.g. Keskin, 2003), or the delamination of the lithosphere inboard of the plate suture (e.g. Kay and Kay, 1993).

The Turkish-Iranian plateau (Fig. 1) is a product of the Cenozoic Arabia-Eurasia collision, and magmatism post-dating initial collision is particularly voluminous from the Late Miocene until the present day, in numerous locations across eastern Turkey, Armenia, and much of Iran (Fig. 1). Erupted products~~,~~ rang~~eing in composition~~ from mafic to felsic, and sodic to ultrapotassic (Pearce et al., 1990; Karapetian et al., 2001; Davidson et al., 2004; Azizi and Moinevaziri, 2009; Saadat et al., 2011; Saadat and Stern, 2012; Allen et al., 2013). In nearby Georgia and the Greater Caucasus, the most recent magmatism appears to have started slightly earlier, in the Middle Miocene, and continued with some gaps in the record until recent times (Lebedev et al., 2006a,b; 2007; 2008a,b; Adamia et al., 2011).

This plateau-wide 'recent' magmatism may be only partly explained by partial melting of asthenospheric ~~and~~ or mantle lithosphere sources ~~resultant from~~due to ~~slab~~ break-off of the southern Neo-Tethys slab (e.g. Keskin, 2003; 2007; Şengör et al., 2008; Dilek et al., 2010; van Hunen and Allen, 2011). ~~Both the Eocene flare-up and~~ Miocene to recent magmatism extends to at least 500 km from ~~their respective~~the Bitlis-Zagros suture zone~~s~~, ~~on~~ a spatial scale akin to the Cenozoic 'ignimbrite flare-up' of the western United States

(Johnson, 1991)~~, with a remarkable co-incidence between the locations of the Eocene and recent magmatism (Verdel et al., 2011)~~. The wide extent of Miocene-Quaternary magmatism hundreds of kilometres from the suture zone indicates that ~~slab break-off is not the sole mantle melting trigger. W~~whole-scale lithospheric delamination (Pearce et al., 1990), ~~on-going under-thrusting of Arabian crust (Allen et al., in press),~~ or other unrecognised processes may be collectively responsible for magmatism in this region.

To further consider the origin of such magmatism, ~~we turn our attention~~this paper focuses on ~~to~~ Armenia (Fig. 1), where ~~the geochemistry of~~ recent volcanism has been under-represented in the international literature ~~(Karapetian et al., 2001; Savov et al., 2007; Lin et al., 2011)~~. We present whole rock elemental and Nd-Sr isotope data from three series of mafic to felsic Pliocene-Quaternary volcanic rocks in the north of Shirak and west of Lori administrative provinces in the northwest of the country (herein referred to ~~simply~~ as 'Shirak') (Fig. 2). The local tectonic setting and relationship to magmatism is highlighted, alongside discussion on magmatic evolution~~fractional crystallisation, crustal contamination~~, mantle sources~~,~~ and partial melting. We finish by assessing how the results fit with regional geodynamic models.

2. Geological setting, structure, and petrography

2.1. The Turkish-Iranian plateau

The Turkish-Armenian-Iranian orogenic plateau (Fig. 1)~~, itself a product of the Arabia-Eurasia continental collision, and~~ developed following the closure of the Neo-Tethys Ocean (Şengör and Kidd, 1979). The basement of the plateau consists of Mesozoic to Early

Cenozoic accretionary belts and arc rocks and also older, Gondwanaland-related micro-continental fragments that all accreted to the southern margin of Eurasia. It is widely assumed that ~~in the region of study,~~ the Neo-Tethys oceanic crust~~Ocean~~ was divided into a northern and a southern segment, the former closed ~~by collisions marked by the Sevan-Akera ophiolite suite (Fig. 2)~~ either during the Late Cretaceous (Lordkinpanidze, 1980; Keskin, 2008) or the Paleocene-Early Eocene (Sosson et al., 2010). The ~~northern and southern~~two segments of Neo-Tethys were separated by ~~rifted~~ micro-continental fragments such as the South Armenian Block and Tauride-Anatolide terranes (Sosson et al., 2010). Destruction of the southern segment of Neo-Tethys brought Arabia and Eurasia together along the Bitlis-Zagros suture zone (Fig. 1).

The timing of initial collision between Arabia and Eurasia is debated, although ~~many~~ most estimates range between 35 and 20 Ma (Agard et al., 2005; Allen and Armstrong, 2008; Morley et al., 2009; Okay et al., 2010; Ballato et al., 2011; McQuarrie and van Hinsbergen, 2013). ~~Furthermore, the timing of plateau growth from this point on is uncertain.~~ Marine carbonates ~~were~~ deposited across much of central Iran and eastern Turkey in the Early Miocene~~,~~ ~~indicating~~ indicate that ~~surface uplift~~growth of the orogenic plateau is a later phenomenon (Bottrill et al., 2012). Deformation is ~~at~~ presently focussed on the plateau margins ~~of the plateau~~, from the Greater Caucasus and Alborz in the north to the Zagros in the south, with no active crustal thickening or thinning occurring between (Jackson et al., 1995; Allen et al., 2011). Lithospheric thickness is highly variable, from >200 km in Iran near the Zagros suture, to only 60 km or less in eastern Anatolia (Priestley and McKenzie, 2006; Angus et al., 2006). The current height of the plateau, ~1750 m above sea level, has been attributed to a combination of Late Cenozoic crustal shortening, and also to the

detachment of mantle lithosphere and/or subducted Tethyan slabs beneath the plateau, allowing the upwelling of hot, buoyant asthenosphere beneath the region (Keskin, 2003).

~~Plateau elevations in northern Armenia are approximately 2 km above sea level at present. Understanding the association between the growth of the plateau and partial melting processes, through interpreting the geochemical patterns of plateau magmatism, can provide key constraints on how the plateau has evolved through time, and give insights into orogenic plateaux in general.~~ The Cenozoic magmatic record ~~within the region of the present plateau~~of the plateau is divided into several stages (see Dilek et al., 2010; Chiu et al., 2013 for reviews~~a review~~). First is an Eocene 'flare-up' of arc magmatism immediately prior to the onset of continental collision, focussed predominantly on the Urumieh-Dokhtar arc in southwest Iran, the Lut Block, Kopeh Dag and Alborz regions of eastern and northern Iran (Verdel et al., 2011), and also in Armenia (Lordkinpanidze et al., 1988). The flare-up has been ~~variously~~ attributed to back-arc extension ~~behind the Iranian margin~~ (Vincent et al., 2005), an episode of flat subduction (Berberian and Berberian, 1981), perhaps coupled with enhanced slab roll-back (Verdel et al., 2011), or break-off of the northern Neo-Tethyan slab in Armenia and North-Central Turkey (Keskin et al., 2008; Sosson et al., 2010). The second stage is a magmatic 'gap' which comprised some 20-30 Myr of ~~very~~ limited magmatic activity between the Eocene and the Late Miocene as continental collision proceeded (Verdel et al., 2011; Richards et al., 2011). The third and final stage is the ~~resumption~~ aforementioned upsurge of ~~ultimately~~ mantle-derived volcanism from the ~~Late~~ Middle to Late Miocene until the present day (Chiu et al., 2013), ~~in numerous locations~~ which forms the basis of this study.

2.2~~1~~. Basement and structure in Armenia

Armenia, including the Lesser Caucasus mountain range, lies at the northern side of the ~~Turkish-Iranian orogenic~~ plateau (Figs. 1, 2). Southern Armenia is underlain by the aforementioned South Armenian Block (SAB), a micro-continental fragment rifted during the early Mesozoic, separating the ~~During the early Mesozoic, the~~ northern and southern branches of the Neo-Tethyan seaway ~~opened between Africa/Arabia and Eurasia, separated by micro-continental fragments of the former Gondawana supercontinent~~ (Stampfli, 2000). ~~Much of southern Armenia is one such fragment, known as the South Armenian Block (SAB), which may link to the Tauride and Anatolide terranes to the west (Sosson et al., 2010). Where exposed beneath Pliocene-Quaternary rocks, t~~The SAB consists of Proterozoic gneisses, mica schists~~,~~ and amphibolites partially overlain by Devonian to Jurassic sediments, Jurassic and younger ophiolitic material, and Paleocene to Early Oligocene volcanic rocks related to subduction of the southern branch of Neo-Tethys (Rolland et al., 2009). ~~The~~ In the north of Armenia, the Armenian Highlands represent the former active continental margin of Eurasia and contains ~~island~~ arc and discontinuous ophiolite sequences formed during the closure of the northern branch of the Neo-Tethyan seaway (Adamia et al., 1981; 2011). ~~There is significant debate over the mode of formation and location within the Neo-Tethyan realm of each ophiolite fragment (Sosson et al., 2010).~~ The largest tract of ophiolitic material in Armenia forms the Sevan-Akera suture zone, a 400 km-long boundary between the SAB and the Mesozoic arc of the Lesser Caucasus to the north. Immediately south of our field area, between Amasia and Stepanavan, is a belt of blueschist-facies mélange (part of the Sevan-Akera ophiolite suite), tectonically overlain by Jurassic to Cretaceous mafic ~~oceanic~~ rocks, ~~which are in turn overlain by~~and two sequences of Cretaceous to Early Oligocene subduction-related volcano-sedimentary rocks (Rolland et al., 2009). ~~^{40}Ar/^{39}Ar phengite ages from the blueschist suggest metamorphism took place during northwards Tethyan subduction in the Late Cretaceous (~95-91 Ma), followed by retrogression which started during collision~~

~~of the SAB with the Lesser Caucasus island arc at ~74-71 Ma, and continued until terminal collision with the Eurasian margin during the Eocene (Rolland et al., 2009).~~

Following the Eocene amalgamation of the Armenian crustal blocks (Rolland et al., 2009), north-directed subduction of the southern ~~branch of~~ Neo-Tethys terminated along the Bitlis-Zagros suture, ~~(~~some 300 km south of Armenia~~)~~. After the last ~~Eocene-Oligocene~~ subduction-related magmatism, the magmatic 'gap' in Armenia extended until the Late Miocene (~~~~<~~10 Ma), based on groundmass and mineral K-Ar ^{40}~~K-~~ ^{40}~~Ar~~ ages from the oldest volcanic rocks of the Gegham Highlands (Arutyunyan et al., 2007). The most voluminous volcanism is ~~however~~ of Pliocene-Quaternary age, covering much of Aragatsotn, Shirak, Kotayk, Gegharkunik, and Syunik provinces, an area >10,000 km^2 (Mitchell and Westaway, 1999; Karapetian et al., 2001; Lebedev et al., 2011) (Fig. 2). ~~If interpretations of crustal structure are correct, the magmas from Shirak in this study may have passed through a complex series of interwoven crustal units including SAB basement, Jurassic arc material, Jurassic-Early Oligocene arc rocks, flysch, and limestone (Sosson et al., 2010).~~

2.3~~2~~. Pliocene - Quaternary magma series

~~Much of t~~The geology of NW Armenia was first studied in detail during Soviet times (Kharazyan, 1983). The oldest Pliocene – Quaternary volcanism is represented by poorly-exposed rhyolites and obsidians at Aghvorik (Fig. 2), covered by ~~. These felsic rocks are covered by Upper Pliocene~~ dolerites ~~(see below). Aside from these felsic rocks, much of the lowest topography in Shirak is covered by mafic rocks, traditionally named as doleritic basalts or Pliocene plateau basalts in Armenian geological literature~~which drape much of the lowest topography in Shirak, often part-filling river valleys for tens of kilometers. ~~These~~

~~flows form a stratigraphic horizon across much of northern and central Armenia, due to presence of extended lava flows cropping out on plateaus and in cross-sections in many of the river valleys.~~ ~~Some r~~Relationships with sedimentary deposits dated using mammalian fossils lead authors to conclude that these mafic lavas were of Late Pliocene age (Kharazyan, 1983 and references therein). A ^{40}~~K~~ ^{40}~~Ar~~ K-Ar age determination from dolerite from the Akhurian river basin within our study area gave a result of 2.5 ± 0.2 Ma (Chernyshev et al., 2002). Groundmass K-Ar ^{40}~~K~~ ^{40}~~Ar~~ results from ~~a wide range of~~numerous mafic to felsic volcanic rocks across the Javakheti Highlands in southern Georgia gave ages of 4.6 ± 0.2 to 1.54 ± 0.10 Ma (Late Pliocene to Quaternary) (Lebedev et al., 2008a,b). The mafic rocks in Armenia and southern Georgia ~~have been described as resulting~~may have resulted from fissure eruptions (Jrbashyan et al., 1996), but the actual source of these lavas has never been found, and may be buried by younger~~, more evolved~~ flows.

~~Also present~~On top of the plateau-like topography formed by the mafic flows in Shirak, are ~~mountainous~~ hills~~areas~~ of intermediate-felsic composition ~~extending~~ of up to 600 m prominence ~~above the plateau-like topography formed by the mafic flows~~, including the ~~prominent~~ north-south trending Javakheti, or Kechut, ridge (Fig. 2). ~~Prior to any radiometric age determinations,~~ Kharazyan (1983) distinguished two ~~age~~ units within the Armenian part of the Javakheti ridge. The first unit (Lower Kechut Suite) ~~is presented by~~is said to contain two-pyroxene basaltic andesites, andesites and hornblende andesites which cover the valley series and are thus assumed to be of Early Pleistocene age (Kharazyan, 2005). SHRIMP U-Pb zircon dating of andesitic vent-proximal ash and breccia layers deposited on the eastern flank of the Javakheti ridge in Lori province at the Karakhach archaeological site (Fig. 2) ~~has~~ gives ~~confirmed~~ maximum eruption ages of 1.94 ± 0.05 to 1.80 ± 0.03 Ma~~, giving a maximum eruption age~~ (Presnyakov et al., 2012). This study also

noted ~~several older grains, two of Eocene age~~two Eocene zircons (40-50 Ma) consistent with Eocene arc rocks found to the east of the study area, plus five Proterozoic grains, consistent with an origin in the underthrust SAB ~~(e.g. Rolland et al., 2009)~~. It is uncertain whether or not these old grains were from xenoliths ripped up during explosive volcanism or zircons assimilated during magma ascent. The Javakheti Ridge extends into southern Georgia, where it is higher and has a sharp little denuded topographic profile compared to further south. Groundmass ^{40}~~K-~~ ^{39}~~Ar~~ K-Ar dating revealed younger ages of ~~<~~<1 Ma for the Samsari volcanic centre ~~which lies~~ to the north of the Javakheti Ridge (Chernyshev et al., 2006). Kharazyan (1983) also defined an Upper Kechut Suite ~~on the Javakheti Ridge,~~ supposedly containing lavas erupted from cinder cones on the western part of the ridge ~~ridge covering eroded lavas and pyroclastic material of the Lower Kechut Suite~~, and considered to be of Middle Pleistocene age (Kharazyan, 2005). We did not find clear evidence of this unit during our studies. The only other Pliocene-Quaternary volcanic products in this part of Shirak are cinder cones to the west of the Javakheti Ridge around Lake Arpi (Fig. 2), which are estimated to be of ~~Lower~~Early-Middle Pleistocene age, based on relationships with ~~valley series~~the mafic rocks and some river terraces (Kharazyan, 1983).

Overall ~~it is evident that~~ there have been no comprehensive geochronological studies carried out in ~~Armenia~~ Shirak using a single reliable technique, unlike those ~~produced~~ for similar sequences in Georgia (Lebedev et al., 2008a,b). ~~Furthermore there is a~~A lack of continuous exposure ~~, which~~ hampers judgement of the relative age of the different lavas. ~~Hence, w~~We have decided to ~~simplify the lavas, and~~ sub-divide the entire Pliocene-Quaternary suite close to the Javakheti Ridge into three ~~main~~ components: mafic flows (the dolerites) largely covering the topography developed on the ~~pre-existing Sevan-Akera suture~~basement (herein termed the *Valley Series*); more evolved flows built up into hills

~~rising up to 600 m~~ above the mafic flows (*Ridge Series*); and scattered cinder cones (*Cone Series*) (Fig. 2).

2.3~~2~~.1. Valley Series

The Valley Series consists of mafic flows ~~which reach~~with a maximum cumulative thickness of 200 m in eastern Lori province (Fig. 2). In the study area, the exposed sequence ~~usually~~ comprises at most four or five stacked flows up to 40 m thick in total, and directly overlies the Sevan-Akera suture and ophiolite sequence in the Dzoraged gorge and near Amasia (Fig. 2). We have collected samples from these locations, as well as from Lake Arpi and near Tashir in western Lori Province (Fig. 2). ~~Jrbashyan et al. (1996) suggested that these flows are likely to have been fissure-fed, and flowed from the north, before following the palaeo-topography of the Debed and Akhuryan river valleys to the east and south.~~ Valley Series samples collected from near Lake Arpi, Amasia, and Tashir (Fig. 2), consist of vesicular sub-ophitic dolerites with rare clinopyroxene or optically zoned plagioclase phenocrysts, set in a groundmass of 1-2 mm grain size consisting of clinopyroxene, plagioclase~~,~~ and oxides (see Supplementary Item 1). Clinopyroxene is commonly rimmed or almost totally replaced by red-brown amphibole, and there is occasional interstitial quartz and rare rounded quartz blebs. ~~None of the samples contain any fresh olivine~~Some samples contain very rare iddingsite crystals, and the few olivines found in thin section are rounded and <0.5 mm in diameter.~~although a number do have very rare 1-2 mm bright red cubic crystals, which may be iddingsite replacing olivine. The vesicles in the selected samples do not contain secondary infill.~~

2.3~~2~~.2. Ridge Series

Magmatism in this series is restricted to ~~more evolved~~ intermediate to felsic lavas ~~which have~~ built up into prominent topographic features. The highest of these is the north to south-trending Javakheti Ridge (Fig. 2), consisting of ~~multiple~~ rounded and glacially eroded ~~centres~~ peaks reaching ~3100 m above sea level, following a clear north-south trend running north into Georgia (Fig. 2). A second series of hills ~~and ridges~~ lie north of the Akhuryan River parallel to the Georgian border, but these are more topographically muted, reaching a maximum elevation of ~2400 m. Rock types from both ridges are almost exclusively ~~flows of~~ andesitic to dacitic ~~composition~~flows, with ~~some~~ rare black dacites and rhyolitic obsidians (Karapetian et al., 2001). ~~The flows that we have analysed~~Analysed flows range from ~~evolved~~ basaltic trachyandesites to dacites, ~~but~~and ~~they display~~there is much compositional and textural variation. Some of the least evolved samples (<60 wt.% SiO_2) contain 1-3 mm phenocrysts and glomerocrysts of clinopyroxene (rarely orthopyroxene) and ~~some~~ plagioclase, set in a flow-banded groundmass of plagioclase, clinopyroxene and Fe-Ti oxides, with accessory apatite and zircon. More evolved samples tend to contain significantly more plagioclase phenocrysts, and several have abundant 1-3 mm euhedral green-brown pleochroic amphiboles, but the presence of amphibole is not ubiquitous even in samples ~~containing~~ of similar SiO_2 and MgO concentrations. Many plagioclase crystals ~~in either clinopyroxene- or amphibole-dominated suites~~ are sieve-textured and some have corroded margins, ~~implying~~ usually taken to imply ~~either~~ the occurrence of magma mixing processes (Tsuchiyama, 1985; Tepley et al., 1999), ~~or rapid decompression during eruption (Nelson and Montana, 1992);~~ and many crystals are also optically zoned. Other evidence for magma mixing is the common occurrence of rounded quartz blebs with dark reaction coronas, and ubiquitous opaque rims on primary hornblende crystals (Tepley et al., 1999; Supplementary Item 1). ~~The~~ A black dacite contains a few clinopyroxene glomerocrysts, but mostly consists of a fine-grained

groundmass dominated by prismatic to acicular feldspars. ~~Two photomicrographs from the Ridge Series are in Supplementary Item 1.~~ The Ridge Series include~~d~~s the only ~~polycrystalline~~ crustal xenoliths noted from our sampling, ~~in a single sample from~~at a single site near Darik, north of Lake Arpi (Fig. 2). The xenoliths consist of a coarse-grained groundmass of plagioclase, clinopyroxene, oxide, and rare iddingsite after olivine; and 2-3 mm phenocrysts of clinopyroxene and plagioclase, most consistent with inclusion of material from the Valley Series. A slight chilled margin is observed within the host~~. Based on petrographic similarities, we suggest that this xenolith has been derived from the Valley Series flows immediately underlying the ridge, and not the deeper crust. The host itself also contains some sub-rounded quartz xenocrysts (see Supplementary Item 1) and degraded plagioclase crystals with a speckled appearance, sometimes rimmed by new growth. The presence of quartz xenocrysts with reaction rims is taken to indicate assimilation of host rocks~~.

2.3~~2~~.3. Cone Series

Scattered cinder cones are present in the Akhuryan valley near Lake Arpi (Fig. 2), often tens of metres high and ~~reaching~~ several hundred metres across. ~~A notable lack of erosion of these cones suggests they represent the youngest volcanism in the area.~~ We have collected samples from Sepasar, Eznasar, and Kaputkogh cones (Fig. 2). Most are composed of poorly welded unsorted glass~~y~~ or scoria~~ceous~~ fragments ~~of various sizes~~, and more coherent scoria bombs reaching a few tens of centimetres in diameter. The Cone Series compositions mirror the least evolved of the ridge series, the majority of samples containing differing proportions of plagioclase and clinopyroxene as phenocrysts and groundmass (Supplementary Item 1). Bombs from Kaputkogh and Eznasar contain ubiquitous mm-scale rounded quartz

xenocrysts, whereas those at Sepasar appear more mafic, and devoid of foreign material. ~~. A photomicrograph of a typical Cone Series sample is available in Supplementary Item 1.~~

3. Analytical methods

Samples were powdered in an agate ball mill at Durham University. Major element analysis was conducted on fused glass beads using a PANalytical Axios Advanced X-Ray Fluorescence (XRF) spectrometer at the University of Leicester. Leftover fractions of the powder from XRF analysis were digested using a standard HF and HNO_3 technique prior to trace element analysis. Solutions were run on a Thermo X2 inductively-coupled plasma mass spectrometer (ICP-MS) at the Northern Centre for Isotopic and Elemental Tracing (NCIET) at Durham University. Accuracy, precision, and reproducibility were monitored using blanks, multi-run and within-run duplicates, Re-Rh spike solutions, and five international reference standards. Standard W2 (n = 15) gave first relative standard deviations of 5% or better for most transition metals (excepting 10% for Sc, 12% for Cr, 6% for Ni), the large ion lithophile elements (LILE) and the rare earth elements (REE) (7% for La, 6% for Ce). Elemental results are recorded in Table 1 and Supplementary Item 2, the latter also containing standard results.

Radiogenic Nd and Sr isotope analysis was conducted at NCIET, with column chemistry for elemental pre-concentration based on the method of Dowall et al. (2007). Powders were digested in HF and HNO_3, and solutions run through 1 ml pipettes containing several drops of dilute Sr-spec resin to collect the Sr-bearing fraction. The high field strength element (HFSE)- and rare earth element (REE)-bearing fraction from these columns was run through 10 ml Bio-Rad polypropylene columns containing 1 ml of Bio-Rad AG1-X8 200-400 mesh anion-exchange resin. Neodymium was collected as part of a general rare earth element

fraction. Analysis was conducted on a Thermo Neptune Mass Collector ICP-MS. Strontium was run in a single batch during which time blanks averaged 88 pg Sr (n = 6). International reference standard NBS987 gave a mean of $^{87}Sr/^{86}Sr = 0.710263 \pm 0.000012$ (2σ, n = 12), comparable to a preferred value of 0.710240, and providing a minimum uncertainty of 16 ppm (2σ). No correction was applied to the final results. Neodymium was run in two separate batches, with blanks averaging 10 pg Nd (n = 6). During the first run, a combination of the J&M standard and a Sm-doped version gave a mean $^{143}Nd/^{144}Nd = 0.511098 \pm 0.000007$ (2σ, n = 13), and a minimum uncertainty of 13 ppm (2σ). During the second run, $^{143}Nd/^{144}Nd = 0.511100 \pm 0.000007$ (2σ, n = 13), giving an uncertainty of 14 ppm (2σ). For consistency between the runs, all results were normalised to a preferred value of 0.511110. Results are presented in Table 2.

4. Geochemistry

4.1. Sample freshness

We collected the freshest available samples at each locality, and this is reflected in loss-on-ignition (LOI) values typically <1 wt.%, mostly un-weathered feldspars and mafic minerals, and an overall lack of sericite and chlorite in thin section. Major and trace element data, particularly element vs. SiO_2 plots (see Section 4.2), have trends consistent with magmatic processes, particularly for CaO, MgO, K_2O, and Na_2O, as opposed to the widespread scatter expected during sub-solidus alteration which easily mobilises these elements (e.g. Cann, 1970; Pearce, 1996). $^{87}Sr/^{86}Sr$ isotope results are commonly affected by hydrothermal alteration, but here are depleted with no sign of a trend towards high $^{87}Sr/^{86}Sr$ at constant $^{144}Nd/^{143}Nd$ (Table 2); nor is there a correlation between LOI and isotopic ratios.

Furthermore, the samples were erupted in an intra-continental high plateau so have not interacted with high $^{87}Sr/^{86}Sr$ seawater or been exposed to tropical weathering.

4.2. Major and trace element characteristics

4.2.1. Valley Series

The Valley Series lavas (~49-55 wt.% SiO_2) are mostly mildly alkaline trachybasalts based on the total alkali-silica classification (Le Bas et al., 1986; Fig. 3a), and belong to the medium-K series of Peccerillo and Taylor (1976; Fig. 3b). They are evolved, with 4-7 wt.% MgO and low molar Mg# from 46 to 58. Overall the samples have low TiO_2, moderate-high Al_2O_3, and a sodic character (Na_2O/K_2O = 2.7-4.1) (Fig. 4). Trace element abundances and trends can be seen on Figure 5. Also, the lavas have low Sc (<25 ppm), moderate Cr, Ni, and large ion lithophile element (LILE) abundances (e.g. Ba = 280-450 ppm and Sr = 540-720 ppm). ~~Of the high field strength elements (HFSE), they have considerable enrichment in Zr (170-210 ppm), and super-chondritic Zr/Hf (47-52), with Nb/Ta (17-22).~~ Chondrite-normalised (CN) ~~Rare Earth Element (REE)~~REE abundances are light REE (LREE) enriched (La/Yb_{CN} = 5-9; calc-alkaline), with flat heavy REE (HREE) patterns around 15-20 times chondritic abundances (Fig. 6a). The patterns are split into two groups, one with lower LREE and higher HREE concentrations and vice versa, the patterns crossing over at around Pr-Nd. There are some very slight negative Eu anomalies relative to the ~~middle REE (~~MREE~~)~~. The extended Primitive Mantle-normalised (PMN) plot (Fig. 6b) shows that the samples have spiky LILE patterns (modest positive Ba, Rb, Th, Sr anomalies), prominent negative K, Nb-Ta, and Ti anomalies and positive Zr-Hf anomalies relative to the REE, with super-chondritic Zr/Hf ratios of 47-55.

399

400 *4.2.2. Ridge Series*

401

402 The more evolved Ridge Series (~57-68 wt.% SiO_2, 2-5 wt.% MgO, Mg# = 41-55) has a
403 wide range of sub-alkaline compositions from basaltic trachy-andesite through to dacite (Fig.
404 3a). Samples largely belong to the medium-K series, although two plot in the high-K field
405 (Fig. 3b). They have noticeably lower TiO_2, $Fe_2O_{3(t)}$ and P_2O_5 concentrations compared to the
406 valley series, and are slightly less sodic (Na_2O/K_2O = 1.4-2.5) (Fig. 4). Transition metal
407 abundances are lower than the Valley Series, but the Ridge Series has higher Ba and Zr and
408 lower Sr and Nb concentrations compared to the mafic lavas (Fig. 5). Chondrite-normalised
409 LREE patterns (Fig. 6c) are similar to the Valley Series, again splitting into two groups with
410 higher or lower LREE concentrations. Ridge samples have La/Yb_{CN} from 8 to 18, with a
411 highly fractionated M-HREE distribution such that some samples have a U-shaped pattern.
412 There are small negative Eu anomalies. Primitive Mantle-normalised patterns (Fig. 6d) differ
413 slightly from the Valley Series in having positive Rb spikes, and more pronounced negative
414 Nb-Ta, P and Ti anomalies.

415

416 *4.2.3. Cone Series*

417

418 The Cone Series splits into three groups, the most mafic being the two cones at Sepasar (58
419 wt.% SiO_2, but low Mg# = 43), and the most felsic at Eznasar (62 wt.% SiO_2, Mg# = 52). The
420 large cone at Kaputkogh has intermediate silica content relative to the other cones, although it
421 has the highest Mg# of 54. The ~~inverted relationship between Mg# and silica content may be~~
422 ~~derived from the most primitive magmas happening to be contaminated by relatively higher~~
423 ~~proportions of associated felsic magmas or crustal components during ascent. This~~

~~relationship means that the Cone Series do not form a significant part of the discussion on overall fractionation and contamination trends in Section 5.2. Finally, t~~The cones have higher Nb and Zr concentrations relative to the other series (Fig. 5); REE patterns for the Cone Series are clearly bimodal (Fig. 6e), whilst the Primitive Mantle-normalised plots look similar to the Valley Series (Fig. 6f).

4.3. Radiogenic isotope geochemistry

Most samples span a narrow range from $^{87}Sr/^{86}Sr$ = 0.70416 to 0.70446 and $^{143}Nd/^{144}Nd$ = 0.51280 to 0.51287, giving a range of values in epsilon notation from εNd = +3.1 to +4.6. No age corrections were applied owing to the young age of the rocks. On Figure 7a, there is overlap between samples from the Valley, Ridge, and Cone series, and the samples display only a little isotopic enrichment with major element evolution (Fig. 7b). Overall, the samples lie on the mantle array between bulk silicate earth and depleted MORB mantle, and there is no clear evidence of any trends which might be related to mixing of different mantle end members (e.g. EMI or EMII) or old, isotopically enriched crustal contaminants. The ~~cones~~ Cone and ~~Valley~~ Ridge Series samples ~~with~~ containing quartz xenocrysts are not isotopically different from the other samples.

Regionally, the samples are significantly more depleted than most Pliocene-Quaternary centres in north-west Iran and Mount Damavand (Alborz), and Tendürek volcano in Eastern Anatolia (Fig. 7a). The Iranian volcanic rocks were erupted through thicker lithosphere than beneath Armenia (e.g. Liotard et al., 2008; Kheirkhah et al., 2009; Mirnejad et al., 2010; Davidson et al., unpublished data; Allen et al., ~~in press~~2013). Samples are also more depleted than asthenospheric melts from eastern Iran which have trends towards the

EM-II mantle end member (Saadat et al., 2011; Saadat and Stern, 2012). Instead, results are closest to the few analyses conducted on the large stratovolcano, Mount Ararat, close to the Armenian border (Pearce et al., 1990; Kheirkhah et al., 2009), and nearly identical in terms of $^{143}Nd/^{144}Nd$ to six analyses of the ~3.25-2.05 Ma valley series lavas from southern Georgia, and from eight Late Miocene sub-alkaline basalts in central Georgia (Lebedev et al., 2006; 2007). Radiogenic isotope results are not yet widely published from other Armenian Pliocene-Quaternary centres, but Savov et al. (2007) and Lin et al. (2011) reported values from $^{87}Sr/^{86}Sr$ = 0.7041 to 0.7051 and $^{143}Nd/^{144}Nd$ = 0.5128 to 0.5129 from ~~across much of the country~~various locations. ~~This is a similar narrow range of results compared to our study, except for some $^{87}Sr/^{86}Sr$ values extending to more enriched compositions outside of the mantle array. The overall lack of enriched, continental crust-like values and crustal or mantle xenoliths is an interesting feature of magmatism across the orogenic plateau in spite of varied basement compositions.~~

5. Discussion

5.1. Volcano-tectonic interaction

Before considering the petrogenesis of the magma series, we first address the location of volcanic activity with respect to major crustal structures. The internal part of the orogenic plateau is not undergoing contractile deformation (Jackson et al., 1995; Vernant et al., 2004), but internal reorganisation of the plateau during the on-going convergence between Arabia and Eurasia means that Eastern Anatolia, the Lesser Caucasus, and northwest Iran are criss-crossed by numerous active strike-slip fault systems (Rebaï et al., 1993; Koçyiğit et al., 2001). These systems, which often tally with pre-existing crustal discontinuities, have been

widely implicated in providing a locus for Quaternary magmatic activity through the production of highly localised pull-apart zones (Dewey et al., 1986; Karakhanian et al., 1997, 2002; Avagyan et al., 2010; Shabanian et al., 2012).

In Armenia, the active Pambak-Sevan-Syunik right-lateral strike-slip fault system is one such structure exploiting the existing discontinuity of the Sevan-Akera suture zone (Fig. 2). All of the magmatism described in this study originated just to the north of the fault zone, and so we propose that this location sat over a region of localised upper crustal extension at the time of magmatism. No active extension is recorded from the Shirak region from earthquake focal mechanisms or geomorphic features. Blanket coverage of most pre-existing fault structures by the Valley Series, and the absence of linear arrays of cinder cones (e.g. Dewey et al., 1986), may have helped obscure this association between faulting and magmatism. The south-eastern termination of the Pambak-Sevan-Syunik fault in the Syunik region is characterised by widespread volcanism in the area south of the fault, with little volcanism to the north (Kharakhanian et al., 2004). The Syunik centres therefore appear to have developed along the complementary trailing imbricate fan (Woodcock and Fischer, 1986) to the Shirak volcanic rocks. The north-south trending volcanism along the Javakheti Ridge is consistent with this idea.

Not all young Armenian centres fit a simple fault-control hypothesis: Aragats volcano, the largest centre in the country, is situated in a region apparently not crossed by presently-active faults (Kharakhanian et al., 2004). It is possible that older faults may be obscured by lava flows, or that some other control on the location of Aragats may apply, such as a local thin-spot in the lithosphere which focussed melting beneath the plateau.

499 5.2. Fractionation and contamination processes

500

501 *5.2.1. Fractional crystallisation – minerals involved*

502

503 No sample ~~of~~ from the mafic Valley Series lavas is close to a primary melt (MgO is typically
504 < 7 wt.%), so it is assumed that they have already evolved at depth involving a typical
505 fractionation assemblage of olivine and spinel. In the major element data, clear falling trends
506 for the Valley Series against typical indices of fractionation, such as SiO_2, TiO_2, MgO, and
507 CaO (Fig. 4), corroborate with the observed mineral assemblages in confirming that clino-
508 and orthopyroxene and Fe-Ti oxides were important in Valley Series evolution. Al_2O_3
509 concentrations cover a narrow range with no trends, indicating that feldspar fractionation was
510 not an important feature of the Valley Series; likewise with P_2O_5 concentrations and apatite.
511 Trace element abundances, such as Ba, Th, and La, display rising trends against SiO_2 in the
512 Valley Series, which confirms their incompatible behaviour (Fig. 5). In the more evolved
513 Ridge and Cone Series, clear falling trends emerge against SiO_2 for Al_2O_3, P_2O_5, Sr, Nb, Zr
514 and La, pointing to addition of plagioclase, along with small proportions of zircon and
515 apatite, to the fractionating assemblage.

516

517 The overall pattern of Shirak magmatism can be compared with Eastern Anatolia.
518 Volcanic centres that display either high- or low-Y trends relative to Rb, are associated with
519 fractionation of anhydrous (plagioclase, olivine, pyroxenes, and magnetite), or hydrous
520 assemblages (including amphibole, which is compatible with Y) respectively (Pearce et al.,
521 1990) (Fig. 8). The mafic Valley Series rocks in Shirak follow the same moderate to low-Y
522 trend as the Kars plateau/Mt. Ararat systems, which may indicate amphibole fractionation has
523 taken place at depth, given that amphibole is not seen in any of the Valley Series thin

sections. Another indication of amphibole fractionation is the compatible middle to heavy REE (Sm-Lu) showing falling trends as the three series evolve (Fig. 6). The ridge series lavas have a steeply falling trend for Y against Rb, which may reflect increased partition coefficients for both clinopyroxene and amphibole for Y as these minerals fractionate from more evolved rocks (Pearce et al., 1990).

5.2.2. Magma mixing

The petrographic evidence for magma mixing (zoned plagioclases, sieve textures, reaction rims and quartz blebs) also needs to be reconciled with geochemical data. Major element plots, especially TiO_2, CaO and MgO vs. SiO_2 (Fig. 4) have straight line trends which are widely associated with mixing of two compositionally distinct magmas (Langmuir et al., 1978), rather than the curved trends associated with fractional crystallisation. In the field, the key observation is that the most evolved rocks found in the area, the obsidians at Agvorik, underlie the mafic Valley Series, so felsic magmas had already been erupted by the time of mafic magma injection.

5.2.3~~2~~. Crustal contamination

Many models (e.g. Keskin et al., 1998) consider assimilation-fractional crystallisation (AFC) processes to be important in magma genesis in the plateau. ~~The extent to which crustal contamination has affected primary magma compositions may vary widely across the collision zone.~~ Keskin et al. (1998) argue~~s~~ that recent mafic to felsic samples from Eastern Anatolia have undergone significant amounts of ~~combined assimilation-fractional crystallisation (AFC)~~AFC coinciding with enriched $^{87}Sr/^{86}Sr$ ratios up to 0.7065 (Pearce et

al., 1990). In Shirak, ~~there is~~samples have only ~~very~~ a slight variation in isotope ~~signatures~~ ratios relative to ~~silica concentration~~SiO_2 (Fig. 7b) ~~in the Valley and Ridge Series~~, and samples containing quartz xenocrysts ~~have neither higher~~ $^{87}Sr/^{86}Sr$ ~~nor lower~~ $^{143}Nd/^{144}Nd$ ~~ratios than~~do not have different isotopic ratios to the other lavas - a feature that should strongly support the hypothesis that fractionation and magma mixing were the dominant processes. Also, preliminary results from elsewhere in Armenia, including the Aragats volcanic system, show little clear isotopic evidence for contamination (Savov et al., 2007; Lin et al., 2011) in spite of Aragats erupting through the SAB basement which has enriched $^{87}Sr/^{86}Sr$ ratios of up to 0.7303 - any contamination should be easily indentified (Bagdasaryan and Gukasyan, 1985). However, along-strike from Shirak at Artvin in eastern Turkey, Eocene rocks have measured $^{143}Nd/^{144}Nd$ of 0.512663 - 0.512854 and $^{87}Sr/^{86}Sr$ of 0.705148 - 0.704233 (Aydinçakir and Şen, in press). These values are very similar to the Shirak lavas (Fig. 7), so partial melting or assimilation of similar Eocene crust may be very difficult to decipher geochemically.

~~In terms of trace element ratios, o~~On a Th/Yb vs. Ta/Yb plot (Pearce, 1983) (Fig. 9), the ~~most mafic Valley Series lavas have enriched Ta/Yb ratios of 2.9-4.7, pointing to lower degrees of melting or a more fertile source than expected for mid-ocean ridge basalts (MORB) (Ta/Yb = 0.9; Sun and McDonough, 1989). The lavas also lie above the mantle array in the calc-alkaline field, indicative of a small subduction-related component (see Section 5.3). The~~ three series form a consistent linear trend sub-parallel to the mantle array, with the felsic rocks having compositions more enriched than those of typical continental ~~upper~~ crust (Rudnick and Gao, 2003). On this diagram, the fractional crystallisation trend for a typical amphibole-bearing assemblage is shown. ~~An important consideration is that t~~The samples plot ~~both~~ to the left of the fractionation trend ~~and left of a direct mixing line with~~

~~upper continental crust (Taylor and McLennan, 1985). This result~~which suggests that AFC processes may be operating ~~-~~ although choice of mineral assemblages and partition coefficients can easily affect the FC trend. AFC modelling (Powell, 1984) using the average composition of the ~~Eocene Turkish~~ Artvin rocks (Aydinçakir and Şen, in press) quite reasonably reproduces the trend of the Shirak lavas, but the ~~and a~~ ratio of assimilation to fractionation is high at~~=~~ 0.8. ~~Results of modelling shown on Figure 9 indicate that this significant level of assimilation may produce a trace element trend more compatible with the composition of the Shirak rocks than attainable by pure FC processes. Unfortunately, isotopic analyses are not available for these Turkish rocks~~. Modelling thus shows that large volumes of isotopically similar material can be incorporated into the Shirak lavas without a significant effect on trace element evolution. Studies of disequilibrium textures and mineral chemistry might better elucidate the processes involved in magma evolution.

5.3. Mantle source and partial melting

5.3.1. ~~Overall nature of the m~~Mantle source of the ~~Shirak lavas~~Valley Series

The presence of LILE and HFSE anomalies on normalised plots of mafic rocks (Fig. 6b) are normally taken to indicate a subduction-modified mantle source owing to the retention of HFSE in the slab, and the comparative mobility of the LILE/REE during slab heating and dewatering into the overlying mantle wedge (e.g. Pearce and Peate, 1995). We have already introduced the Th/Yb vs. Ta/Yb diagram (Fig. 9). The alkali basalts from Shirak plot above the mantle array which is commonly taken to indicate the presence of a subduction-modified source. However, they also have very much higher Ta/Yb ratios than many subduction-related rocks. ~~We take this to indicate that t~~The Shirak lavas are therefore derived from an

incompatible element-enriched mantle source, or ~~one that has undergone a~~are derived from a limited degree of melt extraction. As these lavas erupted >20 Myr after the end of Neo-Tethyan subduction, and there is no evidence for a slab at shallow depths beneath Eastern Anatolia and Armenia at the present day (Zor et al., 2008), it is improbable that a normal supra-subduction zone hydrated asthenospheric mantle wedge was involved in the origin of the Shirak lavas. Therefore, the subduction-like characteristics are likely to be derived from a fertile source within the mantle that had been inherited its slab-related geochemical component from earlier Neo-Tethyan subduction ~~processes~~. Crustal contamination is unlikely be responsible for the subduction-like characteristics of the Shirak lavas, as LILE and HFSE anomalies are significant in even the most mafic samples.

Some of the trace element characteristics of the valley series may help constrain the mineralogy of the mantle source. Overall, the flat normalised HREE patterns (Fig. 6a) indicate a spinel-facies mantle source at <70 km, unless the degree of partial melting was very high (>25%) in order to completely consume any garnet present at depths of >70 km. This is unlikely given the overall LREE-enriched and Nb-Ta/HREE-enriched trace element patterns (Fig. 6b) which point towards modest degrees of partial melting of an enriched source. Low Sc concentrations (<25 ppm) in all Valley Series samples may indicate residual clinopyroxene, another indicator of a low degree of partial melting, but it is also possible that extensive pyroxene fractionation prior to eruption has resulted in these low values. Intra-LILE variations, including low Ba/Rb (<25) and Rb/Sr ratios (<0.05), do not point towards amphiboles or phlogopite playing an important role during melting (e.g. Furman and Graham, 1999). Melting therefore took place beneath the Armenian crust at depths of ~45-70 km.

One unusual feature of the Shirak lavas is high ocean island basalt (OIB)-like Zr concentrations (~200 ppm) and Zr/Hf ratios (41-52) relative to MOR and arc basalts, the latter having chondritic Zr/Hf ratios of 35-39 (Weaver et al., 1987; David et al., 2000; Pfänder et al., 2007). Nb/Ta ratios range from 16-22 relative to the chondritic ratio of 19.9 (Pfänder et al., 2007). Mafic samples from other nearby centres in the plateau, including Tendürek and Ararat, show similar features (Fig. 10). Lower ratios in the Ridge Series compared to the Valley Series might~~can~~ be explained by contamination with crustal material such as the Eocene basement (Fig. 10). However, the high Zr/Hf ratios of 47-52 in the less evolved Valley Series are a primary feature of the magmas.

There is little correlation between Zr and Zr/Hf ratios (not shown), indicating that zircon accumulation cannot be directly responsible for the high Zr-Zr/Hf character of the Shirak lavas. HFSE fractionation in OIBs may be due to: (1) residual or fractionating clinopyroxene (David et al., 2000); (2) fractionation of Ti-bearing phases such as rutile, ilmenite, and amphibole (Foley et al., 2000; Tiepolo et al., 2001); (3) melting of recycled eclogite or garnet pyroxenite (Pfänder et al., 2007); or (4) the occurrence of carbonate metasomatism (Dupuy et al., 1992). For option (1), fractionation of clinopyroxene only has a modest effect upon Zr/Hf ratios (Pfänder et al., 2000). Our modelling of pure clinopyroxene fractional crystallisation from a starting composition with Zr/Hf and Nb/Ta of primitive mantle shows that unrealistic amounts of ~~clinopyroxene~~ fractionation are required to generate the Shirak samples (Fig. 10). In option (2), fractionation of titanate phases such as rutile and ilmenite can generate very high Zr/Hf and Nb/Ta ratios, with $D_{Zr/Hf}$ and $D_{Nb/Ta}$ both <1 (Pfänder et al., 2000); however, titanate fractionation would also strongly reduce overall Nb concentrations, a feature not seen in the Valley Series. Partial melting of garnet-bearing lithologies (option 3) is invoked in many OIB examples (see Pfänder et al., 2007) but can be

ruled out here on the basis of flat normalised HREE patterns in the Shirak lavas – these are not OIB-like magmas (Fig. 6b). Where carbonates are invoked in the mantle source (e.g. Dupuy et al., 1992; Hoernle et al., 2002) (option 4), resultant alkaline melts or mantle xenoliths have very high Sr and Ba of >>1000 ppm, and in spite of high Zr/Hf ratios many carbonatites ~~have very low overall concentrations of these two~~have very low concentrations of these elements (Ionov et al., 1993). This is not the signature of the Shirak samples hence carbonate metasomatism is unlikely in this case. Several studies have shown that amphibole and phlogopite fractionate the HFSE (Moine et al., 2001; Tiepolo et al., 2001; Chakhmouradian, 2006), with Chakhmouradian (2006) demonstrating that low-Ti amphiboles have high Zr/Hf ratios of ~60-200. Hence these minerals can impart high Zr/Hf on a melt; but it is still unclear what the high overall Zr concentrations in the Shirak lavas are caused by - this feature is normally attributed to ancient recycled oceanic crust in OIBs (Weaver, 1991).

5.3.2. Modelling of partial melting

Any model of partial melting conditions for Shirak has to be based on the HREE and HFSE, making the assumption that neither set of elements were transported into the lithospheric mantle source in a slab-derived fluid (Pearce and Peate, 1995). Therefore, we have constructed non-modal batch melting curves using Dy, Yb and Nb (ignoring Zr owing to its anomalous behaviour), in order to constrain the degree of partial melting needed to form the Valley Series. We have taken the approach of Pearce et al. (1990) in assuming that hydrous phases such as amphibole and phlogopite (if present) are completely consumed during melting and do not contribute to the melt model. Given the high Ta/Yb ratios of even the least evolved Valley Series samples (Fig. 9), it is reasonable to compare the melting of depleted MORB mantle (DMM) (Workman and Hart, 2005) with a more incompatible-element

673 enriched source, in this case primitive mantle with 1% bulk continental crust extracted, as
674 used by Fitton and Godard (2004) for the Ontong Java oceanic plateau.
675
676 Although we can easily model HREE and HFSE ratios (see below), fractional
677 crystallisation of olivine, spinel, plagioclase and pyroxene versus fractionation of amphibole
678 from primary magma have competing effects on absolute REE and HFSE concentrations.
679 Often, elemental values for basalts in modelling are back-calculated to 9 wt.% MgO to negate
680 the effects of plagioclase and pyroxene crystallisation (Pearce & Parkinson, 1993). However,
681 valley series Dy and Yb concentrations are near-constant in spite of varying MgO and SiO_2
682 (Fig. 6a), probably due to the competing effects of amphibole and clinopyroxene
683 fractionation, so no realistic back-calculation can be applied. Therefore, we simply attempt to
684 model the elemental ratios of the last-evolved Valley Series lava (7 wt.% MgO) and assume
685 that this best reflects the conditions of partial melting.
686
687 Modelling results (Fig. 11) indicate that melting of a garnet peridotite cannot
688 reproduce the compositions of the Valley Series lavas, a finding consistent with the flat
689 normalised HREE patterns (Fig. 6a). Spinel peridotite partial melting curves do intersect the
690 valley series at low degrees of melting, with the DMM melting curve on Figure 11 giving
691 0.1-0.5% melting. In contrast the more fertile source gives 2-5% melting, which is perhaps
692 more realistic than the tiny proportion of melting required from a DMM source and the
693 difficulties of extracting such a small volume of melt (e.g. Hirth and Kohlstedt, 1995). This
694 spinel peridotite melting outcome is also consistent with geophysical surveys indicating a
695 seismically slow~~, probably partially molten~~ mantle at depths of ~50 km beneath Armenia
696 (e.g. Koulakov et al., 2012).
697

5.4. Reconciliation with geophysical and geodynamic models

5.4.1. Extent of lithospheric delamination

Debate exists over the extent of lithospheric delamination beneath Eastern Anatolia following the cessation of subduction beneath the Bitlis-Zagros suture (e.g. Keskin, 2003). Seismic surveys indicate a crustal thickness of ~40-45 km, but with significant negative P- and S-wave seismic velocity anomalies beneath, extending from ~50 to ~250 km depth, between eastern Turkey, Armenia, the Black Sea and northwest Iran, concurrent with many Pliocene-Quaternary volcanic centres (e.g. Piromallo and Morelli, 2003; Maggi & Priestley, 2005; Zor et al., 2008; Koulakov et al., 2012). The anomaly has been used by these authors to argue for the presence of hot, perhaps partially molten, asthenosphere, but several authors extend these conclusions to the possibility that there is also no mantle lithosphere 'lid' beneath the Anatolian crust (e.g. Keskin, 2003; Zor et al., 2008) and the Caucasus (Koulakov et al., 2012). In this case, mafic magmatism in Shirak would have to have an asthenospheric source.

There are significant implications for magmatism in this scenario. The impact of hot upwelling asthenosphere on the thickened Lesser Caucasus arc crust should result in extensive lower crustal melting, as observed in the Puna Plateau of the Andes, and the Great Basin Altiplano in the western U.S. (Allmendinger et al., 1997; Babeyko et al., 2002; Best et al., 2009). Going back to our geochemical results, this model of whole-scale lithospheric delamination proposed for the Puna Plateau is incompatible with the observed silica-undersaturated magmatism in Shirak, which bears little evidence for large-scale crustal interaction. We conclude that there is sufficient lithospheric mantle beneath the Armenian crust to act as a thermal barrier between the asthenosphere and crust (Fig. 12), protecting the

crust from melting and infiltration by hot asthenospheric melts in the manner described by Babeyko et al. (2002). A~~Furthermore, a~~n asthenospheric source for the Shirak magmas ~~would not~~cannot have been influenced by a subducting slab, because subduction processes ended ~~beneath the region~~ prior to the Miocene. Hence the Shirak magmas would not have subduction-like trace element characteristics, and instead should closely resemble OIB. There are asthenosphere-derived OIB-like lavas without subduction-related geochemical signatures in Eastern Iran (Saadat et al., 2010; Saadat and Stern, 2012) and in the Arabian foreland (Lustrino et al., 2010). The Iranian alkali olivine basalts show trends towards an EMII-like isotope signature (particularly with respect to Pb isotope ratios) (Zindler and Hart, 1986). They also and contain pyroxenite xenoliths from the lithospheric mantle, plagioclase megacrysts of uncertain origin, and some lower crustal gabbroic xenoliths (Saadat and Stern, 2012). These lavas are ~~clearly~~ distinct in terms of xenolith content, trace element signatures and isotope geochemistry from those erupted in Shirak.

5.4.2. Geodynamic model

Our geodynamic model is presented schematically in Figure 12. We propose that, upon the termination of Neo-Tethyan subduction along the Bitlis-Zagros suture during the Oligocene, Armenia lay in a continental back-arc position relative to the former subducting slab and mantle wedge. Modelling studies have suggested that an old slab may be able to persist or 'stall' in the upper mantle without breaking off for up to 20 Myr after terminal collision (van Hunen and Allen, 2011). Delayed break-off of the Neo-Tethyan slab from Arabia beneath Eurasia may thus be responsible for the upsurge in magmatism since 10 Ma, and particularly in the Pliocene-Quaternary, across the orogenic plateau (e.g. Keskin, 2003), concurrent with the influx of hot asthenosphere into the region the slab once occupied. In Eastern Anatolia,

748 the region immediately above the detached slab might lack mantle lithosphere, and
749 asthenospheric and crustal melting would combine to produce arc-like magmas (Fig. 12)
750 (Keskin, 2003). However, as we have already discussed, it is improbable that whole-scale
751 lithospheric mantle delamination occurred beneath Armenia because we do not see attendant
752 whole-scale lower crustal melting. The former asthenospheric mantle wedge of the Neo-
753 Tethyan arc system would be refrigerated by the presence of a stalled slab, and rapidly
754 converted into lithospheric mantle over the 15-25 Myr following terminal collision (c.f. Holt
755 et al., 2010). This depleted lithospheric mantle could be stable and buoyant enough to be at
756 least partially preserved following the eventual detachment of the underlying oceanic slab,
757 whilst the aforementioned influx of convecting asthenosphere would trigger partial melting in
758 the overlying lithospheric mantle, as well as providing a thermal support for the orogenic
759 plateau (Fig. 12).
760
761 Another potentially important consideration is that, although much of the LILE and
762 LREE budget of the southern Neo-Tethyan slab may have been delivered to the lithosphere
763 before continental collision, a stalled slab and associated sediments would continue
764 dewatering before break-off. This would contribute to the subduction-like signature on the
765 mantle frozen-in beneath Armenia. Other Pliocene-Quaternary centres in the collision zone,
766 such as the foreland volcanic system at Karacadağ, may result from asthenospheric melting
767 beneath thin spots in the lithosphere (Lustrino et al., 2010; Ekici et al., 2012). Mantle-derived
768 volcanism is also apparent even in the 50+ km thick crust of the Elbrus region of the Greater
769 Caucasus (Lebedev et al., 2006b; Koulakov et al., 2012), and it is here that magmatism may
770 be related to melting during collisional thickening of lithospheric mantle and the breakdown
771 of hydrous mineral phases such as micas and amphiboles (e.g. Pearce et al., 1990; Allen et

al., ~~in press~~2013) or to asthenospheric upwelling during lithospheric dripping (see Sosson et al., 2010) (Fig. 12)~~ - further work is required to distinguish these hypotheses~~.

6. Conclusions

- Mafic and more evolved Pliocene-Quaternary lavas in Shirak, NW Armenia, were emplaced through a former continental margin arc sequence as a result of localised extensional tectonics within the present-day Arabia-Eurasia collision zone.
- Magmas evolved from mafic through to dacitic compositions by fractional crystallisation dominated by pyroxene, amphibole and plagioclase; and although evolved samples contain quartz xenocrysts, none preserves clear isotopic evidence for large-scale crustal assimilation - magma mixing appears to be the dominant petrogenetic process. We conclude that if assimilation did occur, it was of local ~~Mesozoic to Early Cenozoic~~ arc-related crust of a similar isotopic composition to the ~~primary~~ Shirak melts.
- The least-evolved magmas preserve trace element evidence for derivation by moderate degrees of melting (~3-4%) from a shallow, spinel-facies lithospheric mantle source with an inherited subduction component probably related to earlier Tethyan subduction processes. T~~Unusually, t~~hey contain high Zr concentrations and high Zr/Hf ratios which ~~cannot be explained by fractional crystallisation processes, and~~ are an intrinsic feature of the source or partial melting process.
- ~~I~~The presence of lithospheric mantle beneath Armenia is a requirement for geodynamic models of the region~~,~~ in order to prevent the occurrence of whole-scale lower crustal melting.

Acknowledgements

This work is funded by the Natural Environment Research Council project, 'Orogenic Plateau Magmatism' [NE/H021620/1]. Nick Marsh conducted the XRF analyses; Geoff Nowell and Chris Ottley assisted with, and partly conducted, radiogenic isotope and trace element analyses, respectively. We are grateful to *Lithos* guest editor Ioan Seghedi, along with Evgenii Sharkov and an anonymous reviewer for their constructive comments. Ivan Savov and Douwe van Hinsbergen are thanked for discussion on some of the ideas presented within.

References

Adamia, S.A., Chkhotua, T., Kekelia, M., Lordkipanidze, M., Shavishvili, I., 1981. Tectonics of the Caucasus and adjoining regions: implications for the evolution of the Tethys ocean. Journal of Structural Geology 3, 437-447.

Adamia, S.A., Zakariadze, G., Chkhotua, T., Sadradze, N., Tsereteli, N., Chabukiani, A., Gventsadze, S., 2011. Geology of the Caucasus: A Review. Turkish Journal of Earth Sciences 20, 489-544.

Agard, P., Omrani, J., Jolivet, L., Mouthereau, F., 2005. Convergence history across Zagros (Iran): constraints from collisional and earlier deformation. International Journal of Earth Sciences 94, 401-419.

Allen, M.B., Armstrong, H.A., 2008. Arabia-Eurasia collision and the forcing of mid Cenozoic global cooling. Palaeontology Palaeoclimatology Palaeoecology 265, 52-58.

822

823 Allen, M.B., Kheirkhah, M., Emami, M.H., Jones, S.J., 2011. Right-lateral shear across Iran
824 and kinematic change in the Arabia-Eurasia collision zone. Geophysical Journal International
825 184, 555-574.

826

827 Allen, M.B., Kheirkhah, M., Neill, I., Emami, M.H., Mcleod, C., in press. Generation of arc
828 and within-plate chemical signatures in collision zone magmatism: Quaternary lavas from
829 Kurdistan Province, Iran. Journal of Petrology, doi: 10.1093/petrology/egs090.

830

831 Allmendinger, R.W., Isacks, B.L., Jordan, T.E., Kay, S.M., 1997. The evolution of the
832 Altiplano-Puna plateau of the Central Andes. Annual Reviews of Earth Science 25, 139-174.

833

834 Angus, D.A., Wilson, D.C., Sandvol, E., Ni, J.F., 2006. Lithospheric structure of the Arabian
835 and Eurasian collison zone in eastern Turkey from S-wave receiver functions. Geophysical
836 Journal International 166, 1335-1346.

837

838 Avagyan, A., Sosson, M., Karakhanian, A., Philip, H., Rebai, S., Rolland, Y., Melkonyan, R.,
839 Davtyan, V., 2010. Recent tectonic stress evolution in the Lesser Caucasus and adjacent
840 regions. In: Sosson, M., Kaymakci, N., Stephenson, R.A., Bergerat, F., Starostenko, V.
841 (Eds.). Sedimentary Basin Tectonics from the Black Sea and Caucasus to the Arabian
842 Platform. Geological Society of London Special Publications, v. 340, p.p. 393-408.

843

844 Aydinçakir, E., Şen, C, 2013. Petrogenesis of the post-collisional volcanic rocks from the
845 Borçka (Artvin) area: Implications for the evolution of the Eocene magmatism in the Eastern
846 Pontides (NE Turkey). Lithos, in press, doi:10.1016/j.lithos.2013.04.007.

Azizi, H., Moinevaziri, H., 2009. Review of the tectonic setting of Cretaceous to Quaternary volcanism in northwestern Iran. Journal of Geodynamics 47, 167-179.

Babeyko, A.Yu., Sobolev, S.V., Trumbull, R.B., Oncken, O., Lavier, L.L., 2002. Numerical models of crustal-scale convection and partial melting beneath the Altiplano-Puna plateau. Earth and Planetary Science Letters 199, 373-388.

Baghdasaryan, G.P., Ghukasyan, R.Kh., 1985. Geochronology of magmatic, metamorphic and ore formations of Armenian SSR. Publication of the Academy of Sciences of Armenian Soviet Socialist Republic (in Russian).

Ballatto, P., Uba, C.E., Landgraf, A., Strecker, M.R., Sudo, M., Stockli, D.F., Friedrich, A., Tabatabaei, S.H., 2011. Arabia-Eurasia continental collision: Insights from late Tertiary foreland-basin evolution in the Alborz Mountains, northern Iran. Geological Society of America Bulletin 123, 106-131.

Berberian, F., Berberian M., 1981. Tectono-plutonic episodes in Iran. In: Gupta, H.K., Delany, F.M. (Eds.). Zagros, Hindu Kush, Himalaya Geodynamic Evolution. American Geophysical Union Geodynamic Series v. 3, p.p. 5-32.

Best, M.G., Barr, D.L., Christiansen, E.H., Gromme, S., Deino, A.L., Tingey, D.G., 2009. The Great Basin Altiplano during the middle Cenozoic ignimbrite flareup: insights from volcanic rocks. International Geology Review 51, 589-633.

872 Bottrill, A.D., van Hunen, J., Allen, M.B., 2012. Insight into collision zone dynamics from
873 topography: numerical modelling results and observations. Solid Earth 3, 387-399.
874
875 Cann, J.R., 1970. Rb, Sr, Zr and Nb in some ocean floor basaltic rocks. Earth and Planetary
876 Science Letters 10, 7-11.
877
878 Chakhmouradian, A., 2006. High-field-strength elements in carbonatitic rocks:
879 Geochemistry, crystal chemistry and significance for constraining the source of carbonatites.
880 Chemical Geology 235, 138-160.
881
882 Chernyshev, I.V., Lebedev, V.A., Arakelyants, M.M., Jrbashyan, R.T., Ghukasyan, Y.G.,
883 2002. Geochronology of the Aragats volcanic centre, Armenia: Evidence from K-Ar dating.
884 Doklady Earth Sciences 384, 393-398 (in Russian).
885
886 Chernyshev, I.V., Lebedev, V.A., Arakelyants, M.M., 2006. K-Ar dating of Quaternary
887 volcanics: Methodology and interpretation of results. Petrologiya (Petrology) 14, 69-89.
888
889 Chiu, H.-Y., Chung, S.-L., Zarrinkoub, M.H., Mohammadi, S.S., Khatib, M.M., Iizuka, Y.,
890 2013. Zircon U-Pb constraints from Iran on the magmatic evolution related to Neotethyan
891 subduction and Zagros orogeny. Lithos 162, 70-87.
892
893 David, K., Schiano, P., Allégre, C.J., 2000. Assessment of the Zr/Hf fractionation in oceanic
894 basalts and continental materials during petrogenetic processes. Earth and Planetary Science
895 Letters 178, 285-301.
896

Davidson, J.P., Hassanzadeh, J., Berzins, R., Stockli, D.F., Bashukooh, B., Turrin, B., Pandamouz, A., 2004. The geology of Damavand volcano, Alborz Mountains, northern Iran. Geological Society of America Bulletin 116, 16-29.

Dewey, J.F., Hempton, M.R., Kidd, W.S.F., Saroglu, F., Şengör, A.M.C., 1986. Shortening of continental lithosphere: the neotectonics of Eastern Anatolia – a young collision zone. In: Coward, M.P., Ries, A.C. (Eds.). Collision Tectonics. Geological Society of London Special Publication, v. 19, p.p. 3-36.

Dilek, Y., Imamverdiyev, N., Altunkaynak, Ş., 2010. Geochemistry and tectonics of Cenozoic volcanism in the Lesser Caucasus (Azerbaijan) and the peri-Arabian region: collision-induced mantle dynamics and its magmatic signature.

Dowall, D.P., Nowell, G.M., Pearson, D.G., 2007. Chemical pre-concentration procedures for high-precision analysis of Hf-Nd-Sr isotopes in geological materials by plasma ionisation multi-collector mass spectrometry (PIMMS) techniques. In: Holland, J.G., Tanner, S.D. (Eds.) Plasma Source Mass Spectrometry: Applications and Emerging Technologies. Cambridge: The Royal Society of Chemistry, p.p. 321-337.

Drew, S.T., Ducea, M.N., Schoenbohm, L.M., 2009. Mafic volcanism on the Puna Plateau, NW Argentina: Implications for lithospheric composition and evolution with an emphasis on lithospheric foundering. Lithosphere 1, 305-318.

Dupuy, C., Liotard, J.M., Dostal, J., 1992. Zr/Hf fractionation in intraplate basaltic rocks: Carbonate metasomatism in the mantle source. Geochimica et Cosmochimica Acta 56, 2417-2423.

Ekici, T, Macpherson, C.G., Otlu, N, 2012. Polybaric melting of a single mantle source during the Neogene Siverek phase of the Karacadağ Volcanic Complex, SE Turkey. Lithos 146, 152-163.

Fitton, J.G., Godard, M., 2004. Origin and evolution of magmas on the Ontong Java Plateau. In: Fitton, J.G., Mahoney, J.J., Wallace, P.J., Saunders, A.D. (Eds.). Origin and Evolution of the Ontong Java Plateau. Geological Society of London Special Publication, v. 229, p.p. 151-178.

Foley, S.F., Barth, M.G., Jenner, G.A., 2000. Rutile/melt partition coefficients for trace elements and an assessment of the influence of rutile on the trace element characteristics of subduction zone magmas. Geochimica et Cosmochimica Acta 64, 933-939.

Furman, T., Graham, D., 1999. Erosion of lithospheric mantle beneath the East African Rift System: geochemical evidence from the Kivu volcanic province. Lithos 48, 237-262.

Jackson, J., Haines, J., Holt, W., 1995. The accommodation of Arabia-Euasia Plate convergence in Iran. Journal of Geophysical Research 100, B8, P15205.

943 Johnson, C.M., 1991. Large-scale crust formation and lithosphere modification beneath
944 middle to late Cenozoic calderas and volcanic fields, western North America. Journal of
945 Geophysical Research 96, 13485-13507.
946
947 Jrbashian, R.T., Kazarian, G.A., Karapetian, S.G., Meliksetian, Kh.B., Mnatsakanian, A.,
948 Shirinian, K.G., 1996. Meso-Cenozoic basaltic volcanism in the northeastern part of
949 Armenian Highland. Letters of the Armenian Academy of Sciences, Earth Sciences 49, 19-32
950 (in Russian).
951
952 Hirth, G., Kohlstedt, D.L., 1995. Experimental constraints on the dynamics of the partially
953 molten upper mantle: deformation in diffusion creep regime. Journal of Geophysical
954 Research 100, 1981-2001.
955
956 Hoernle, K., Tilton, G., Le Bas, M.J., Duggan, S., Garbe-Schönberg, D., 2002. Geochemistry
957 of oceanic carbonatites compared with continental carbonatites: mantle recycling of oceanic
958 crustal carbonate. Contributions to Mineralogy and Petrology 142, 520-542.
959
960 Holt, P.J., Allen, M.B., van Hunen, J., Bjørnseth, H.M., 2010. Lithospheric cooling and
961 thickening as a basin forming mechanism. Tectonophysics 495, 184-194.
962
963 Ionov, D.A., Dupuy, C., O'Reilly, S.Y., Kopylova, M.G., Genshaft, Y.S., 1993. Carbonated
964 peridotite xenoliths from Spitsbergen: implications for trace element signature of mantle
965 carbonate metasomatism. Earth and Planetary Science Letters 119, 283-297.
966

967 Karapetian, S.G., Jrbashian, R.T., Mnatsakanian, A.Kh., 2001. Late collision rhyolitic
968 volcanism in the north-eastern part of the Armenian Highland. Journal of Volcanology and
969 Geothermal Research 112, 189-220.
970
971 Kharazyan, E.Kh., 1983. Geology of recent volcanism of north-west part of Armenian SSR
972 (basins of rivers Dzoraget and Akhuryan). PhD thesis, unpublished, ArmGeologia, Yerevan,
973 55 pp.
974
975 Kharazyan, E.Kh., 2005. Geological Map of Armenia. Ministry of Nature Protection of
976 Republic of Armenia.
977
978 Keskin, M., Pearce, J.A., Mitchell, J.G., 1998. Volcano-stratigraphy and geochemistry of
979 collision-related volcanism on the Erzurum-Kars Plateau, northeastern Turkey. Journal of
980 Volcanology and Geothermal Research 85, 355-405.
981
982 Keskin, M., 2003. Magma generation by slab steepening and breakoff beneath and
983 subduction-accretion complex: An alternative model for collision-related volcanism in
984 Eastern Anatolia, Turkey. Geophysical Research Letters 30, 1-4.
985
986 Keskin, M., 2007. Eastern Anatolia: a hot spot in a collision zone without a mantle plume. In:
987 Foulger, G.R., Jurdy, D.M. (Eds.) Plates, Plumes, and Planetary Processes. Geological
988 Society of America Special Paper, vol. 409, p.p. 1-25.
989

Keskin, M., Can Genç, Ş, Tüysüz, O., 2008. Petrology and geochemistry of post-collisional Middle Eocene volcanic units in North-Central Turkey: Evidence for magma generation by slab breakoff following the closure of the Northern Neotethys Ocean. Lithos 104, 267-305.

Karakhanian, A.S., Trifonov, V.G., Azizbekian, O.G., Hondkarian, D.G., 1997. Relationship of late Quaternary tectonics and volcanism in the Khanarassar active fault zone, the Armenian Upland. Terra Nova 9, 131-134.

Karakhanian, A., Djrbashian, R., Trifonov, V., Philip, H., Arakelian, S., Avagian, A., 2002. Holocene-historical volcanism and active faults as natural risk factors for Armenia and adjacent countries. Journal of Volcanology and Geothermal Research 113, 319-344.

Karakhanian, A., Abgaryan, Y., 2004. Evidence of historical seismicity and volcanism in the Armenian Highland (from Armenian and other sources). Annals of Geophysics 47, 793-810.

Kay, R.W., Kay, S.M., 1993. Delamination and delamination magmatism. Tectonophysics 219, 177-189.

Kheirkhah, M., Allen, M.B., Emami, M.H., 2009. Quaternary syn-collision magmatism from the Iran/Turkey borderlands. Journal of Volcanology and Geothermal Research 182, 1-12.

Koçyiğit, A., Yilmaz, A., Adamia, S., Kuloshvili, S., 2001. Neotectonics of East Anatolian Plateau (Turkey) and Lesser Caucasus: implications for transition from thrusting to strike-slip faulting. Geodinamica Acta 14, 177-195.

Langmuir, C.H., Vocke, R.D., Hanson, G.N., Hart, S.R., 1978. A general mixing equation with applications to Icelandic basalts. Earth and Planetary Science Letters 37, 380-392.

Koulakov, I., Zabelina, I., Amanatashvili, I., Meskhia, V., 2012. Nature of orogenesis and volcanism in the Caucasus region based on results of regional tomography. Solid Earth 3, 327-337.

Lebedev, V.A., Chernyshev, I.V., Chugaev, A.V., Dudauri, O.Z., Vashakidze, G.T., 2006a. K-Ar age and Sr-Nd characteristics of subalkali basalts in the Central Georgian neovolcanic region. Doklady Earth Sciences 408, 657-661.

Lebedev, V.A., Bubnov, S.N., Chernyshev, I.V., Gol'tsman, Y.V., 2006b. Basic magmatism in the geological history of the Elbrus neovolcanic area, Greater Caucasus: Evidence from K-Ar and Sr-Nd isotope data. Doklady Earth Sciences 406, 37-44.

Lebedev, V.A., Bubnov, S.N., Chernyshev, I.V., Chugaev, A.V., Dudauri, O.Z., Vashakidze, G.T., 2007. Geochronology and genesis of subalkaline basaltic lava rivers at the Dzhavakheti Highland, Lesser Caucasus: K-Ar and Sr-Nd isotopic data. Geochemistry International 45, 211-225.

Lebedev, V.A., Bubnov, S.N., Dudauri, O.Z., Vashakidze, G.T., 2008a. Geochronology of Pliocene volcanism in the Dzhavakheti Highland (the Lesser Caucasus). Part 1: Western part of the Dzhavakheti Highland. Stratigraphy and Geological Correlation 16, 204-224.

1039 Lebedev, V.A., Bubnov, S.N., Dudauri, O.Z., Vashakidze, G.T., 2008b. Geochronology of
1040 Pliocene volcanism in the Dzhavakheti Highland (the Lesser Caucasus). Part 2: Eastern part
1041 of the Dzhavakheti Highland. Regional geological correlation. Stratigraphy and Geological
1042 Correlation 16, 553-574.
1043
1044 Lebedev, V.A., Chernyshev, I.V., Chugaev, A.V., Gol'tsman, Y.V., Bairova, E.D., 2010.
1045 Geochronology of eruptions and parental magma sources of Elbrus volcano, the Greater
1046 Caucasus: K-Ar and Sr-Nd-Pb isotope data. Geochemistry International 48, 41-67.
1047
1048 Lebedev, V.A., Chernyshev, I.V., Yakushev, A.I., 2011. Initial time and duration of
1049 Quaternary magmatism in the Aragats neovolcanic area (Lesser Caucasus, Armenia).
1050 Doklady Earth Sciences 437, 532-536.
1051
1052 Le Bas, M.J., Le Maitre, R.W., Streckeisen, A., Zanettin, B., 1986. A chemical classification
1053 of volcanic rocks based on the total alkali-silica diagram. Journal of Petrology 27, 745-750.
1054
1055 Lin, Y.C., Chung, S.L., Karakhanian, A., Jrbashyan, R., Navasardyan, G., Galoyan, G., Chiu,
1056 H.Y., Lin, I.J., Chu, C.H., Lee, H.Y., 2011. Geochemical and Sr-Nd isotopic constraints on
1057 the petrogenesis of pre- to post-collisional volcanic rocks in Armenia. Geophysical Research
1058 Abstracts 13, EU2011-5422.
1059
1060 Liotard, J.M., Dautria, J.M., Bosch, D., Condomines, M., Mehdizadeh, H., Ritz, J.F., 2008.
1061 Origin of the absarokite-banakite association of the Damavand volcano (Iran): trace elements
1062 and Sr, Nd, Pb isotope constraints. International Journal of Earth Sciences 97, 89-102.
1063

Lordkipanidze, M., 1980. Alpine volcanism and geodynamics of the central segment of the Mediterranean belt. Metsniereba, Tiblisi (in Russian).

Lordkipanidze, M., Meliksetian, B., Jrbashian, R., 1988. Mesozoic-Cenozoic magmatic evolution of the Pontian-Crimean-Caucasian region. Mémoire de la Société Géologique de France 154, 103-124.

Lustrino, M., Keskin, M., Mattioli, M., Lebedev, V.A., Chugaev, A., Sharkov, E., Kavak, O., 2010. Early activity of the largest Cenozoic shield volcano in the circum-Mediterranean area: Mt. Karacadağ, SE Turkey. European Journal of Mineralogy 22, 343-362.

Maggi, A., Priestley, K., 2005. Surface waveform tomography of the Turkish-Iranian plateau. Geophysical Journal International 160, 1068-1080.

McDonough, W.F., Sun, S.-S., 1995. The composition of the Earth. Chemical Geology 120, 223-253.

McQuarrie, N., van Hinsbergen, D.J.J., 2013. Retrodeforming the Arabia-Eurasia collision zone: Age of collision versus magnitude of continental subduction. Geology 41, 315-318.

Mirnejad, H., Hassanzadeh, J., Cousens, B.J., Taylor, B.E., 2010. Geochemical evidence for deep mantle melting and lithospheric delamination as the origin of the inland Damavand volcanic rocks of northern Iran. Journal of Volcanology and Geothermal Research 198, 288-296.

Mitchell, J., Westaway, R., 1999. Chronology of Neogene and Quaternary uplift and magmatism in the Caucsus: constraints from K-Ar dating of volcanism in Armenia. Tectonophysics 304, 157-186.

Mo, X., Hou, Z., Niu, Y., Dong, G., Qu, X., Zhao, Z., Yang, Z., 2007. Mantle contributions to crustal thickening during continental collision: Evidence from Cenozoic igneous rocks in southern Tibet. Lithos 96, 225-242.

Moine, B.N., Grégoire, M., O'Reilly, S.Y., Sheppard, S.M.F., Cottin, J.Y., 2001. High field strength element fractionation in the upper mantle: evidence from amphibole-rich composite mantle xenoliths from the Kerguelen Islands (Indian Ocean). Journal of Petrology 42, 2145-2167.

Morley, C.K., Kongwung, B., Julapour, A.A., Abdolghafourian, M., Hajian, M., Waples, D., Warren, J., Otterdoom, H., Srisuriyon, K., Kazemi, H., 2009. Structural development of a major late Cenozoic basin and transpressional belt in central Iran: The Central Basin in the Qom-Saveh area. Geosphere 5, 325-362.

~~Nelson, S.T., Montana, A., 1992. Sieve-textured plagioclase in volcanic rocks produced by rapid decompression. American Mineralogist 77, 1242-1249.~~

Okay, A.I., Zattin, M., Cavazza, W., 2010. Apatite fission-track data for the Miocene Arabia-Eurasia collision. Geology 38, 35-38.

1113 Pagé, P., Bédard, J.H., Tremblay, A., 2009. Geochemical variations in a depleted fore-arc
1114 mantle: The Ordovician Thetford Mines Ophiolite. Lithos 113, 21-47.
1115
1116 Pearce, J.A., 1983. Role of the sub-continental lithosphere in magma genesis at active
1117 continental margins. In: Hawkesworth, C.J., Norry, M.J. (Eds.). Continental Basalts and
1118 Mantle Xenoliths. Shiva, Natwich, p.p. 230-249.
1119
1120 Pearce, J.A., Bender, J.F., Delong, S.E., Kidd, W.S.F., Low, P.J., Guner, Y., Sargolu, F.,
1121 Yilmaz, Y., Moorbath, S., Mitchell, J.G., 1990. Genesis of collision volcanism in eastern
1122 Anatolia, Turkey. Journal of Volanology and Geothermal Research 44, 189-229.
1123
1124 Pearce, J.A., Parkinson, I.J., 1993. Trace element models for mantle melting: application to
1125 volcanic arc petrogenesis. In: Prichard, H.M., Alabaster, T., Harris, N.B.W., Neary, C.R.
1126 (Eds.). Geological Society Special Publication 76, 373-403.
1127
1128 Pearce, J.A., Peate, D.W., 1995. Tectonic implications of the composition of volcanic arc
1129 magmas. Annual Review of Earth and Planetary Sciences 23, 251-285.
1130
1131 Pearce, J.A., 1996. A users guide to basalt discrimination diagrams. In: Wyman, D.A. (Ed.).
1132 Trace Element Geochemistry of Volcanic Rocks: Applications for Massive Sulphide
1133 Exploration. Geological Association of Canada Short Course Notes 12, 79-113.
1134
1135 Peccerillo, R., Taylor, S.R., 1976. Geochemistry of Eocene calc-alkaline volcanic rocks from
1136 the Kastamonu area, northern Turkey. Contributions to Mineralogy and Petrology 58, 63-81.
1137

1138 Pfänder, J.A., Münker, C., Stracke, A., Mezger, K., 2007. Na/Ta and Zr/Hf in ocean island
1139 basalts – Implications for crust-mantle differentiation and the fate of Niobium. Earth and
1140 Planetary Science Letters 254, 158-172.
1141
1142 Piromallo, C., Morelli, A., 2003. P-wave tomography of the mantle under the Alpine-
1143 Mediterranean area. Journal of Geophysical Research 108, B2, doi:10.1029/2002JB001757.
1144
1145 Powell, R., 1984. Inversion of the assimilation and fractional crystallisation (AFC) equations;
1146 characterisation of contaminants from isotope and trace element relationships in volcanic
1147 suites. Journal of the Geological Society of London 141, 447-452.
1148
1149 Presnyakov, S.L., Belyaeva, E.V., Lyubin, V.P., Rodionov, N.V., Antonov, A.V., Saltykova,
1150 A.K., Berezhnaya, N.G., Sergeev, S.A., 2012. Age of the earliest Paleolithic sites in the
1151 northern part of the Armenian Highland by SHRIMP-II U-Pb geochronology of zircons from
1152 volcanic ashes. Gondwana Research 21, 929-938.
1153
1154 Priestley, K.F., McKenzie, D.P., 2006. The thermal structure of the literature from shear
1155 wave velocities. Earth and Planetary Science Letters 244, 285-301.
1156
1157 Rebaï, S., Philip, H., Dorbath, L., Borissoff, B., Haessler, H., Cisternas, A., 1993. Active
1158 tectonics in the Lesser Caucasus: coexistence of compressive and extensional structures.
1159 Tectonics 12, 1089-1114.
1160
1161 Richards, J.P., Spell, T., Rameh, E., Razique, A., Fletcher, T., 2012. High Sr/Y magmas
1162 reflect arc maturity, high magmatic water content, and porphyry Cu ± Mo ± Au potential:

1163 examples from the Tethyan arcs of central and eastern Iran and western Pakistan. Economic
1164 Geology 107, 295-332.
1165
1166 Rolland, Y., Billo, S., Corsini, M., Sosson, M., Galoyan, G., 2009. Blueschists of the
1167 Amassia-Stepanavan suture zone (Armenia): linking Tethys subduction history from E-
1168 Turkey to W-Iran. International Journal of Earth Sciences 98, 533-550.
1169
1170 Saadat, S., Karimpour, M.H., Stern, C., 2010. Petrochemical characteristics of Neogene and
1171 Quaternary alkali olivine basalts from the western margin of the Lut Block, eastern Iran.
1172 Iranian Journal of Earth Sciences 2, 87-106.
1173
1174 Saadat, S., Stern, C.R., 2012. Petrochemistry of a xenolith-bearing Neogene alkali olivine
1175 basalt from northeastern Iran. Journal of Volcanology and Geothermal Research 225, 13-29.
1176
1177 Savov, I.P., Luhr, J., D'Antonio, M., Connor, C., Karakhanian, A., Ghukasyan, Y.,
1178 Djrbashian, R., 2007. Variable slab and subarc mantle signatures within dying arc setting –
1179 clues from the volcanology and geochemistry of Quaternary volcanic rocks from Armenia.
1180 American Geophysical Union Spring Meeting Abstracts, V53A-02.
1181
1182 Sen, P.A., Temel, A., Gourgaud, A., 2004. Petrogenetic modelling of Quaternary post-
1183 collisional volcanism: a case study of central and eastern Anatolia. Geological Magazine 141,
1184 81-98.
1185
1186 Şengör, A.M.C., Kidd, W.S.F., 1979. Post-collisional tectonics of the Turkish-Iranian plateau
1187 and a comparison with Tibet. Tectonophysics 55, 361-376.

Şengör, A.M.C., Özeren, M.S., Keskin, M., Sakinç, M., Özbakir, A.D., Kayan, I., 2008. Eastern Turkish high plateau as a small Turkic-type orogen: Implications for post-collisional crust-forming processes in Turkic-type orogens. Earth Science Reviews 90, 1-48.

Shabanian, E., Acocella, V., Gioncada, A., Ghasemi, H., Bellier, O., 2012. Structural control on volcanism in intraplate post collisional settings: Late Cenozoic to Quaternary examples of Iran and Eastern Turkey. Tectonics 31, TC3013, doi:10.1029/2011TC003042.

Skhirtladse, N.N., 1958. Post-Paleogene Volcanism in Georgia (Postpaleogenovyi effuzivnyi vulkanizm Gruzii). Report of the Georgian Soviet Socialist Republic Academy of Sciences, Tblisi, 368 pp (in Russian).

Sosson, M., Rolland, Y., Müller, C., Danelian, T., Melkonyan, R., Kekelia, S., Adamia, A., Babazadeh, V., Kangarli, T., Avagyan, A., Galoyan, G., Mosar, J., 2010. Subudctions, obduction and collision in the Lesser Caucasus (Armenia, Azerbaijan, Georgia), new insights. In: Sosson, M., Kaymakci, N., Stephenson, R.A., Bergerat, F., Starostenko, V. (Eds.). Sedimentary Basin Tectonics from the Black Sea and Caucasus to the Arabian Platform. Geological Society of London Special Publications 340, 329-352.

Stampfli, G.M., 2000. Tethyan oceans. In: Bozkurt, E., Winchester, J.A., Piper, J.D.A. (Eds.). Tectonics and Magmatism in Turkey and the Surrounding Area. Geological Society of London Special Publications 173, 1-23.

1212 Sun, S.-S., McDonough, W.F., 1989. Chemical and isotopic systematics of oceanic basalts:
1213 implications for mantle composition and processes. In: Saunders, A.D., Norry, M.J. (Eds.)
1214 Magmatism in the Ocean Basins. Geological Society of London Special Publication, vol.42,
1215 p.p. 313-345.
1216
1217 Tepley III, F.J., Davidson, J.P., Clynne, M.A., 1999. Magmatic interactions as recorded in
1218 plagioclase phenocrysts of Chaos Crags, Lassen Volcanic Centre, California. Journal of
1219 Petrology 40, 787-806.
1220
1221 Tiepolo, M., Bottazzi, P., Foley, S.F., Oberti, R., Vannucci, R., Zanetti, A., 2001.
1222 Fractionation of Nb and Ta from Zr and Hf at mantle depths: the role of Titanian pargasite
1223 and kaersutite. Journal of Petrology 42, 221-232.
1224
1225 Tsachiyama, A., 1985. Dissolution kinetics of plagioclase in the melt system diopsite-albite-
1226 anorthite, and origin of dusty plagioclase in andesites. Contributions to Mineralogy and
1227 Petrology 89, 1-16.
1228
1229 van Hunen, J., Allen, M.B., 2011. Continental collision and slab break-off: A comparison of
1230 3-D numerical models with observations. Earth and Planetary Science Letters 302, 27-37.
1231
1232 Verdel, C., Wernicke, B.P., Hassanzadeh, J., Guest, B., 2011. A Paleogene extensional arc
1233 flare-up in Iran. Tectonics 30, TC3008, doi:10.1029/2010TC002809.
1234
1235 Vernant, P., Nilforoushan, F., Hatzfeld, D., Abbassi, M., Vigny, C., Masson, F., Nankali, H.,
1236 Martinod, J., Ashtiani, A., Bayer, R., Tavakoli, F., Chery, J., 2004. Contemporary crustal

deformation and plate kinematics in Middle East constraints by GPS measurements in Iran and northern Iran. Geophysical Journal International 157, 381-398.

Vincent, S.B., Allen, M.B., Ismail-Zadeh, A.D., Flecker, R., Foland, K.A., Simmons, M.B., 2005. Insights from the Talysh of Azerbaijan into the Paleogene evolution of the South Caspian region. Geological Society of America Bulletin 117, 1513-1533.

Weaver, B.L., Wood, D.A., Tarney, J., Joron, J.L., 1987. Geochemistry of ocean island basalts from the South Atlantic: Ascension, St. Helena, Gough and Tristan da Cunha. In: Fitton, J.G., Upton, B.G.J. (Eds.). Alkaline Igneous Rocks. Geological Society of London Special Publications 30, 253-267.

Weaver, B.L., 1991. The origin of ocean island basalt end-member compositions: trace element and isotope constraints. Earth and Planetary Science Letters 104, 381-397.

Williams, H.M., Turner, S.P., Pearce, J.A., Kelley, S.P., Harris, N.B.W., 2004. Nature of the source regions for post-collisional, potassic magmatism in southern and northern Tibet from geochemical variations and inverse trace element modelling. Journal of Petrology 45, 555-607.

Woodcock, N.H., Fischer, M., 1986. Strike-slip duplexes. Journal of Structural Geology 8, 725-735.

Workman, R.K., Hart, S.R., 2005. Major and trace element composition of the depleted MORB mantle (DMM). Earth and Planetary Science Letters 231, 53-72.

Zindler, A., Hart, S., 1986. Chemical Geodynamics. Annual Reviews in Earth and Planetary Sciences 14, 493-571.

Zor, E., 2008. Tomographic evidence of slab detachment beneath eastern Turkey and the Caucasus. Geophysical Journal International 175, 1273-1282.

Table captions

Table 1. Major and trace element data for selected samples from the valley, ridge, and cone series, Shirak. LOI = loss-on-ignition.

Table 2. Measured Nd and Sr isotope compositions of the valley, ridge, and cone series, Shirak.

Supplementary Items

Item 1. Selected photomicrographs of samples from the valley, ridge, and cone series, Shirak.

Item 2. Complete whole rock major and trace element data for the Shirak lavas, including trace element standards.

Figures

Figure 1. Map of the Turkish- Iranian plateau with shaded digital topography, showing locations of Pliocene-Quaternary volcanic centres (cones) and the study area (rectangle).

Figure 2. Digital topography map of the study region with geological features simplified from work by Khachatur Meliksetian, Gevorg Navasardyan and Sergey Karapetyan of the Institute of Geology of the National Academy of Sciences of Armenia, plus outline map of Armenia showing administrative boundaries and regional coverage of Late Miocene-Quaternary magmatic products.

Figure 3. (a) Total alkali-silica classification (Le Bas et al., 1986) and (b) K_2O vs. SiO_2 classification (Peccerillo and Taylor, 1976).

Figure 4. Major element variation diagrams for the Shirak lavas.

Figure 5. Minor and trace element variation in the Shirak lavas.

Figure 6. Rare earth element and extended trace element normalised plots. Chondrite normalisation values from McDonough and Sun (1995) and Primitive Mantle and OIB values from Sun and McDonough (1989).

Figure 7. (a) Nd-Sr isotope plot for Shirak lavas, compared to mafic centres within the collision zone. Pliocene-Pleistocene valley series in southern Georgia and Late Miocene mafic lavas from the Elbrus region of Southern Russia - Lebedev et al. (2007; 2010); NW

Iran minor centres, Tendurek, Ararat, Kurkistan - Kheirkhah et al. (2009), Allen et al. (~~in press~~2013); Damavand - Davidson et al. (unpublished data), Mirnejad et al. (2010); Artvin, Eastern Turkey - Aydiçakir and Şen, in press). Mantle end members and array - Zindler & Hart (1986). (b) Variation of Nd and Sr isotopes as a function of magmatic evolution.

Figure 8. Fractional crystallisation (FC) trends within the Shirak lavas (symbols as per previous diagrams). Data and FC vectors for basic to acidic rocks for Eastern Anatolia are from Pearce et al. (1990). pl = plagioclase; o = olivine; opx = orthopyroxene; cpx = clinopyroxene; hb = hornblende; gnt = garnet.

Figure 9. Th/Yb vs. Ta/Yb diagram (Pearce, 1983) for the Shirak lavas, showing a ~~fractional crystallisation (FC)~~an FC vector for a hydrous assemblage, taking into account increasing partition coefficients during magmatic evolution (after Keskin et al., 1998), and an ~~assimilation FC~~AFC vector as described on the figure. Eocene rocks from ~~North-Central~~Eastern Turkey, likely to be similar to those directly underlying the Shirak lava series, are plotted (~~Keskin et al., 2008~~Aydinçakir and Şen, in press). ~~Upper crust - Taylor and McLennan (1985),~~Crust (UCC: upper continental crust; MCC: middle crust; LCC: lower crust; BCC: bulk continental crust, all from Rudnick and Gao, 2003). A~~a~~ctive margins - Pearce (1983). See text for discussion.

Figure 10. Zr/Hf vs. Nb/Ta plot for Shirak lavas and selected mafic Pliocene-Quaternary lavas from the Arabia-Eurasia collision. Ararat and Tendürek are from lithospheric mantle sources, Karacadağ in southern Turkey has an OIB source. Sources: ~~Eocene arc rocks – Keskin et al. (2008);~~ Tendürek, Ararat – Kheirkhah et al. (2009); Karacadağ - Sen et al.

(2004), Lustrino et al. (2010); clinopyroxene fractionation based on partition coefficients of Pagé et al. (2009); other references as per Figure 9.

Figure 11. Non-modal batch partial melting models for the valley series lavas using depleted MORB mantle (Workman and Hart, 2005) and incompatible element enriched oceanic plateau (Fitton and Godard, 2004) sources. Source modes: spinel lherzolite - ol = 0.578, opx = 0.27, cpx = 0.119, sp = 0.033; garnet lherzolite - 0.598, 0.211, 0.076, gnt = 0.115. Melt modes: spinel lherzolite - 0.1, 0.27, 0.5, sp = 0.13; garnet lherzolite - 0.05, 0.2, 0.3, gnt = 0.45. Partition coefficients are from the GERM Partition Coefficient Database (http://earthref.org/KDD).

Figure 12. A schematic cross-section through the present-day Arabia-Eurasia collision zone highlighting potential processes involved in Pliocene-Quaternary magmatism. Hatchings represent regions of partial melting. Crustal thicknesses estimated from Zor et al. (2008).

Figure 1

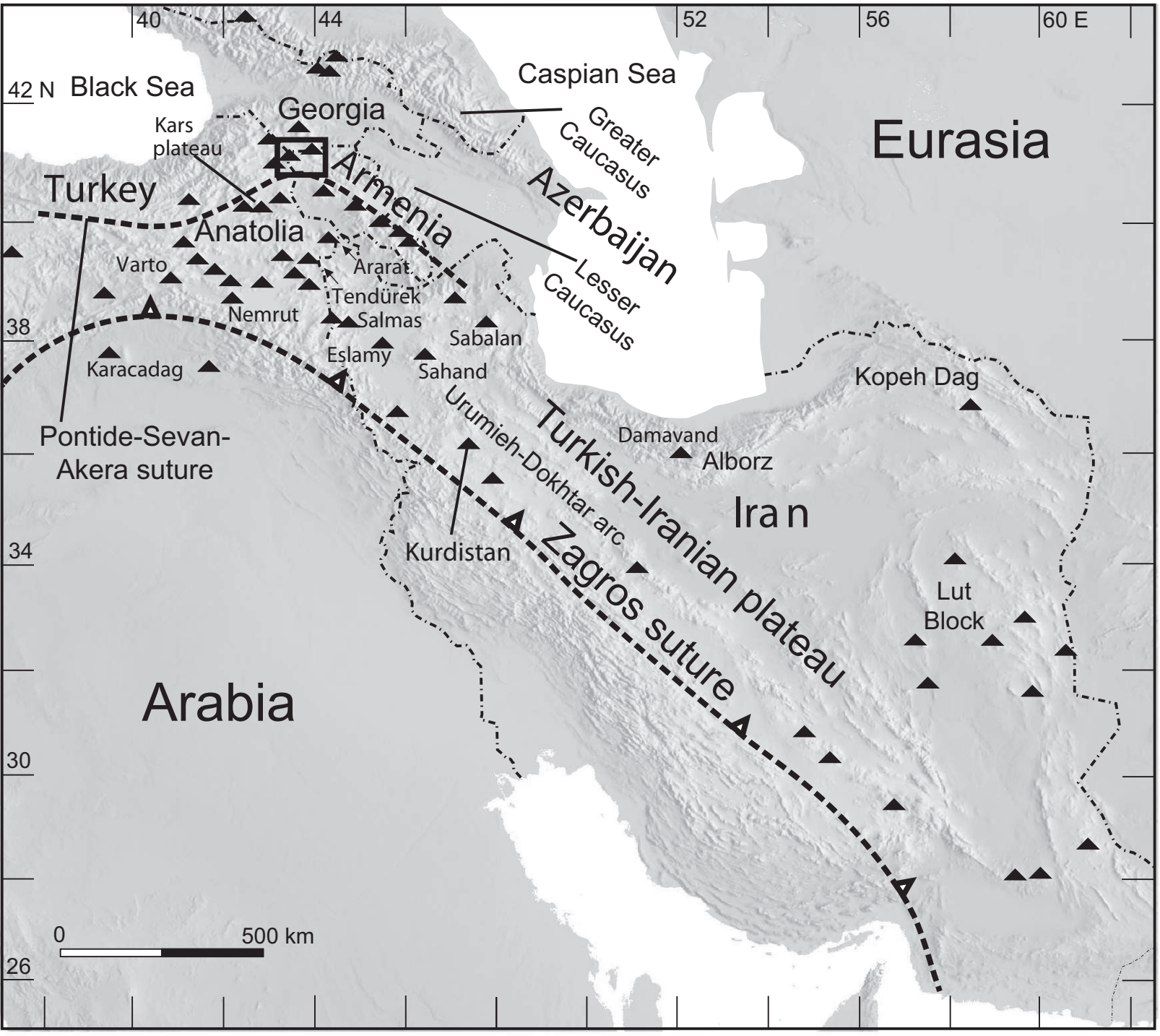
40
44
52
56
60 E
42 N
Black Sea
Caspian Sea
Georgia
Kars
plateau
Greater
Caucasus
Eurasia
Turkey
Armenia
Azerbaijan
Anatolia
Lesser
Caucasus
Varto
Ararat
Tendürek
Nemrut
Salmas
38
Sabalan
Eslamy
Sahand
Karacadag
Kopeh Dag
Pontide-Sevan-
Akera suture
Urumieh-Dokhtar arc
Turkish-Iranian plateau
Damavand
Alborz
Iran
34
Kurdistan
Zagros suture
Lut
Block
Arabia
30
0
500 km
26

Figure 2

Click here to download high resolution image

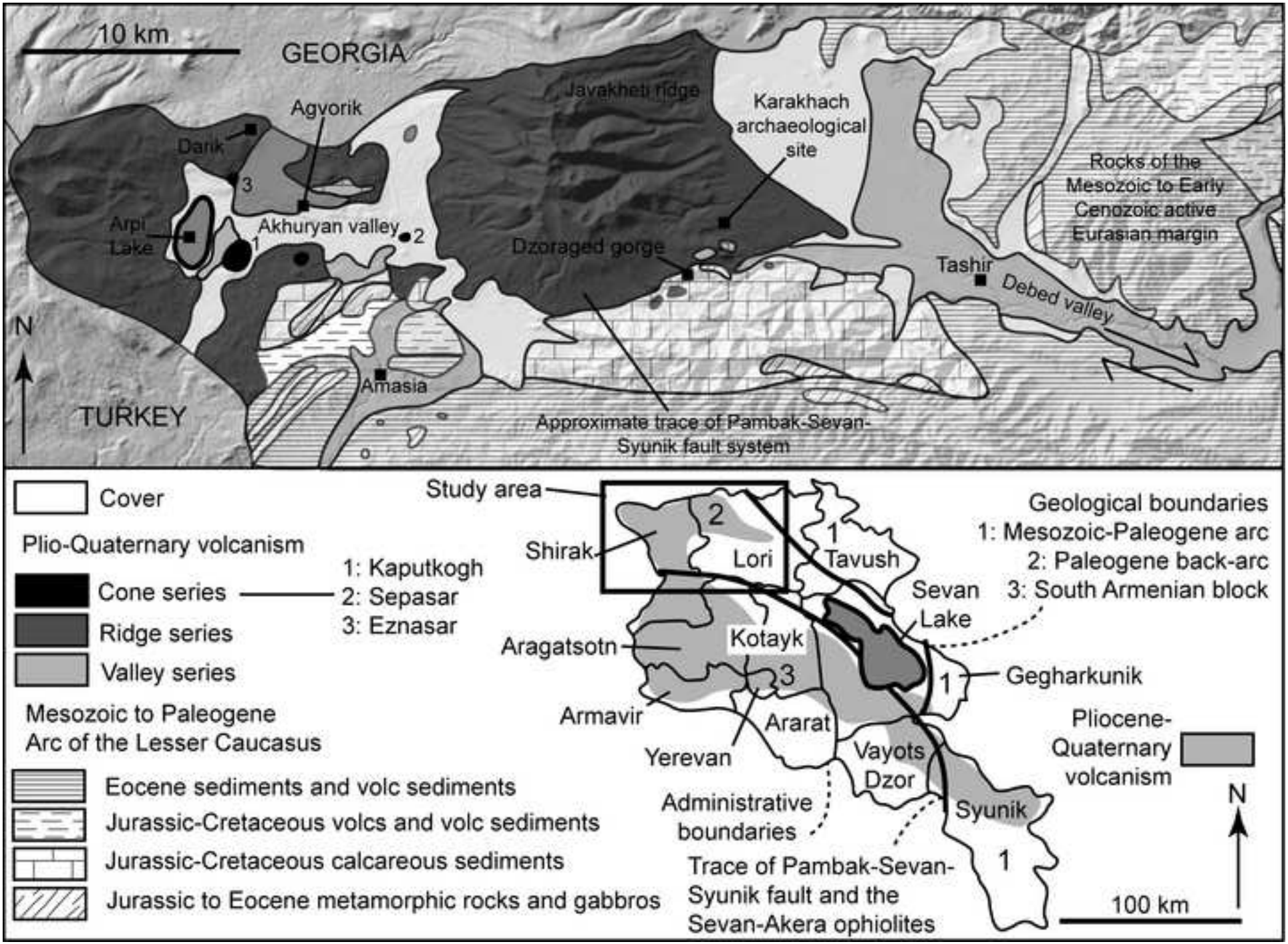

Figure 3

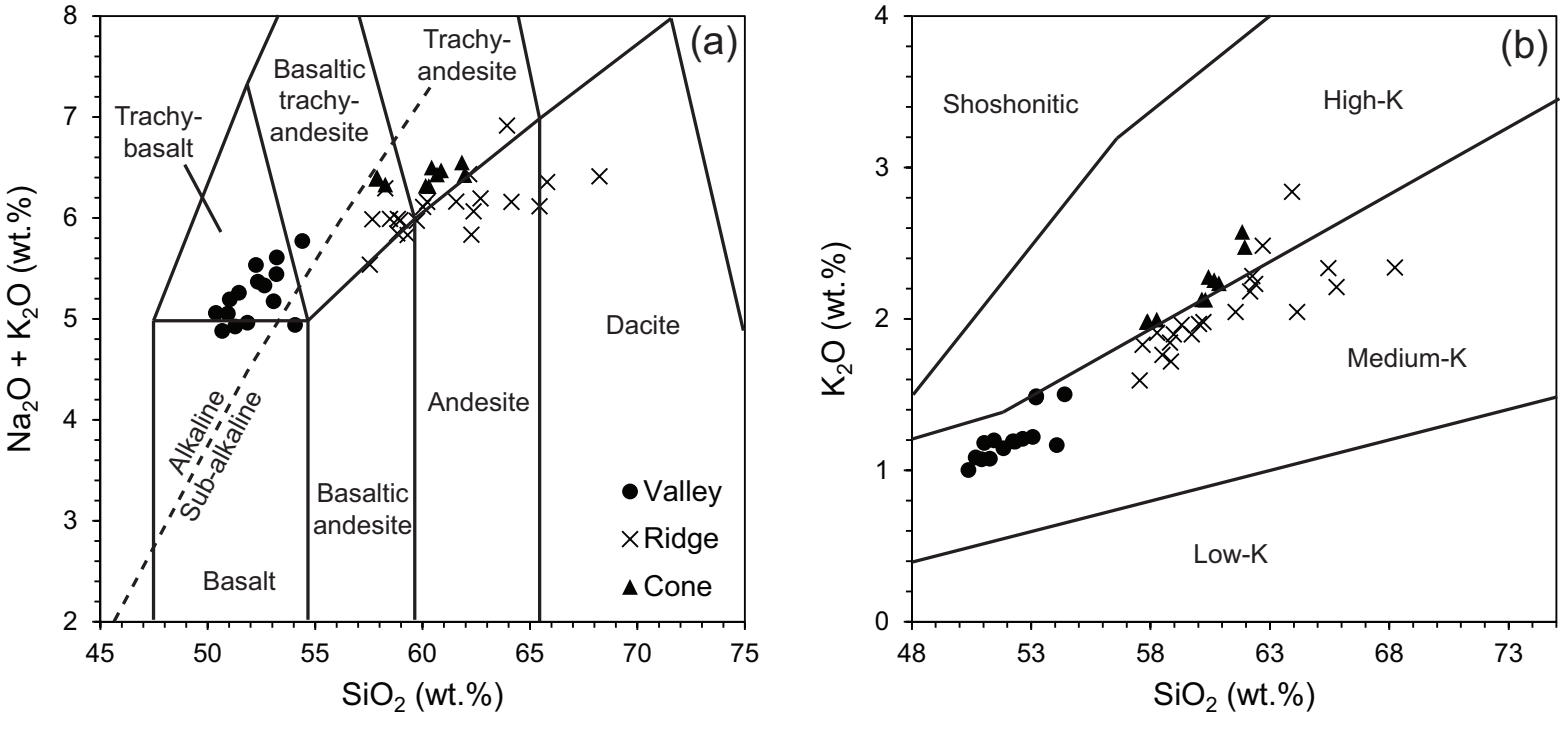
(a)
Trachy-basalt
Basaltic trachy-andesite
Trachy-andesite
Dacite
Andesite
Basaltic andesite
Basalt
Alkaline
Sub-alkaline
Valley
Ridge
Cone
$Na_2O + K_2O$ (wt.%)
SiO_2 (wt.%)
(b)
Shoshonitic
High-K
Medium-K
Low-K
K_2O (wt.%)
SiO_2 (wt.%)

Figure 4

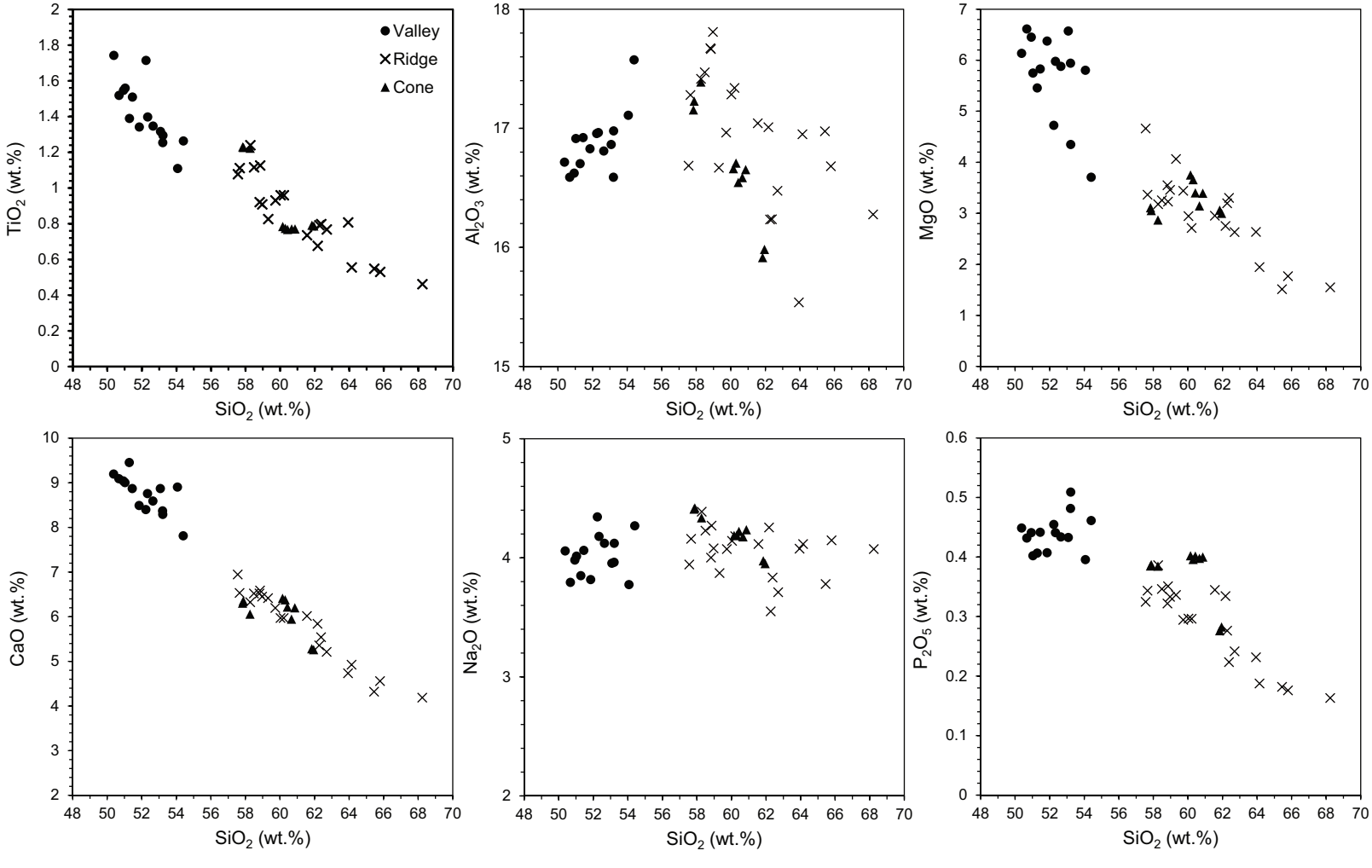
Valley
Ridge
Cone
TiO2 (wt.%)
Al2O3 (wt.%)
MgO (wt.%)
CaO (wt.%)
Na2O (wt.%)
P2O5 (wt.%)
SiO2 (wt.%)

Figure 5

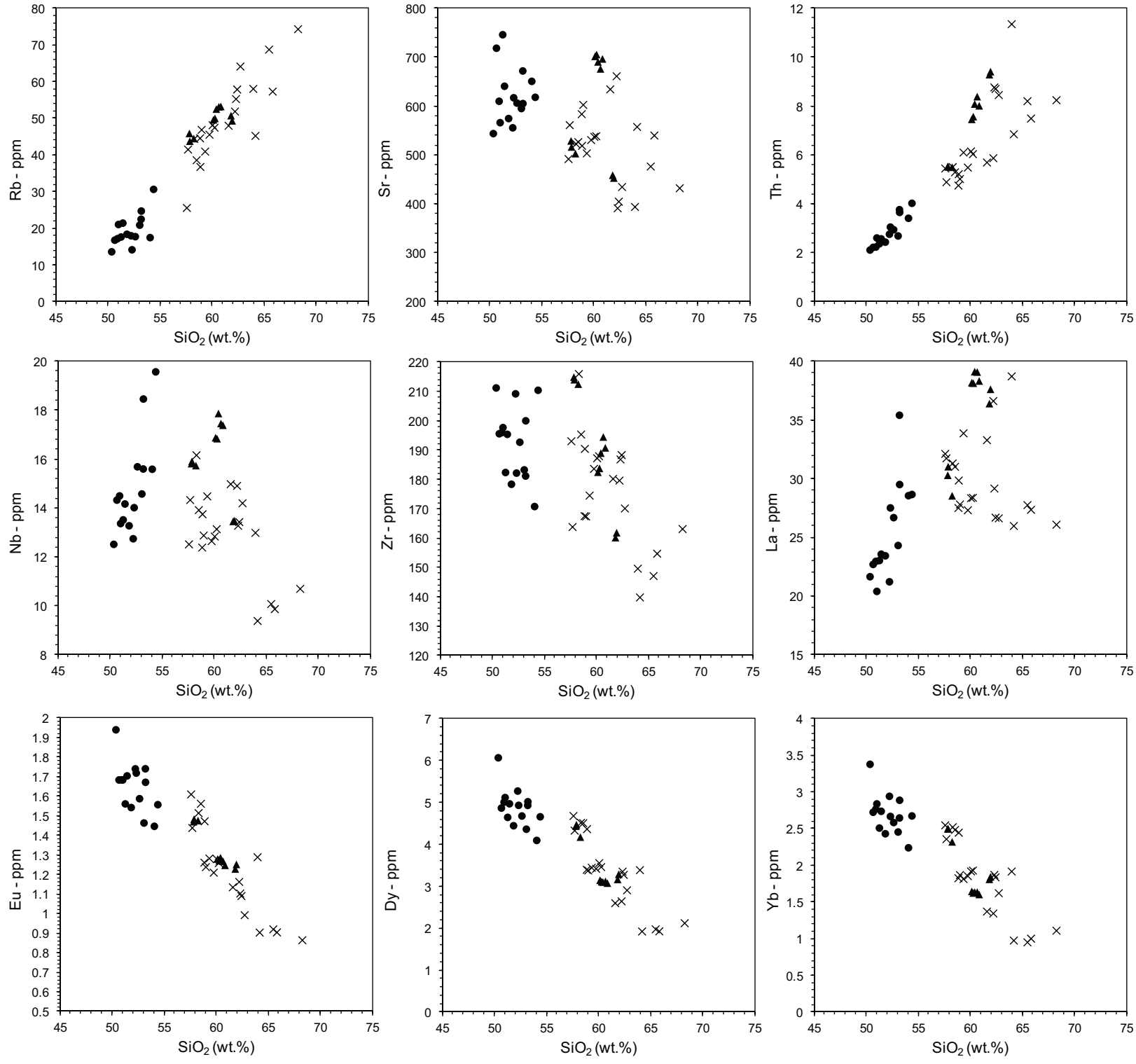
Rb - ppm
Sr - ppm
Th - ppm
Nb - ppm
Zr - ppm
La - ppm
Eu - ppm
Dy - ppm
Yb - ppm
SiO2 (wt.%)

Figure 6

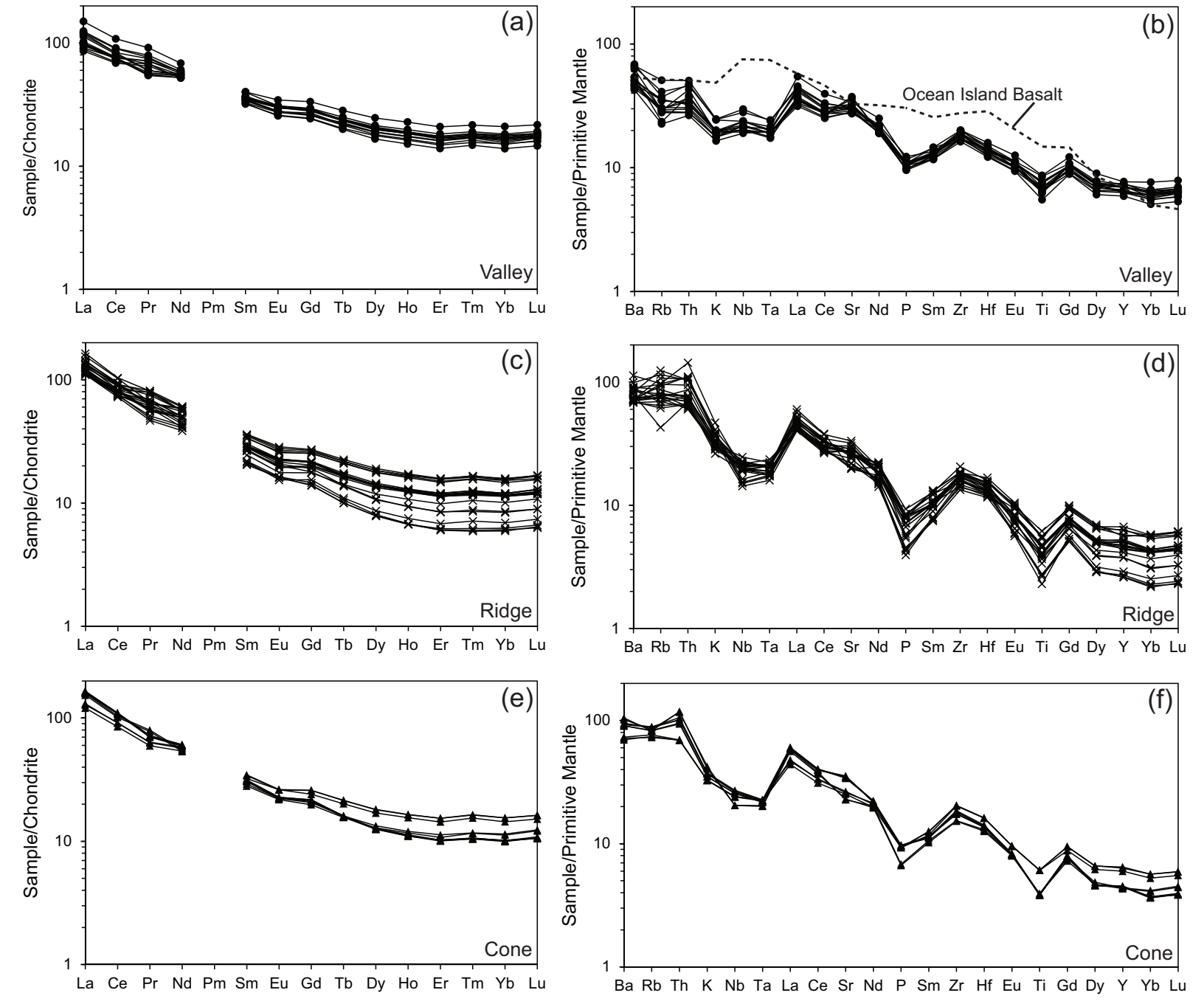
(a)
Sample/Chondrite
100
10
1
Valley
La Ce Pr Nd Pm Sm Eu Gd Tb Dy Ho Er Tm Yb Lu
(b)
Sample/Primitive Mantle
Ocean Island Basalt
Valley
Ba Rb Th K Nb Ta La Ce Sr Nd P Sm Zr Hf Eu Ti Gd Dy Y Yb Lu
(c)
Ridge
(d)
Ridge
(e)
Cone
(f)
Cone

Figure 7

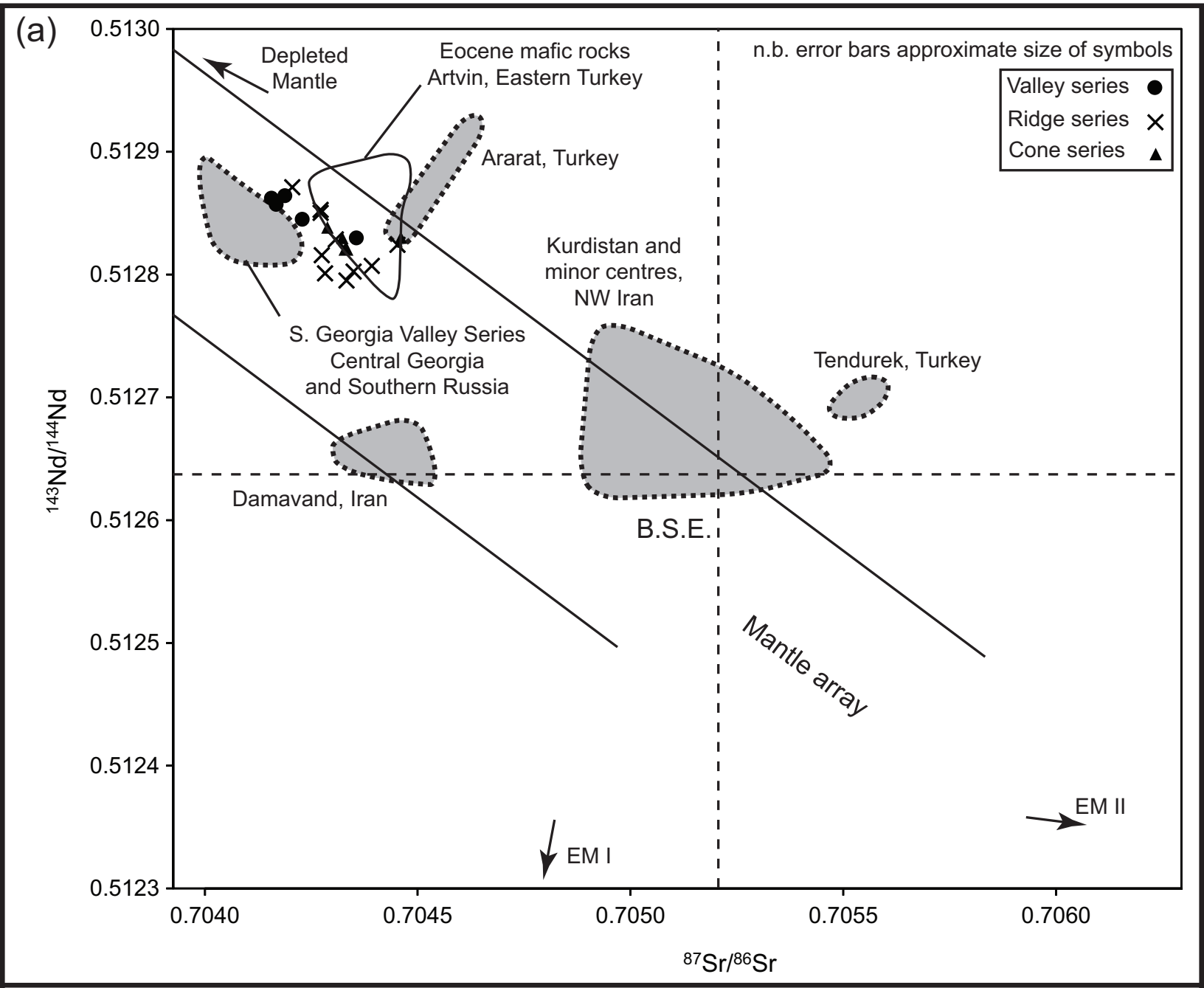
(a)
Depleted Mantle
Eocene mafic rocks Artvin, Eastern Turkey
Ararat, Turkey
Kurdistan and minor centres, NW Iran
S. Georgia Valley Series Central Georgia and Southern Russia
Tendurek, Turkey
Damavand, Iran
B.S.E.
Mantle array
EM I
EM II
n.b. error bars approximate size of symbols
Valley series
Ridge series
Cone series
143Nd/144Nd
87Sr/86Sr
0.5130
0.5129
0.5128
0.5127
0.5126
0.5125
0.5124
0.5123
0.7040
0.7045
0.7050
0.7055
0.7060

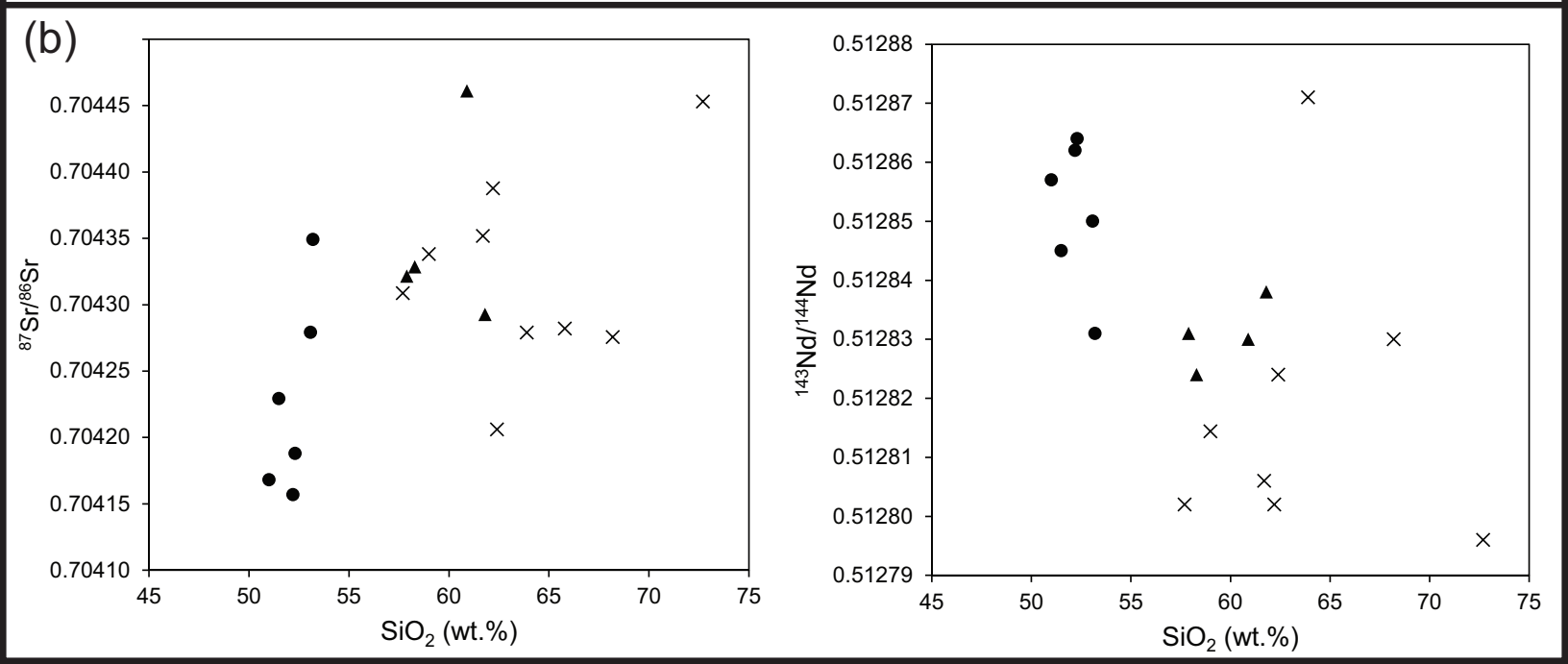
(b)
87Sr/86Sr
SiO2 (wt.%)
143Nd/144Nd
SiO2 (wt.%)
0.70445
0.70440
0.70435
0.70430
0.70425
0.70420
0.70415
0.70410
0.51288
0.51287
0.51286
0.51285
0.51284
0.51283
0.51282
0.51281
0.51280
0.51279
45
50
55
60
65
70
75

Figure 8

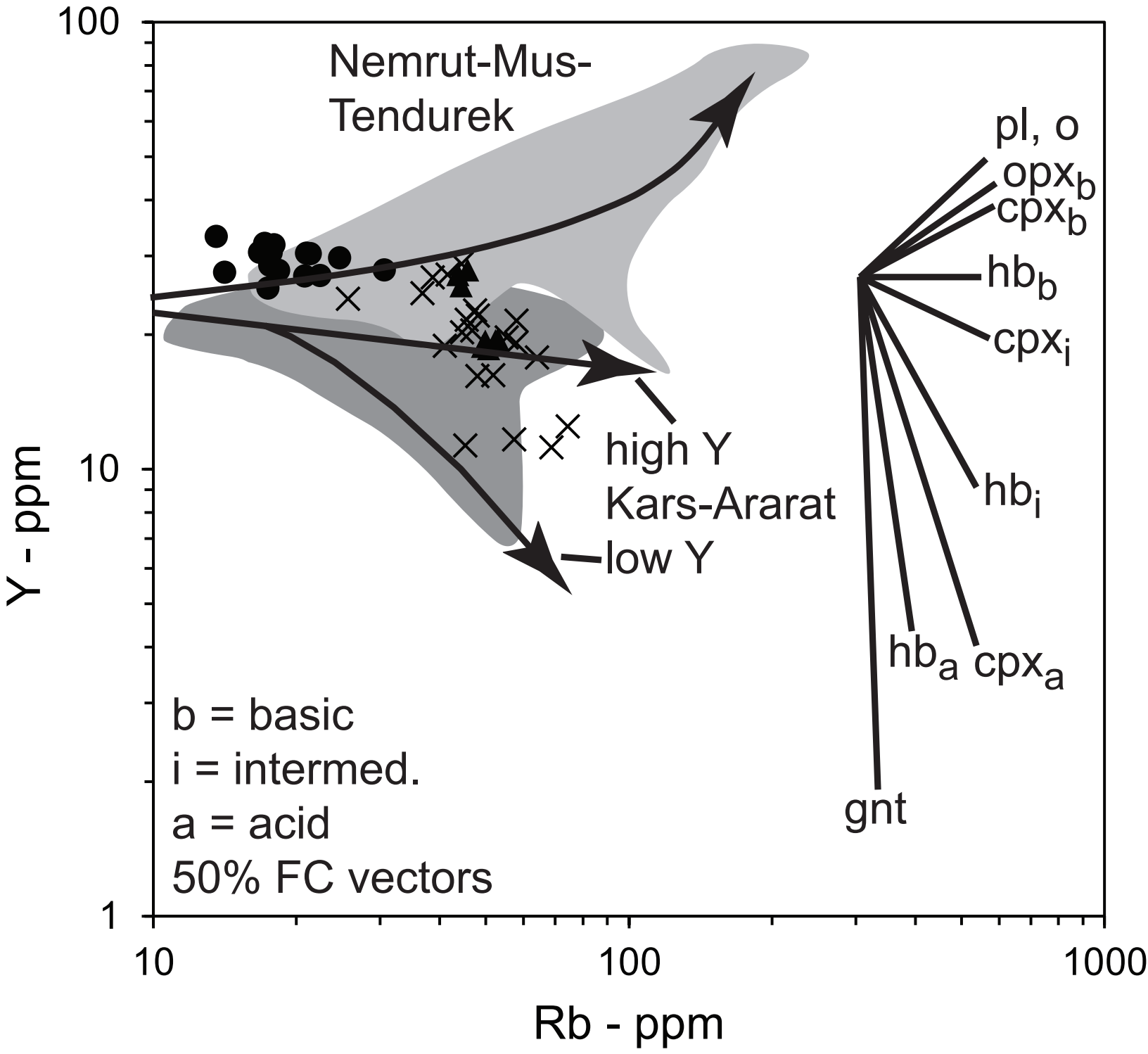
100
10
1
Y - ppm
10
100
1000
Rb - ppm
Nemrut-Mus-
Tendurek
high Y
Kars-Ararat
low Y
pl, o
opx$_b$
cpx$_b$
hb$_b$
cpx$_i$
hb$_i$
hb$_a$ cpx$_a$
gnt
b = basic
i = intermed.
a = acid
50% FC vectors

Figure 9

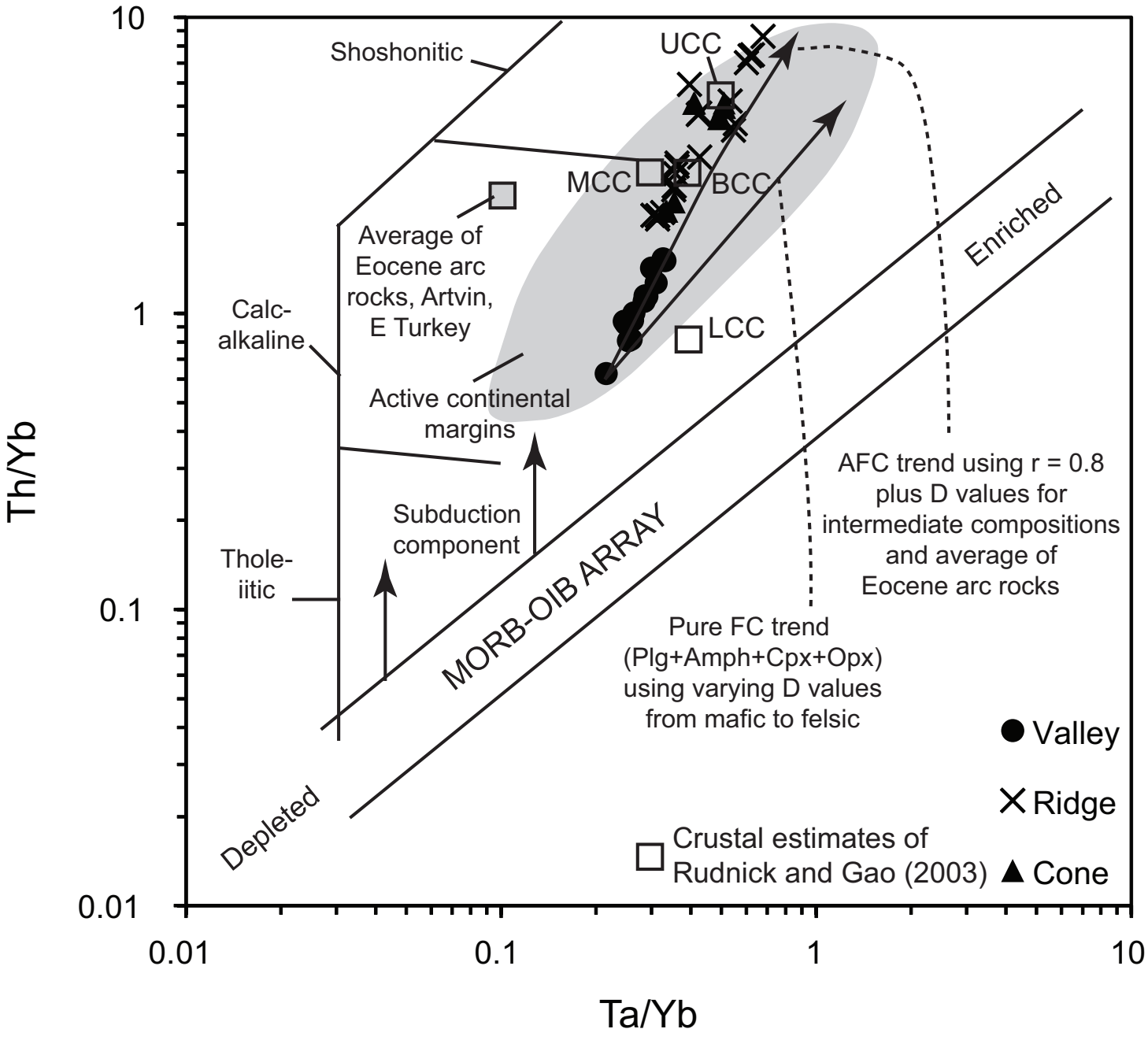
10
1
0.1
0.01
0.01
0.1
1
10
Th/Yb
Ta/Yb
Shoshonitic
Calc-
alkaline
Thole-
iitic
Depleted
UCC
MCC
BCC
LCC
Average of
Eocene arc
rocks, Artvin,
E Turkey
Active continental
margins
Subduction
component
MORB-OIB ARRAY
Enriched
AFC trend using r = 0.8
plus D values for
intermediate compositions
and average of
Eocene arc rocks
Pure FC trend
(Plg+Amph+Cpx+Opx)
using varying D values
from mafic to felsic
Valley
Ridge
Crustal estimates of
Rudnick and Gao (2003)
Cone

Figure 10

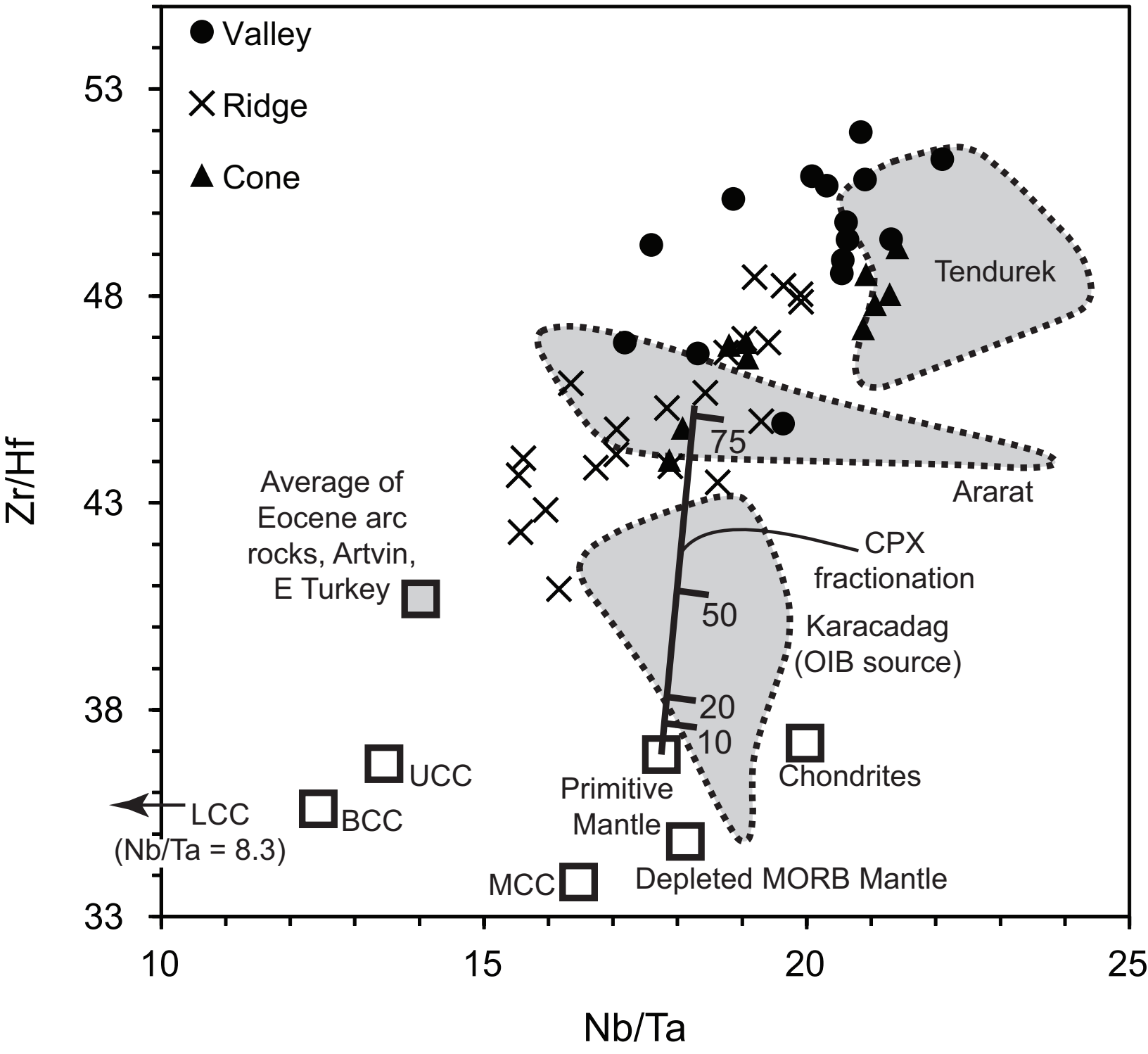
Valley
Ridge
Cone
Tendurek
Ararat
75
CPX
fractionation
50
Karacadag
(OIB source)
20
10
Average of
Eocene arc
rocks, Artvin,
E Turkey
UCC
BCC
LCC
(Nb/Ta = 8.3)
Primitive
Mantle
Chondrites
MCC
Depleted MORB Mantle
53
48
43
38
33
Zr/Hf
10
15
20
25
Nb/Ta

Figure 11

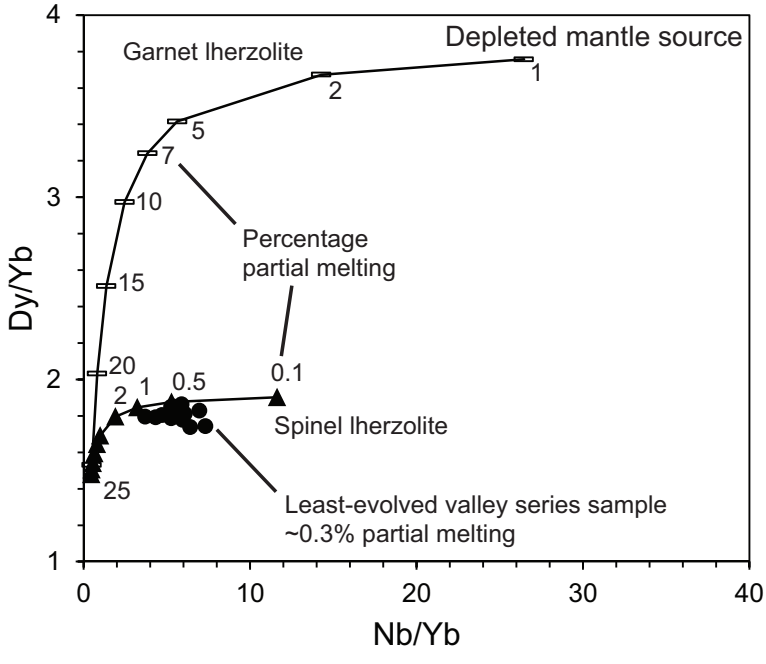
Depleted mantle source
Garnet lherzolite
Percentage
partial melting
Spinel lherzolite
Least-evolved valley series sample
~0.3% partial melting
Dy/Yb
Nb/Yb

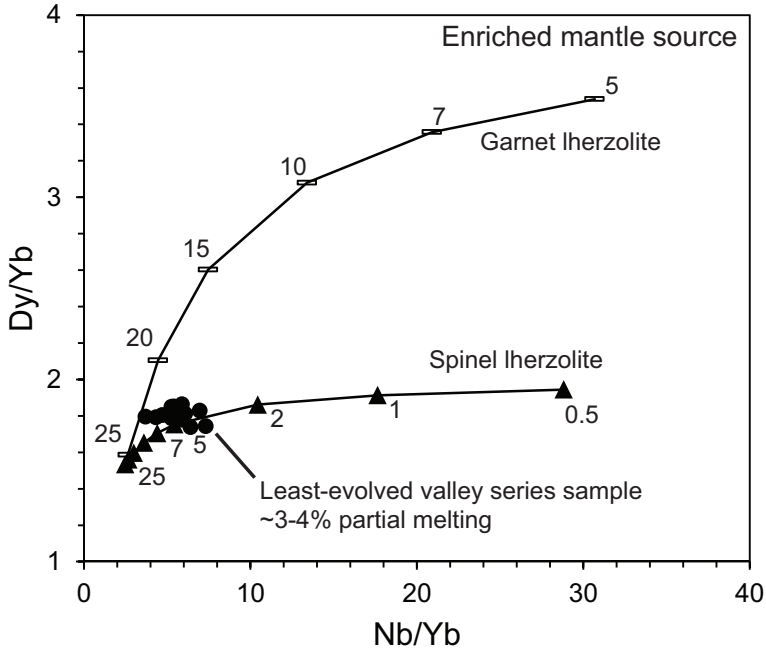
Enriched mantle source
Garnet lherzolite
Spinel lherzolite
Least-evolved valley series sample
~3-4% partial melting
Dy/Yb
Nb/Yb

Figure 12

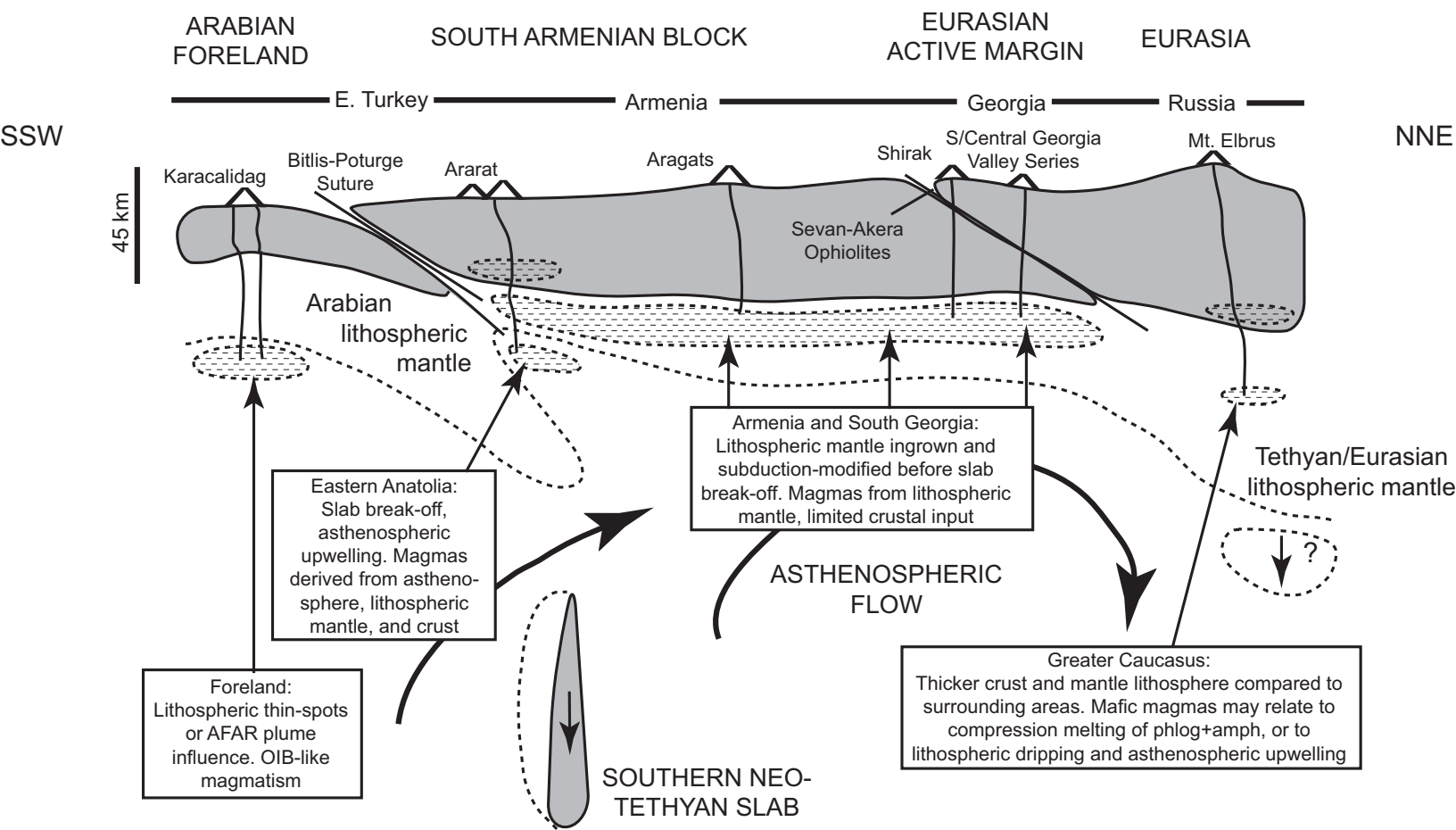
ARABIAN FORELAND
SOUTH ARMENIAN BLOCK
EURASIAN ACTIVE MARGIN
EURASIA
E. Turkey
Armenia
Georgia
Russia
SSW
NNE
45 km
Karacalidag
Bitlis-Poturge Suture
Ararat
Aragats
Shirak
S/Central Georgia Valley Series
Mt. Elbrus
Sevan-Akera Ophiolites
Arabian lithospheric mantle
Armenia and South Georgia: Lithospheric mantle ingrown and subduction-modified before slab break-off. Magmas from lithospheric mantle, limited crustal input
Tethyan/Eurasian lithospheric mantle
?
Eastern Anatolia: Slab break-off, asthenospheric upwelling. Magmas derived from astheno-sphere, lithospheric mantle, and crust
ASTHENOSPHERIC FLOW
Foreland: Lithospheric thin-spots or AFAR plume influence. OIB-like magmatism
Greater Caucasus: Thicker crust and mantle lithosphere compared to surrounding areas. Mafic magmas may relate to compression melting of phlog+amph, or to lithospheric dripping and asthenospheric upwelling
SOUTHERN NEO-TETHYAN SLAB

Table 1

Click here to download Table: Neilletal Table1.docx

Table 1. Major and trace element data for selected samples from the valley (v), ridge (r), and cone (c) series, Shirak.

Number	S14.4	S14.5	S19.1	S25.2	S26.2	S28.1	S29.1	S4.2	S5.1	S6.1	S9.2	S21.1	S23.1	S30.2	S30.3	S1.1	S2.1	S7.3	S20.2
Series	V	V	V	V	V	V	V	R	R	R	R	R	R	R	R	C	C	C	C
SiO_2	50.68	53.21	52.33	53.08	52.24	51.45	51.03	57.67	51.57	52.18	65.80	63.94	62.39	58.97	68.23	57.88	58.27	60.68	61.84
TiO_2	1.52	1.25	1.40	1.32	1.71	1.51	1.56	1.11	0.73	0.68	0.53	0.81	0.80	0.91	0.46	1.23	1.22	0.77	0.79
Al_2O_3	16.59	16.59	16.96	16.86	16.96	16.92	16.91	17.28	17.04	17.01	16.68	15.54	16.23	17.81	16.28	17.23	17.39	16.65	15.91
Fe_2O_3(T)	10.20	9.03	9.27	9.58	10.43	10.16	10.52	7.35	5.56	5.25	4.07	5.40	5.55	6.63	3.56	7.76	7.85	5.82	5.70
MnO	0.16	0.15	0.15	0.15	0.16	0.18	0.17	0.12	0.09	0.09	0.07	0.10	0.09	0.11	0.06	0.11	0.10	0.10	0.10
MgO	6.61	5.94	5.98	6.57	4.72	5.83	5.75	3.36	2.95	2.75	1.77	2.63	3.30	3.46	1.55	3.05	2.87	3.39	3.06
CaO	9.09	8.37	8.75	8.87	8.40	8.87	9.00	6.53	6.02	5.84	4.56	4.73	5.54	6.45	4.19	6.35	6.06	6.20	5.28
Na_2O	3.79	3.96	4.12	3.95	4.34	4.06	4.01	4.16	4.11	4.25	4.15	4.07	3.83	4.08	4.07	4.42	4.33	4.24	3.97
K_2O	1.09	1.48	1.19	1.22	1.19	1.20	1.18	1.83	2.05	2.18	2.21	2.84	2.23	1.90	2.34	1.94	2.00	2.24	2.58
P_2O_5	0.43	0.48	0.44	0.43	0.46	0.44	0.40	0.34	0.35	0.33	0.18	0.23	0.22	0.33	0.16	0.39	0.39	0.40	0.28
LOI	0.73	-0.30	-0.14	-0.23	-0.09	0.05	-0.14	-0.07	0.45	-0.06	0.63	0.17	0.74	0.09	0.00	-0.06	0.11	-0.11	0.84
Total	100.89	100.16	100.52	101.81	100.56	100.67	100.40	99.68	100.92	100.50	100.64	100.47	100.94	100.74	100.91	100.34	100.58	100.55	100.37
Sc	15.6	23.1	19.3	20.3	21.7	22.1	22.2	bd	bd	bd	bd	bd	12.7	15.0	bd	bd	bd	bd	11.5
V	167	179	164	169	188	185	184	131	103	100	71	85	105	142	68	147	140	112	101
Cr	154	162	162	175	131	153	129	bd	45	44	bd	38	72	bd	bd	bd	bd	73	47
Co	37.6	33.0	36.5	36.5	35.0	41.4	42.2	22.9	16.1	15.3	9.8	18.9	19.0	23.1	9.5	20.6	20.3	18.1	17.6
Ni	106.8	113.8	113.5	125.6	65.4	106.3	101.5	bd	16.6	bd	bd	47.2	52.1	32.9	bd	bd	bd	39.2	36.7
Rb	16.7	22.5	14.1	20.8	17.9	21.4	21.0	41.6	48.1	51.9	57.4	58.1	57.9	46.9	74.4	43.7	44.4	53.2	50.7
Sr	718	671	617	595	555	640	566	562	635	662	540	395	405	603	433	516	503	696	458
Y	30.5	27.1	27.6	27.0	31.7	30.3	30.4	27.2	16.1	16.2	11.7	21.5	19.2	20.4	12.5	27.2	25.7	19.2	18.6
Zr	195.5	181.1	182.1	183.2	209.1	195.3	197.6	163.9	180.3	179.7	154.8	149.7	188.4	167.5	163.2	213.9	212.4	190.7	160.1
Nb	14.3	15.6	14.0	14.6	12.7	14.2	13.4	14.3	15.0	14.9	9.9	13.0	13.4	12.9	10.7	15.9	15.7	17.4	13.5
Ba	329	452	356	340	288	334	312	449	556	599	589	742	471	491	545	474	460	609	670
Hf	3.9	4.0	3.9	3.5	4.3	3.8	3.9	3.7	3.8	3.8	3.5	3.3	4.3	3.6	3.7	4.6	4.6	3.9	3.6
Ta	0.7	0.8	0.8	0.7	0.7	0.7	0.7	0.7	0.8	0.8	0.6	0.8	0.8	0.7	0.7	0.8	0.8	0.8	0.7
Pb	4.6	6.6	5.5	5.1	4.3	4.6	4.7	8.0	9.0	9.6	11.6	10.6	8.9	8.3	11.1	8.7	8.0	11.8	9.9
Th	2.2	3.8	3.1	2.7	2.8	2.6	2.6	4.9	5.7	5.9	7.5	11.4	8.7	5.0	8.3	5.5	5.5	8.0	9.3
U	0.7	0.9	0.3	0.8	0.3	0.8	0.6	1.2	1.3	1.4	1.9	2.0	2.2	1.3	2.2	1.5	1.4	1.8	1.7
La	22.7	35.4	27.5	24.3	21.2	23.6	20.4	31.8	33.3	36.6	27.4	38.7	26.7	27.8	26.1	31.0	28.5	38.3	26.4
Ce	45.6	66.2	51.1	47.1	43.0	47.0	42.1	54.6	58.1	62.7	46.3	63.6	48.2	50.9	46.0	55.8	52.1	66.3	62.0
Pr	5.2	8.5	6.9	6.3	6.3	6.6	6.0	5.9	5.7	6.1	4.5	7.5	5.9	6.4	5.5	5.9	5.5	6.6	7.2
Nd	24.7	31.3	26.8	23.7	25.1	26.0	23.9	26.6	23.3	25.2	18.6	25.4	20.7	22.7	18.7	26.7	24.7	27.7	24.5
Sm	5.3	5.9	5.3	4.7	5.4	5.4	5.2	5.0	3.9	4.2	3.1	4.3	3.9	4.2	3.2	5.1	4.8	4.5	4.2
Eu	1.7	1.7	1.7	1.5	1.7	1.7	1.7	1.4	1.1	1.2	0.9	1.3	1.1	1.2	0.9	1.5	1.5	1.3	1.2
Gd	5.6	5.8	5.6	4.9	5.9	5.7	5.7	5.0	3.6	3.8	2.8	4.2	3.9	4.3	3.1	5.2	4.8	4.3	3.9
Tb	0.8	0.9	0.9	0.7	0.9	0.9	0.9	0.8	0.5	0.5	0.4	0.6	0.6	0.6	0.4	0.8	0.7	0.6	0.6
Dy	4.9	4.9	4.9	4.3	5.3	5.0	5.1	4.3	2.6	2.7	1.9	3.4	3.3	3.4	2.1	4.5	4.2	3.1	3.2
Ho	1.0	1.0	1.0	0.9	1.1	1.0	1.0	0.9	0.5	0.5	0.4	0.7	0.7	0.7	0.4	0.9	0.9	0.6	0.6
Er	2.7	2.7	2.7	2.4	2.9	2.7	2.8	2.4	1.4	1.4	1.0	0.9	1.8	1.8	1.1	2.5	2.3	1.6	1.7
Tm	0.4	0.4	0.4	0.4	0.5	0.4	0.5	0.4	0.2	0.2	0.2	0.3	0.3	0.3	0.2	0.4	0.4	0.3	0.3
Yb	2.7	2.6	2.7	2.5	2.9	2.7	2.8	2.4	1.4	1.4	1.0	1.9	1.8	1.9	1.1	2.5	2.3	1.6	1.8
Lu	0.4	0.4	0.4	0.4	0.4	0.4	0.5	0.4	0.2	0.2	0.2	0.3	0.3	0.3	0.2	0.4	0.4	0.3	0.3

LOI = loss on ignition; b.d. = below detection

Table 2

Click here to download Table: Neilletal Table2.docx

Table 2. Measured Nd and Sr isotope compositions of the valley, ridge, and cone series, Shirak.

	$^{143}Nd/^{144}Nd$	± 1σ	εNd	± 1σ	$^{87}Sr/^{86}Sr$	± 1σ
Valley series						
S14.5	0.512831	0.000004	+3.76	0.08	0.704349	0.000009
S19.1	0.512864	0.000005	+4.41	0.10	0.704188	0.000007
S25.2	0.512850	0.000006	+4.14	0.12	0.704279	0.000007
S26.2	0.512862	0.000006	+4.37	0.12	0.704157	0.000008
S28.1	0.512845	0.000005	+4.04	0.10	0.704229	0.000008
S29.1	0.512857	0.000005	+4.27	0.10	0.704168	0.000007
Ridge series						
S4.2	0.512830	0.000007	+3.75	0.14	0.704309	0.000007
S5.1	0.512802	0.000007	+3.20	0.14	0.704352	0.000008
S6.1	0.512806	0.000005	+3.28	0.10	0.704388	0.000010
S9.2	0.512802	0.000005	+3.20	0.09	0.704282	0.000008
S21.1	0.512848	0.000004	+4.10	0.08	0.704279	0.000006
S23.1	0512871	0.000005	+4.55	0.10	0.704206	0.000007
S30.2	0.512796	0.000005	+3.08	0.10	0.704338	0.000010
S30.3	0.512814	0.000005	+3.44	0.10	0.704276	0.000007
Cone series						
S1.1	0.512831	0.000005	+3.76	0.10	0.704321	0.000007
S2.1	0.512824	0.000005	+3.63	0.10	0.704329	0.000007
S7.3	0.512830	0.000003	+3.75	0.06	0.704461	0.000007
S20.2	0.512838	0.000004	+3.90	0.09	0.704293	0.000007

Supplementary Item 1

Click here to download Background dataset for online publication only: NeilletalSUP1photomicrographs copy.pdf

Supplementary Item 2

Click here to download Background dataset for online publication only: Neilletal Shirak SUP 2.xlsx